

# PXIE Design Handbook

---

Draft, v1.0, edited by S. Nagaitsev, December 28, 2012

## Table of Contents:

Introduction.....	3
1. PXIE Overview.....	6
2. PXIE Beam Optics Design.....	12
3. Ion Source and Low Energy Beam Transport.....	19
4. Radio-Frequency Quadrupole.....	28
5. Medium Energy Beam Transport.....	34
6. Half-Wave Resonator Cryomodule Design .....	45
7. SSR1 Cryomodule Design .....	53
8. Diagnostics Line and Beam Dump .....	63
9. Facility Layout .....	71
10. Shielding and Radiation safety .....	73
11. Beam Instrumentation.....	82
12. Cryogenic Systems.....	89
13. RF Power Systems .....	93
14. Vacuum Systems.....	96
15. Controls.....	99
16. Low Level RF System .....	101
17. PXIE Machine Protection System .....	103
Summary .....	106

## **Introduction**

Steve Holmes

Project X is a proposed multi-MW, multi-functional proton accelerator complex aimed to support Fermilab's leading role in the intensity frontier research over next several decades [1]. It is currently under development by Fermilab with national and international partners. The Project X will include a 1-GeV, 2-mA CW linac, followed by a 3-GeV, 1-mA CW linac accelerating half of the beam delivered to 1 GeV further to 3 GeV, and a pulsed linac accelerating protons from 3 to 8 GeV for injection into the existing Main Injector synchrotron, as well as to various high-power beam targets associated with corresponding experiments. Project X will replace the existing 40-year old Fermilab injector complex and will add powerful new capabilities to support a large number of experiments in the energy range from 1 to 120 GeV. The 3-GeV CW linac is the centerpiece of the facility. It has to deliver proton beams to several experiments quasi-simultaneously with a beam structure which can be adjusted to the needs of each experiment. The time structure required by each experiment will be obtained by removing undesired bunches from the 162 MHz RFQ bunch stream in the medium energy beam transport (MEBT) at beam energy of 2.1 MeV using a wideband chopper (see Section 5 below). Separation of the beams to multiple experiments will be achieved by RF deflection of the beam after acceleration to 1 and 3 GeV points.

The Project X Reference Design [2] achieves its goals via a configuration that provides unique capabilities for the delivery of high power beams to multiple experiments with differing energy and bunch structure requirements. The front end of the Project X linac is key to the unique capabilities provided by the Reference Design, and the Project X Collaboration is planning a program of research and development aimed at integrated systems testing of critical components comprising the Project X front end. This program, known as the Project X Injector Experiment (PXIE), is being undertaken as a major element of the ongoing Project X R&D program. Successful completion of PXIE over the period FY12-17 will validate the concept for the front end, thereby minimizing the primary technical risk element within Project X.

### **Mission Goals**

The goal of the PXIE program is to validate critical technologies required to support the Project X Reference Design concept. PXIE will provide a platform for demonstrating operations of Project X front end components at full design parameters. Specific goals of the integrated systems test are:

- Deliver 1 mA average current with 80% bunch-by-bunch chopping of beam delivered from the RFQ.
- Demonstrate efficient acceleration with minimal emittance dilution through at least 15 MeV.

## Scope

The scope of PXIE includes:

- CW H<sup>-</sup> source delivering 5 mA at 30 keV
- LEBT with beam pre-chopping
- CW RFQ operating at 162.5 MHz and delivering 5 mA at 2.1 MeV
- MEBT with integrated wide band chopper and beam absorbers capable of generating arbitrary bunch patterns at 162.5 MHz, and disposing of up to 5 mA average beam current
- Two low beta superconducting cryomodules based on half-wave (HWR) and spoke (SSR1) resonators and capable of accelerating 1 mA beam to at least 15 MeV
- Associated beam diagnostics
- Beam dump capable of accommodating 1 mA at full beam energy for extended periods.
- Associated utilities and shielding

## Rationale

A concept for delivery of high power, high duty factor beam to multiple experiments with differing beam structure requirements is incorporated into the Project X Reference Design. This capability is unique among high power proton facilities either operating or under development anywhere in the world. The concept is based on a fast programmable beam chopper (aka wideband chopper) integrated into the linac front end, capable of removing bunches spaced at 6 ns in arbitrary patterns and paired with transverse rf deflecting cavities to send beam quasi-simultaneously to three or more different experimental areas at either 1 or 3 GeV. While the utilization of RF deflection to support multiple experiments has already been demonstrated at the CEBAF facility at TJNAF, the wideband chopper is a unique device currently beyond the state of the art.

The delivery of multi-MW CW proton beams requires a linac front end capable of efficient acceleration of low- $\beta$  beams with minimal halo formation. The utilization of superconducting accelerating structures in this regime is unique and presents significant technical challenges. In addition the outlined capabilities are critical to establishing routine operations meeting extremely stringent beam loss criteria – typically less than 1 W/m. At 3 GeV this translates into a fractional beam loss of  $<3 \times 10^{-7}/m$ . The initial stage of acceleration, utilizing accelerating structures at  $\beta \approx 0.1$  and 0.2 up to  $\approx 40$  MeV, is crucial in meeting this performance goal.

The purpose of PXIE is to demonstrate that the technologies selected for the Project X front end can indeed meet the performance requirements established in the Reference Design, thereby mitigating the primary technical risk element associated with Project X. PXIE will utilize components constructed to Project X specifications wherever possible and will explore, and provide feedback into the Project X Front End design regarding, the following specific technical concerns:

- Ion source lifetime
- LEBT pre-chopping
- Vacuum management in the LEBT/RFQ region,
- Validation of chopper performance
- Measurement of extinction level for removed bunches
- Effectiveness and lifetime of MEBT beam absorber
- MEBT vacuum management
- Operation of HWR in close proximity to 10 kW absorber subjected to blistering and sputtering introduced by the incoming beam
- Operation of SSR1 with beam
- Emittance preservation and beam halo formation through the front end

PXIE will be developed by U.S. and Indian institutions who are expected to participate in the proposed Project X construction. PXIE will thus provide an opportunity to develop the working relationships and management processes necessary for the construction phase.

### **Plan**

PXIE is part of the Project X R&D program and the development of PXIE will be coordinated from within the Project X organization. PXIE development will require close cooperation with the SRF and General Accelerator Development programs at Fermilab. The effort will be provided initially by Fermilab, LBNL, ANL, and SLAC with opportunities for collaboration with Indian colleagues who are developing similar systems for their domestic programs. Opportunities to integrate additional collaborators with similar interests will be pursued.

The goal is to complete PXIE, meaning delivery of beam to at least 15 MeV with final parameters (1 mA CW, 5 mA peak, arbitrary bunch chopping) in the fall of 2016.

### **References**

- [1] “Project X Functional Requirements Specification”, Project X Document 658 (<http://projectx-docdb.fnal.gov/cgi-bin/ShowDocument?docid=658>)
- [2] “Project X Reference Design”, Project X Document 776 (<http://projectx-docdb.fnal.gov/cgi-bin/ShowDocument?docid=776>).



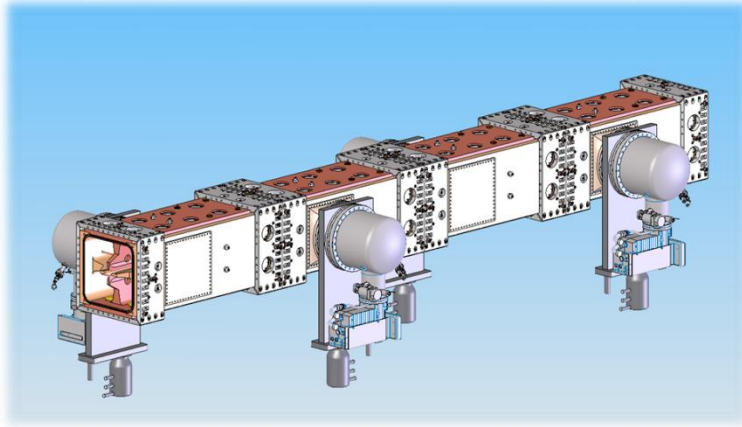


**Figure 1.2:** The RFQ conceptual design

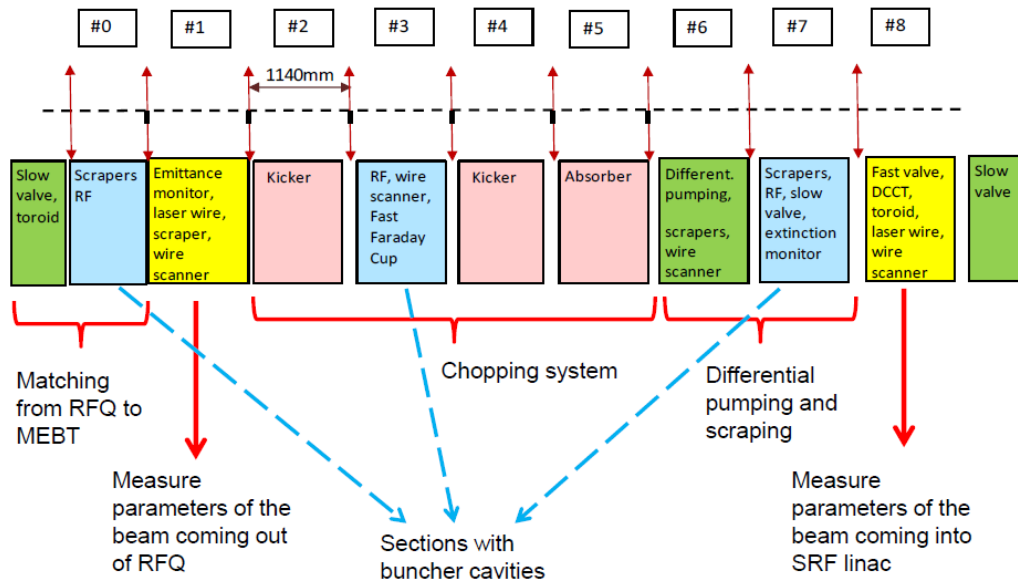


**Figure 1.3:** The conceptual MEBT schematic.

The PXIE MEBT serves the following functions:

- Forms the bunch structure required by the Project X users ;
- Matches optical functions between the RFQ and the SRF cavities;
- Includes tools to measure the properties of the beam coming out of the RFQ and transported to the SRF cavities;
- Plays a role in a machine protection system.

Figure 1.3 shows the conceptual MEBT schematic. The MEBT has a periodic transverse focusing structure comprised of 9 drift sections (65 cm each) separated by quadrupole triplets. The overall length of the MEBT is about 10 m. Each drift section serves a distinct purpose as

described in Figure 1.3. Several main ideas drive such a concept. First, to reduce the kick voltage, the MEBT chopper employs two kickers separated by 180 deg. in betatron phase. Second, the RFQ frequency was chosen sufficiently low so as to reduce the kicker bandwidth to a manageable value ( $\leq 1$  GHz). Third, the MEBT beam absorber [3] is being designed to absorb the beam power of 21 kW allowing operations with up to 10 mA beam current; and, fourth, the differential pumping section isolates the absorber and the cryomodules to reduce the gas load to the cold section. The vacuum at the HWR cryomodule entrance was specified to be at or below  $10^{-9}$  Torr to prevent potential performance degradation of the SRF cavities because of high vacuum pressure. Figure 1.4 presents the transverse and longitudinal rms beam envelopes at a nominal beam current.

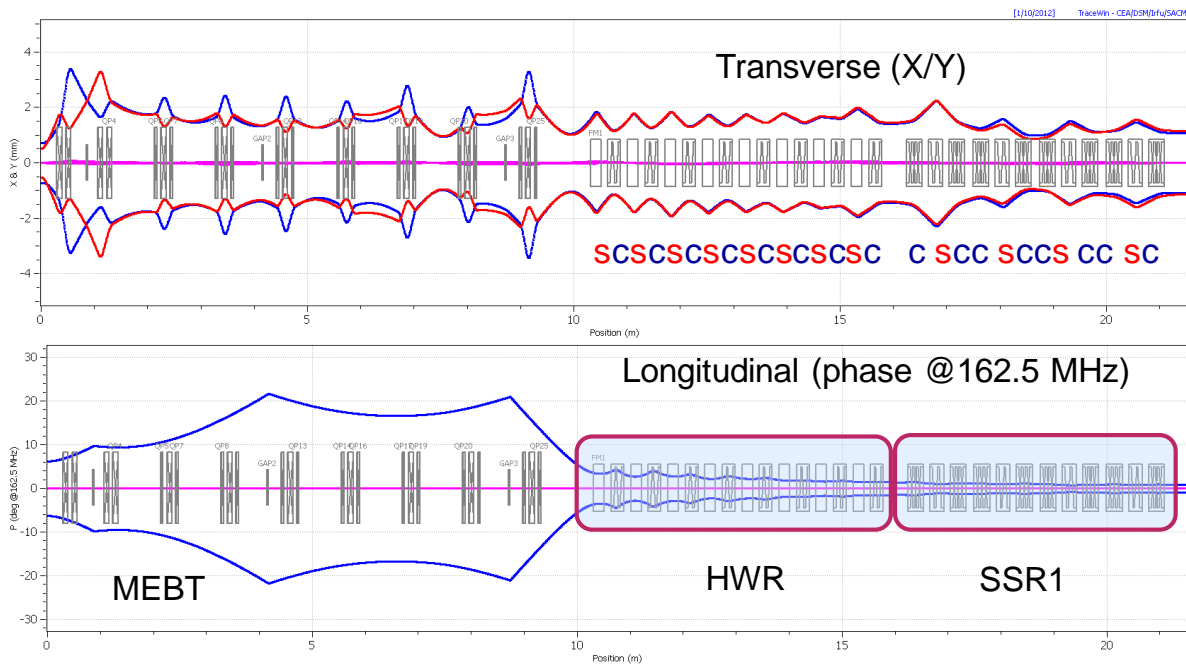


**Figure 1.4:** Transverse (mm) and longitudinal (degrees of 162.5 MHz) rms beam envelopes from the RFQ exit (2.1 MeV) to the exit of the SSR1 cryomodule (22 MeV). Peak beam current is 5 mA ( $1.9 \cdot 10^8$  ppb).

The PXIE cryogenic section consists of two SRF cryomodules (CM), operating at 2K, separated by a warm section. The half-wave resonator (HWR) cryomodule [4] has eight HW  $\beta = 0.11$  cavities [5] operating at 162.5 MHz and separated by 8 superconducting focusing solenoids. Each solenoid accommodates a pair of transverse corrector coils and a BPM. The HWR CM (being designed by ANL) is  $\sim 5.9$  m long and accelerates the beam from 2.1 MeV to  $\sim 11$  MeV. The nominal operational accelerating gradient was chosen to be 1.75 MV/cavity (at  $\beta = 0.11$ ). The gradient is reduced at the first few cavities to avoid longitudinal beam overfocusing. Figure 1.5 shows the HWR CM cavity and solenoid string assembly.

The single-spoke resonator (SSR1) cryomodule is being designed by FNAL [6]. It consists of eight 325-MHz single-spoke resonators ( $\beta = 0.22$ ) [7] and 4 focusing solenoids. Figure 1.6 shows the cavity and solenoid string assembly. Similar to the HWR CM, all solenoids will have corrector coils and BPMs. Its overall length (flange-to-flange) is about 5.3 m and it accelerates the beam from 11 to  $\sim 25$  MeV. The operational accelerating gradient was chosen to be 2 MV/cavity (at  $\beta = 0.22$ ).

The high-energy test beam line (downstream of SSR1 CM) is designed to accommodate the beam diagnostics to measure the beam properties and the beam extinction for rf buckets emptied by MEBT chopper [8]. Finally, the PXIE beam dump at the end of the beam line is being designed for 50 kW. The dipole magnet immediately upstream of the beam dump will serve as a spectrometer to measure the beam energy. A variety of diagnostic tools will be installed throughout the PXIE beam line to support the commissioning and the R&D program [9].

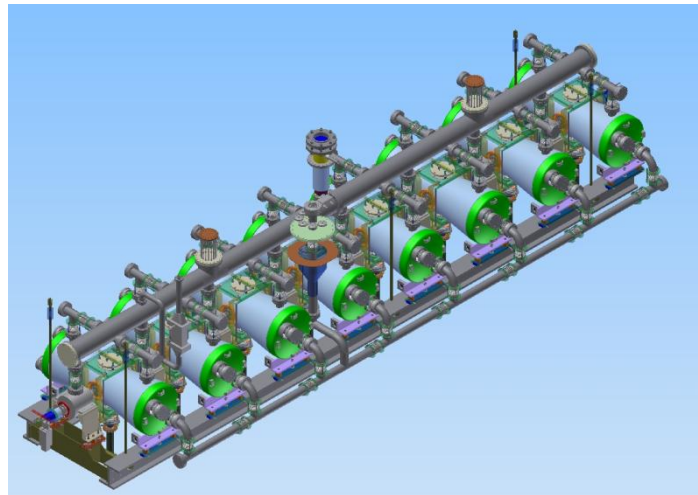


**Figure 1.5:** The HWR cavity and solenoid string assembly.

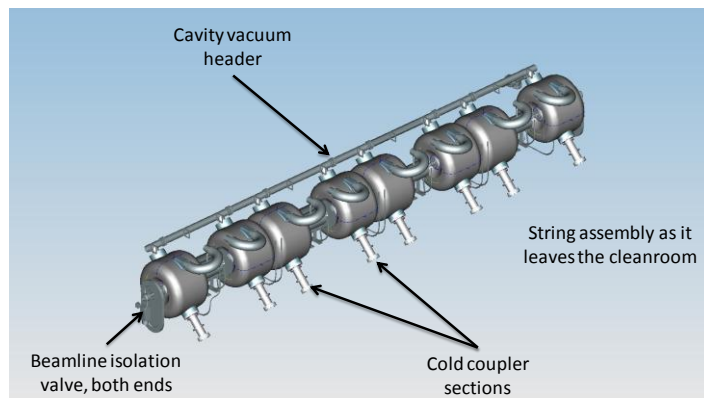


**Figure 1.6:** The SSR1 cavity and solenoid string assembly.

PXIE will be located in the existing Cryomodule Test Facility (CMTF) building which also will include an enclosure for ILC cryomodules testing. A cryo-plant supporting operation of both installations will have 500 W cooling power at 2 K and 4.1 kW at 40 K. It is expected that at normal operations PXIE will require cryo-power not exceeding 100 W at 2 K.

Many PXIE subsystems and components are being designed and constructed in collaboration with LBNL (LEBT and MEBT), SLAC (MEBT chopper driver) and Indian laboratories (high-level rf, beam instrumentation).

### **Summary**

The PXIE program is being designed and constructed at Fermilab as the centerpiece of the Project X R&D program. It will provide an integrated systems test for Project X front end components and validate the concept for the Project X front end, thereby minimizing the primary technical risk element within the Reference Design.

Main technical issues to be addressed by PXIE are:

- LEBT: the beam neutralization, the chopper performance, and the beam stability;
- RFQ: the longitudinal halo formation and the high average power;
- MEBT: the beam dynamics, the chopper kicker and its driver, the absorber, the diagnostics, the extinction, and vacuum near SRF cavities;
- HWR and SSR1: Issues associated with operating SRF cryomodules near a high power absorber, beam losses, beam acceleration, the effect of solenoids magnetic field on SRF cavities, microphonics and LLRF control of low beta CW cavities at 2K;
- Beam line: the beam properties, the beam extinction, the beam losses and halo.

### **References**

- [3] <http://www.dehnel.com/>
- [4] S. Virosek et al., “Design and Analysis of the PXIE CW Radio-frequency Quadrupole (RFQ)”, IPAC12 proceedings.
- [5] C. Baffes et al., “Design Considerations For An MEBT Chopper Absorber of 2.1MeV H<sup>-</sup> at the Project X Injector Experiment”, IPAC12 proceedings.
- [6] Z. Conway et al., “A New Half-Wave Resonator Cryomodule Design for Project-X”, IPAC12 proceedings.
- [7] P. Ostroumov et al., “Development of a Half-Wave Resonator for Project X”, IPAC12 proceedings.
- [8] T. Nicol et al., “SSR1 Cryomodule Design PXIE”, IPAC12 proceedings.

- [9] L. Ristori et al., “Design of SSR1 Single Spoke Resonators for PXIE”, IPAC12 proceedings.
- [10] V. Lebedev et al., “PXIE Optics and Layout”, IPAC12 proceedings.
- [11] V. Scarpine et al., “Fermilab PXIE Beam Diagnostics Development and Testing at the HINS Beam Facility”, IPAC12 proceedings.

## 2. PXIE Beam Optics Design

Valeri Lebedev

### PXIE OPTICS

Measurements of ion source beam emittance resulted in the beam normalized rms emittance to be within 0.09-0.12 mm mrad for a current range 2 to 10 mA [1]. The LEBT section transports the beam to the RFQ. It includes a switching dipole and normal conducting solenoids to match the beam phase space to the RFQ. The edge focusing of switching dipole is adjusted to minimize asymmetry between its horizontal and vertical focusing. The beam space charge introduces non-linear focusing which strongly effects single particle motion and results in emittance growth. To mitigate it space charge compensation by residual gas ions will be used.

Bunching and acceleration in the RFQ was designed to minimize the beam loss and the emittance growth in the current range of 4 to 10 mA [4]. Simulations in the current range 4 to 10 mA yield the normalized rms emittances at the RFQ exit to be 0.15 mm mrad and 0.22-0.25 mm mrad for transverse and longitudinal planes, correspondingly. RFQ vanes are extended by a few centimeters to make a matcher reducing transverse beta-functions in the MEBT matching section.

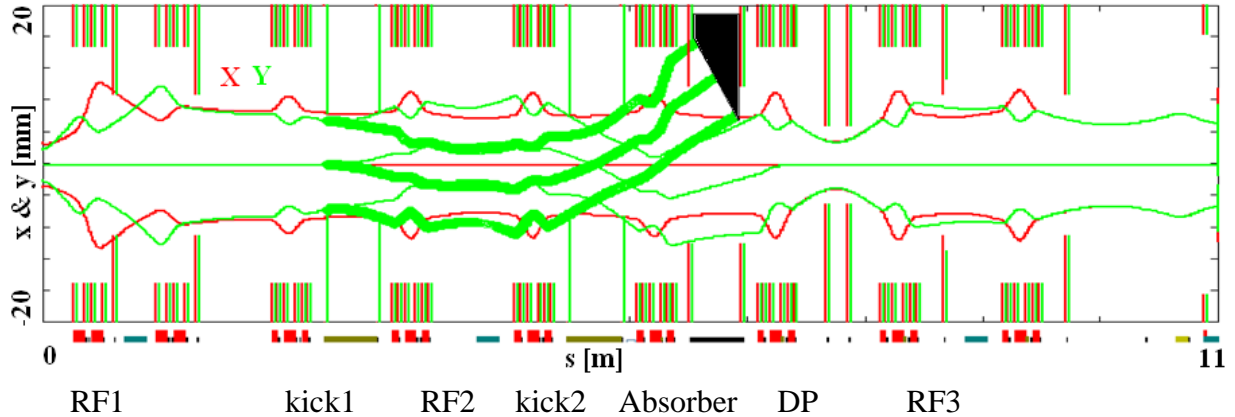
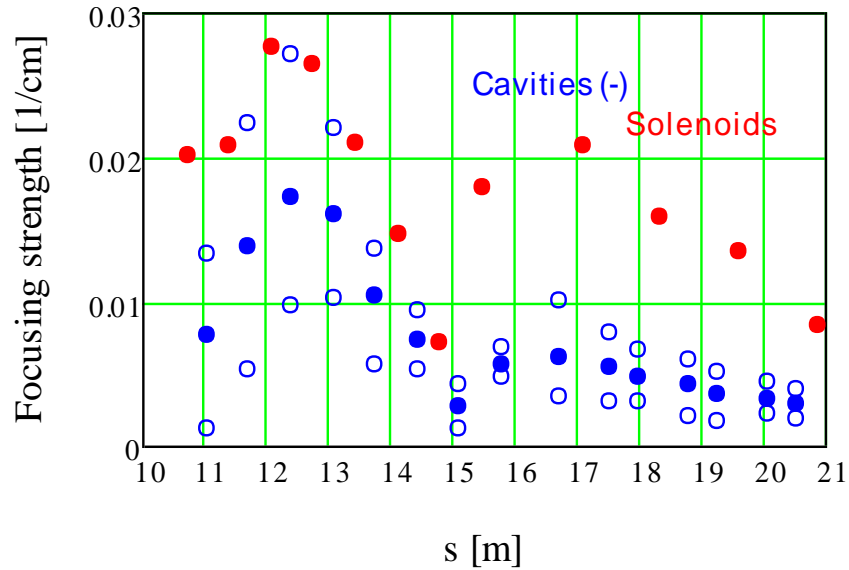


**Figure 2.1:** The  $3\sigma$  beam envelopes ( $\epsilon_{rms,n}=0.25$  mm mrad) for accepted and removed bunches through MEBT; red – horizontal plane, green – vertical plane, red and green vertical lines show aperture limitations for  $x$  and  $y$  planes.

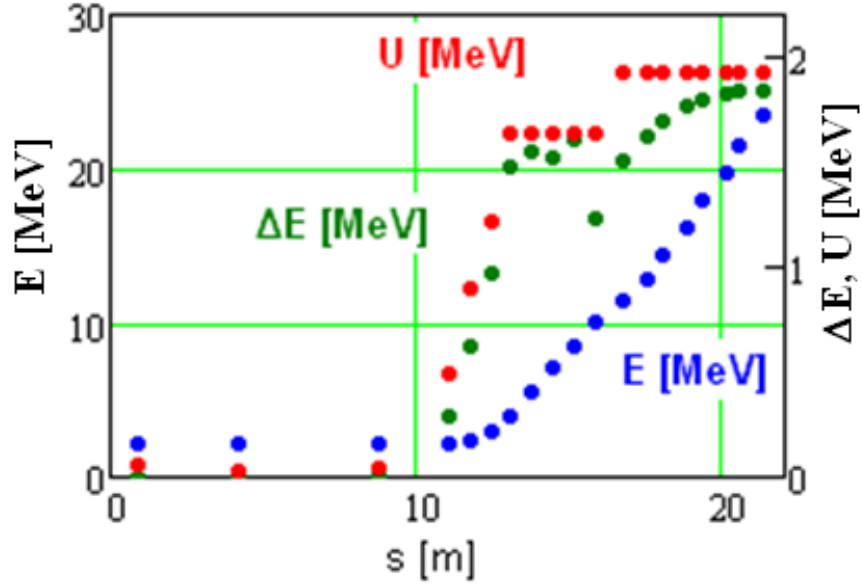
Figure 2.1 presents beam envelopes through the MEBT. Triplet focusing with  $\sim 90$  deg. phase advance per cell was chosen for the MEBT. It minimizes the beam size and creates sufficiently “smooth” focusing resulting in sufficiently small emittance growth. To obtain acceptable voltage (power) for the bunch-by-bunch MEBT kickers they are separated by 180 deg in the betatron phase. It minimizes the gap between kicker plates and the required driving voltage. Each kicker [3] has 16 mm gap with 13 mm aperture restriction, 500 mm length, and is driven differentially by two power amplifiers with  $\pm 250$  V voltage each. Bunches deflected down (see Figure 2.1) pass the beam absorber and proceed for further acceleration. Bunches deflected up (shown by

thick green line in Figure 2.1) are stopped at the beam absorber. The drift section immediately following the absorber section has a reduced aperture (10 mm) to introduce effective differential pumping required to prevent performance degradation of the SC cavities due to high gas load from the absorber. The MEBT has three 162.5 MHz normal conducting cavities to prevent beam debunching and to match the longitudinal beam envelope between RFQ and SC linac. The maximum accelerating RF voltage is 100 kV (amplitude).

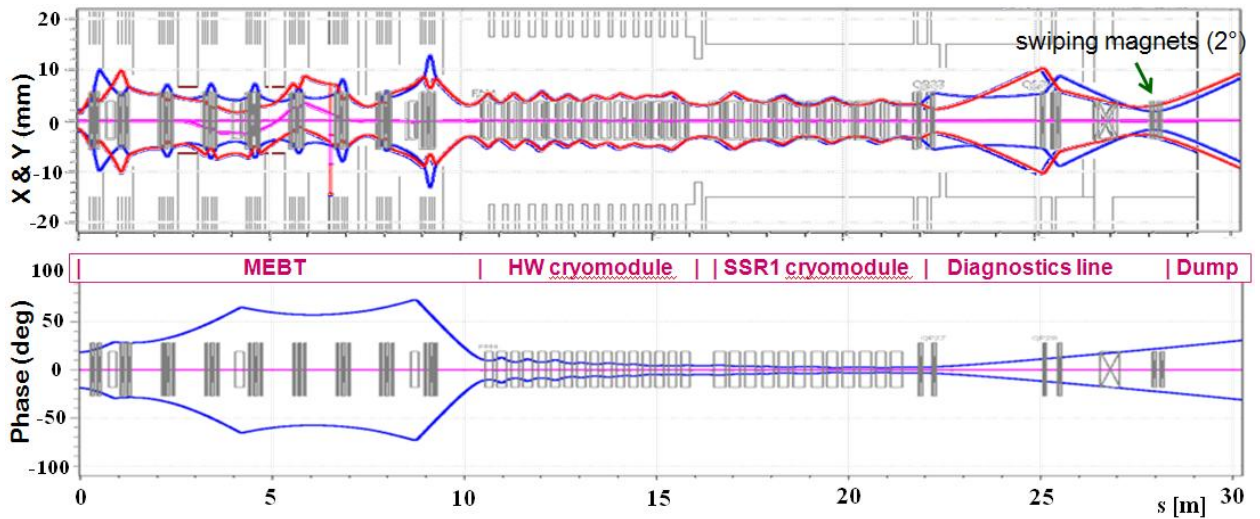
To fully exploit the high value of RF voltage delivered by SC cavities the accelerating structure has to be compact. This requirement determines the optics structure for the cryomodules. Both of them have solenoidal focusing which in the 2 to 30 MeV energy range makes more compact focusing than quadrupoles. High accelerating gradient in the first cryomodule where energy gain per cavity is comparable with the energy itself creates two problems. The first one is related to longitudinal overfocusing and the second one to transverse defocusing by electro-magnetic fields of the cavities. The transverse defocusing depends on a particle position in a bunch and therefore it requires stronger focusing than one would need for reference particle focusing (see Figure 2.2). These considerations led to the choice that an optical cell of the first cryomodule includes one cavity per solenoid. In spite of that compact focusing structure the accelerating voltage for the first three cavities of the HW cryo-module is reduced (see Figure 2.3) so that the longitudinal phase advance would not significantly exceed 90 degree.



**Figure 2.2:** Focusing strength of solenoids (red) and nearby SC cavities for the reference particle (solid blue) and  $\pm 4\sigma$  longitudinal bunch ends. Sign of the cavity focusing is changed from negative to positive.



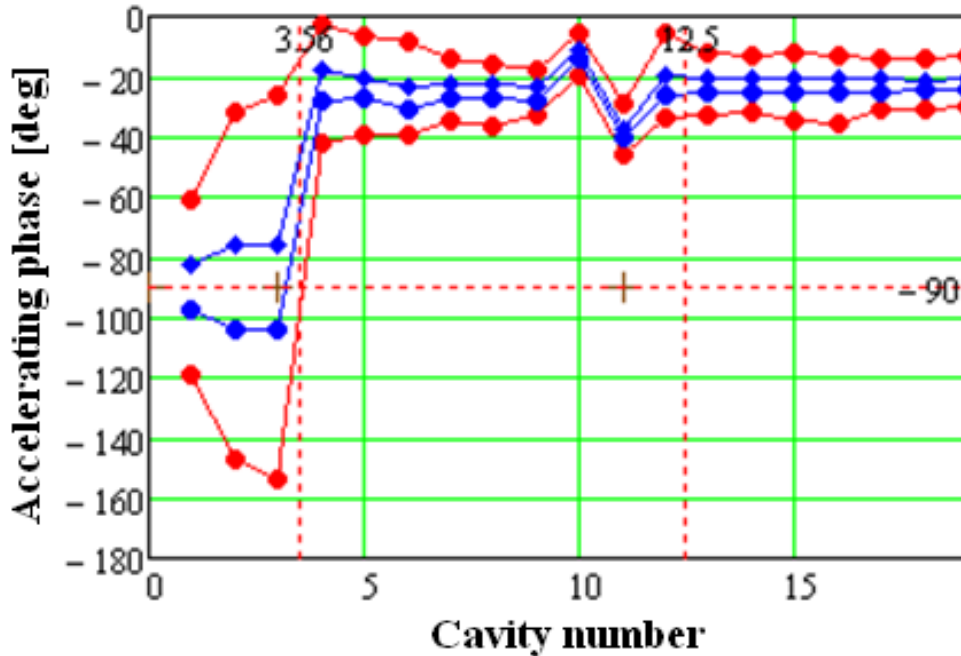
**Figure 2.3:** Dependences of beam energy (blue), cavity voltage (red) and actual beam energy change in a cavity (green) on cavity longitudinal coordinates.



**Figure 2.4:** The  $3\sigma$  bunch sizes from RFQ end to beam dump; top - blue and red lines represent horizontal and vertical planes, correspondingly; bottom -  $3\sigma$  bunch length.

Both the longitudinal overfocusing and the transverse defocusing decrease with beam energy. That allows reduction in the number of focusing solenoids in the second cryomodule where one solenoid follows after two cavities. The relative strengths of space charge effects for both transverse and longitudinal planes are about the same through the beam acceleration. However longitudinal dynamics is additionally affected by the strong non-linearity of the accelerating field focusing; therefore a diligent approach is required for the treatment of longitudinal motion. To reduce the longitudinal motion perturbation at the transition between

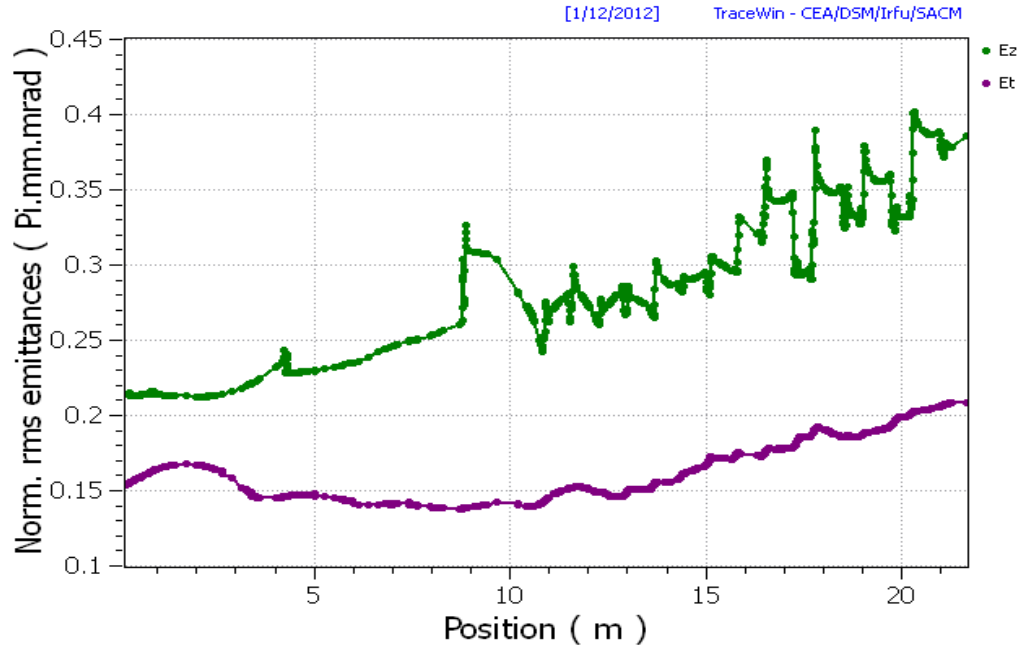
cryomodules the HW cryomodule is ended with a cavity and the SSR1 cryomodule starts from a cavity. Thus the cryomodules have the following structure: (S-C-S-C-S-C-S-C-S-C-S-C-S-C-S-C) for the HW and (C-S-CC-S-CC-S-CC-S-C) for the SSR1, where C stands for a cavity and S for a solenoid. Using a solenoid as the first element in the HW cryomodule also improves differential pumping between the beam absorber and SC cavities due to cryo-pumping of a cold vacuum chamber located in the solenoid. Its low temperature ( $2K^{\circ}$ ) results in good cryo-pumping for all gases including hydrogen. Figure 2.4 presents the bunch envelopes through PXIE (from the end of RFQ to the beam dump). Figure 2.5 shows corresponding accelerating phases and the bunch length inside RF cavities (expressed in degrees of corresponding cavity phase).



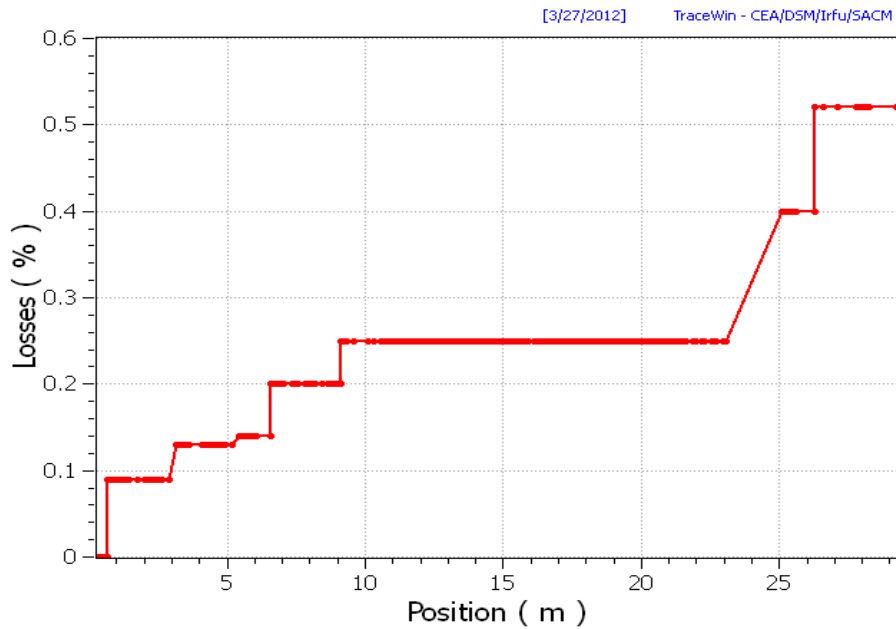
**Figure 2.5:** Accelerating phases for  $1\sigma$  and  $4\sigma$  bunch boundaries; vertical lines mark cryomodule boundaries.

Figure 2.6 presents results of simulations of the beam emittance evolution. An emittance growth for both transverse planes is moderate and is within specifications. There is significantly larger growth for the longitudinal emittance mainly related to longitudinal focusing non-linearity. The requirements on the longitudinal emittance growth in Project X are not too strict. However if necessary the emittance growth can be reduced by lowering an accelerating rate. Note also that non-linearities introduced by different cavities can be compensated by minor adjustments of accelerating phases. That presents considerable freedom for further possible improvements.

We also studied the implication of a single cavity failure on machine operation. Calculations show that machine operation remains possible with acceptable performance degradation even when the missing cavity is the lowest energy one.



**Figure 2.6:** Dependence of longitudinal (green) and transverse (red and blue) rms emittances on longitudinal coordinate from the RFQ exit to the SSR1 end for 5 mA peak beam current.



**Figure 2.7:** Integrated particle loss along PXIE.

### BEAM LOSS AND BEAM EXTINCTION

Figure 2.7 shows the particle loss integrated along the machine. There are two areas where particle loss is observed: the MEBT ( $s \leq 10$  m) and the diagnostic section ( $s \geq 22$  m). In the both areas the loss happens at the designated transverse scrapers. The particle loss from the

accelerating bucket is more than an order of magnitude smaller. It happens due to long non-Gaussian tails of the RFQ longitudinal distribution (see Figure 2.8). In contrast to the transverse tails it is close to impossible to intercept the major fraction of longitudinal tails at designated scrapers even if they are located inside the SC cryomodules. Simulations show that particles in far tails are lost extremely fast. If a particle slips out of acceleration its energy deviates significantly after passing just one cavity. Then, overfocusing in the downstream solenoid results in its loss in the next cavity. Simulations show that even if beam collimators would be installed near each solenoid they cannot intercept major fraction of longitudinal beam loss. Fortunately the RFQ tails are expected to be sufficiently small and should not yield the beam loss exceeding few watts at cryogenic surfaces.

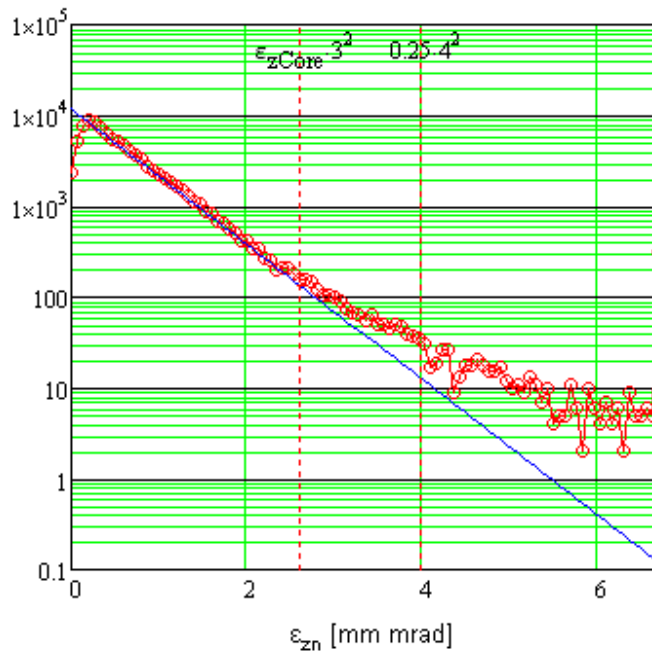


**Figure 2.8:** Particle longitudinal distribution at the end of RFQ simulated for 5 mA beam current.

Some of Project X experiments may require extremely good extinction for removed bunches. The target value is smaller than  $10^{-9}$ , *i.e.* much less than one particle per bunch. A finite population of longitudinal RFQ tails can be the main limitation for achieved beam extinction. Although there is very good rejection of the tails in the first SC cryomodule the weak longitudinal focusing in MEBT and its large length allow momentum tails of allowed bunches to move to the nearby rejected bunches and be accepted in their RF bucket. Figure 2.9 presents the phase space at the bunch chopper for particles which will be accepted for further acceleration. Lanes above and below the main bunch will be accepted in the nearby buckets. Thus, the longitudinal RFQ tails suppression is the key to achieve good extinction for removed bunches.

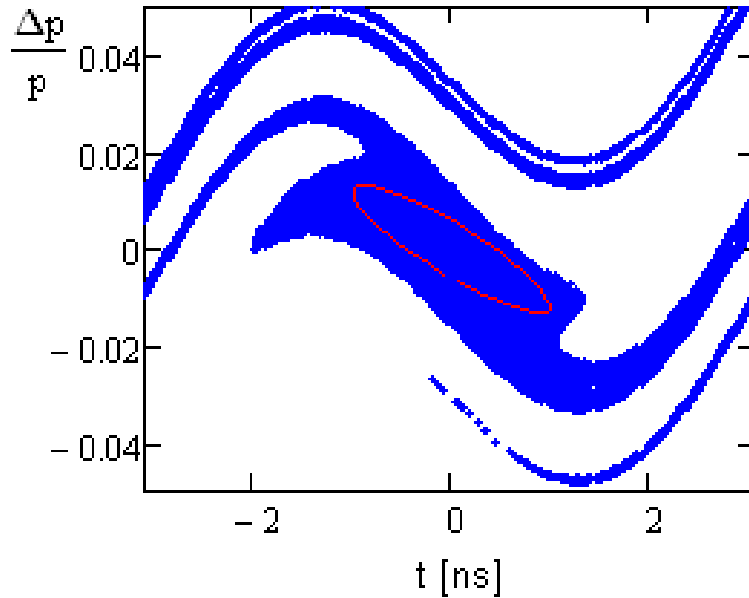


**Figure 2.9:** Longitudinal phase space at the beam chopper location for particles accepted for further acceleration (blue dots). Red line shows  $4\sigma$  bunch boundary.

### References

- [1] Q. Ji, “PXIE LEPT Concept”, <https://indico.fnal.gov/conferenceOtherViews.py?view=standard&confId=5300>, (2012).
- [2] Steve Virostek et al., “Design and Analysis of the PXIE CW Radio-frequency Quadrupole”, IPAC-12 proceedings.
- [3] V. Lebedev et al. “Progress with PXIE MEPT Chopper”, IPAC-12 proceedings.

### 3. Ion Source and Low Energy Beam Transport

Lionel Prost

#### Ion Source

The PXIE Ion Source is a DC,  $H^-$  source designed to be capable of delivering 5 mA (nominal) at 30keV to the Low Energy Beam Transport (LEBT) section. The Ion Source assembly consists of the ion source attached to a vacuum chamber body (Figure 3.1;  $H^-$  Volume-Cusp Ion Source procured from D-Pace Inc. [1]). The source can deliver up to 15 mA, which allows for a possible upgrade, where the average Linac current would be increased to 2mA (up from 1 mA for the nominal design).

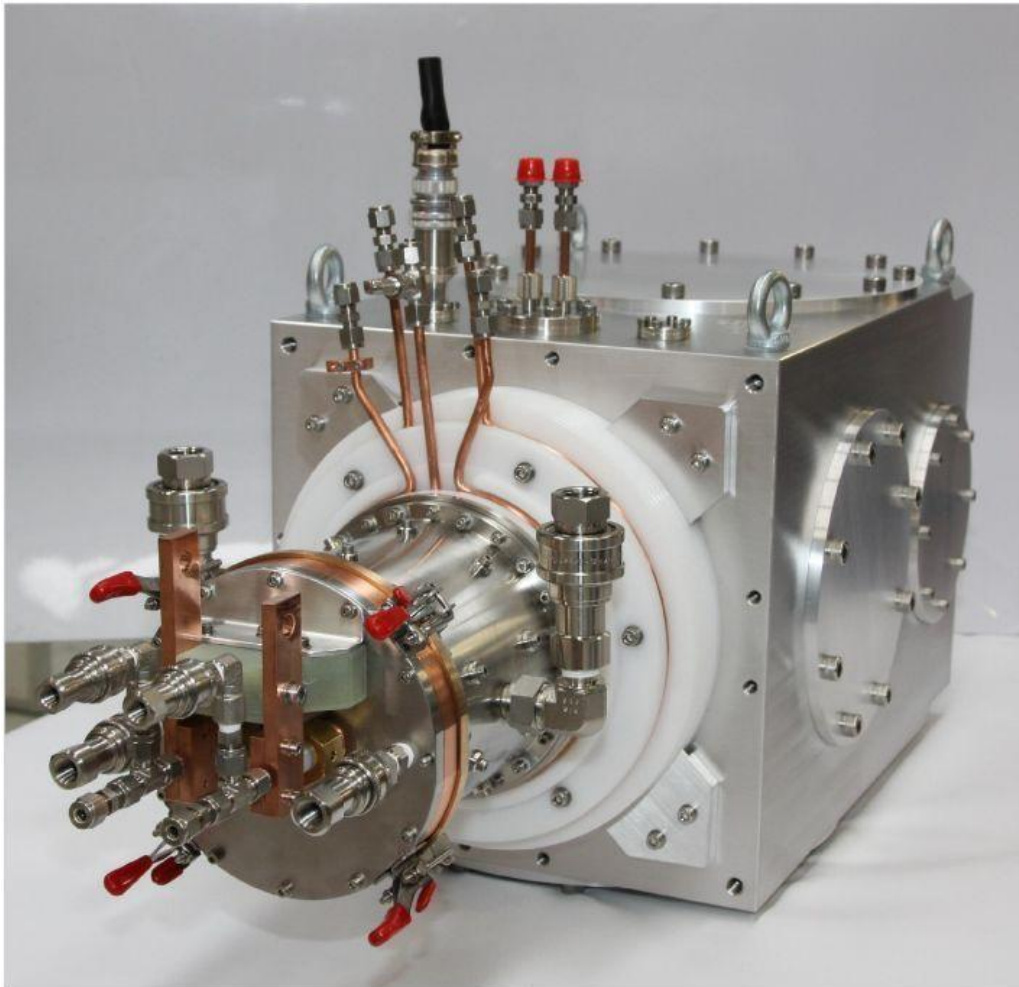


**Figure 3.1:** Photograph of the ion source with the vacuum chamber.

Table 3.1 shows the functional requirement specifications for the ion source [2]. These requirements are the same for PXIE and for Project X, although the ‘Uptime’ requirements are not critical for PXIE which is an R&D beam line and not a user facility. Nevertheless, they should be demonstrated.

**Table 3.1:** Ion Source Assembly Requirements

Beam		
	Ion type	H <sup>-</sup>
	Nominal output kinetic energy	30 keV
	Kinetic energy stability	0.5% rms
	Nominal beam current	5 mA
	Maximum beam current	10 mA
	Beam current stability [for frequencies $f > 1$ Hz (ripples)]	±5%
	Duty factor	100%
	Transverse emittance over 1-10 mA current range	< 0.2 mm mrad
	Electron beam current at LEBT input	< 100 μA
	Beam turn off time (after fault detection)	< 1ms
Uptime		
	Mean time between maintenance (beam ON time)	> 350 hours
	Pre-conditioned ion source turn-on time <sup>a</sup>	< 10 min
	Ion source replacement time <sup>b</sup> (with closed-loop control circuit)	8 hours
Vacuum		
	Gas flow to LEBT (with beam on)	≤ 4×10 <sup>-3</sup> torr l s <sup>-1</sup>

*a* - "Pre-conditioned ion source turn-on time" refers to the scenario in which, the on-line ion source fails, and the second ion source has been pre-conditioned i.e. demonstrated stable beam at nominal current - the source has then be maintained under vacuum with the gate valve closed. The operator needs to turn on the second ion source and configure the switching magnet such that the beam gets back online.

*b* - "Ion source replacement time" refers the scenario that the on-line ion source suddenly fails, but there is no pre-conditioned ion source available. The operator needs to either mount the 2nd ion source, or replace the filament of the failed source. In both cases, the system must be pumped down and the filament conditioned to the point where the closed-loop control system can provide stable beam downstream.

Acceptance measurements of the source made before its delivery showed that it meets all beam quality requirements [3] for  $2 < I_{Beam} < 10$  mA. In fact, the maximum measured emittance on a test bench was 0.12 mm·mrad at 10 mA. The uptime requirements are based on years of experience of using the same type of source at TRIUMF. For PXIE as for Project X, the ion source will be included in the machine protection and personnel safety systems. In both cases, the ion source will be inhibited to provide beam until normal conditions are restored.

It should be noted that while the PXIE design only accounts for one ion source, for Project X, two will be available. When one source will be in use, the second can be serviced and

conditioned so that there is always one source available for quick turnaround. This is especially important because of the relatively short lifetime of the source's filament, which needs to be replaced regularly. In that regards, for Project X, it would be beneficial to develop an alternate source design with much longer lifetime. The most promising technology is currently to use a RF antenna *outside* the plasma chamber to replace the current design with a filament. This approach has already been implemented for pulsed ion sources.

### **Low Energy Beam Transport**

The PXIE LEBT includes all of the beam line components necessary to transport the beam from the exit of the Ion Source assembly to the RFQ and match the optical functions to the RFQ's.

In addition, the LEBT shall:

- Serve as the primary sub-system for machine protection by preventing the beam to propagate downstream.
- Allow for pulsed beam operation during commissioning of the downstream beam line.

Table 3.2 shows the functional requirement specifications [4].

The LEBT consists of 3 solenoids, a slow switching dipole magnet, a chopper assembly (i.e. a kicker followed by a beam absorber) and various diagnostics to characterize and tune the beam. A schematic of the beam line is shown on Figure 3.2. Although it may not be exactly the final configuration, all the elements shown on the figure will be present. Note that the capability of scraping the transverse tails of the beam may also be included. In addition, while the total length of the LEBT is relatively long, longitudinal space available for each element is tight and must be taken into consideration in their designs.

For Project X, the LEBT has to accommodate two ion sources (not running concurrently) and consequently needs to include a slow switching dipole magnet. On the other hand, only one ion source is incorporated in the PXIE front-end design. Nevertheless, a switching dipole is included in the PXIE LEBT section in order to validate its design. The Project X front-end design with two sources, 60° apart, brings additional space limitations (in the horizontal direction). Again, they are not an issue for the PXIE layout, but must be taken into consideration when designing the beam line components. Issues like where to route water tubing and electrical cables may become considerable. To avoid interference between the two legs before the switching magnet, the transverse size of the components must not be ignored.

As shown on Figure 3.2, the two main beam diagnostics instruments will be an emittance scanner upstream [5] (located in the ion source vacuum chamber, before the first solenoid), a DCCT after the first solenoid and a toroid right next to the chopper. In addition, several electrically isolated diaphragms (fixed) will be installed along the beam line (most likely within the solenoids) in order to measure the beam size and its position, and to some extent beam halo. Just in front of the RFQ, there will be a movable electrically isolated 'scraper'. The scraper will serve as a beam position monitor (e.g.: segmentation in 4 quadrants) and beam size measuring

device. In addition, the default configuration for the aperture is to remain in front of the RFQ, acting as an additional protection device. In its completely inserted position, it may also serve as a beam dump.

**Table 3.2: LEBT Requirements**

Beam		
	Ion type	H <sup>-</sup>
	Input kinetic energy	30 keV
	Output kinetic energy	30 keV
	Kinetic energy stability	0.5% RMS
	Nominal beam current	5 mA
	Maximum beam current	10 mA
	Beam current stability [for frequencies $f > 1$ Hz (ripples)]	$\pm 5\%$
	Duty factor	100%
	Input transverse emittance over 1-10 mA current range	$< 0.2$ mm mrad
	Output transverse emittance over 1-10 mA current range	$< 0.25$ mm mrad
	Beam loss outside gaps (i.e. un-chopped beam)	$< 10\%$
Uptime		
	Turn-on time (after source switch e.g.: tuning)	$< 2$ hours
Chopper		
	Extinction ratio	$10^{-4}$
	Rise/fall time (10% - 90%)	$< 100$ nsec
	Single pulse length ( $> 90\%$ of maximum intensity)	1 $\mu$ sec - DC
	Maximum pulsing frequency <sup>#</sup>	1 MHz <sup>E</sup>
Machine protection		
	Beam shut-off time <sup>†</sup>	$< 1$ $\mu$ s
	Beam stop insertion time (after fault detection)	$< 1$ sec
Vacuum		
	Max. Pressure	$\leq 10^{-6}$ torr
	Gas flow to RFQ (beam on)	$< 2 \times 10^{-3}$ torr l s <sup>-1</sup>

<sup>#</sup> 1 to 100  $\mu$ sec beam pulses at 10-60 Hz will be used for commissioning, troubleshooting and machine tuning

<sup>E</sup> If 'pre-chopping' becomes necessary for realizing the required bunch patterns downstream

<sup>†</sup> This is the time it takes for the beam to be diverted onto the absorber with the chopper kicker once a fault is detected

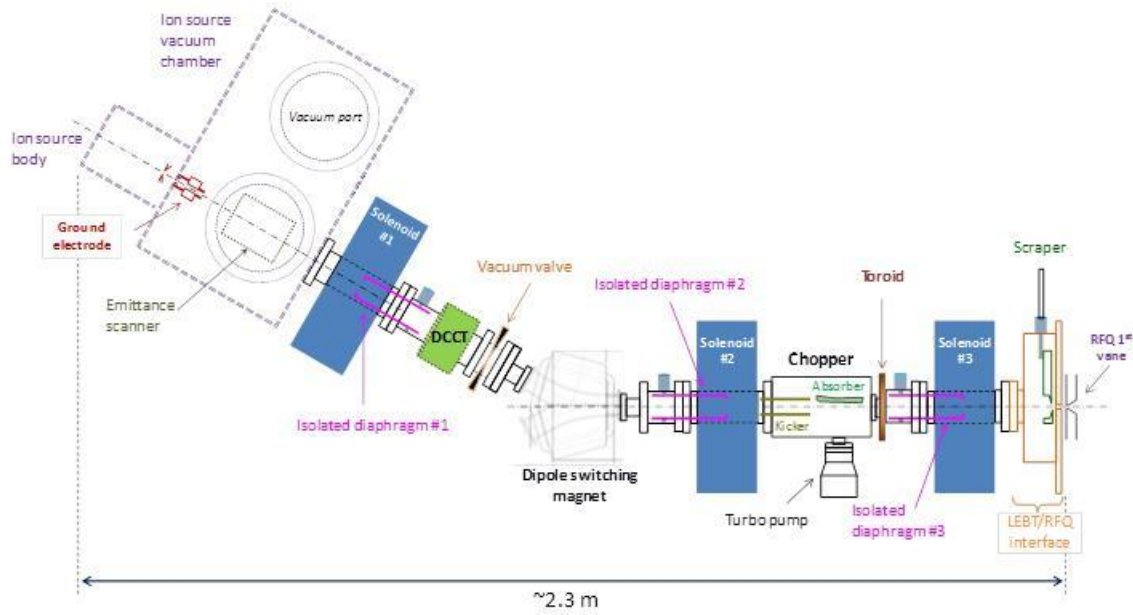


**Figure 3.2:** Main components of the LEBT.

Machine protection and pulsed beam operation are achieved via the chopper assembly that comprises a kicker followed by an absorber. For machine protection, the beam is diverted onto the absorber with the chopper kicker when a fault is detected. This is the fastest way to interrupt the beam. Similarly, beam pulses for machine tuning are obtained by power cycling the chopper kicker, alternatively diverting the beam onto the absorber or letting the beam pass. Note that the final time structure of the beam is realized in the Medium Energy Beam Transport (MEBT) [6]. However, provision shall be made for the chopper assembly, in particular the kicker, to be capable of delivering high frequency beam pulses hence providing an additional stage for the realization of the appropriate bunch pattern downstream.

A 3-solenoid transport scheme has been adopted for PXIE. The baseline optics design [7] (Figure 3.3) incorporates two regions: the beam is considered to be fully neutralized as it exits the ion source assembly; further downstream and to the RFQ entrance, the beam dynamics is space charge dominated (and completely un-neutralized in the calculations). The transition region occurs shortly upstream of the chopper kicker and is applied in one step in the code.

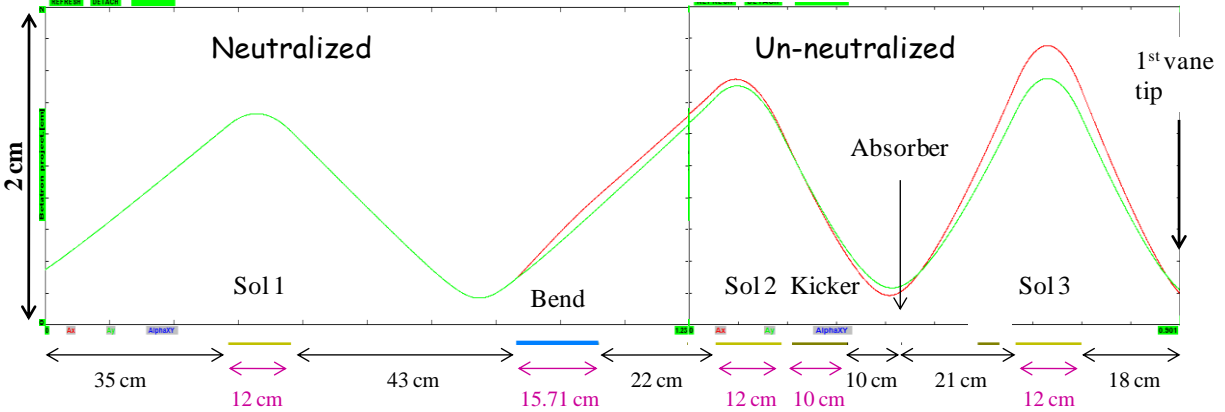


**Figure 3.3:** Optics simulation of the LEBT for 10 mA, 30 keV beam (with OptiM). Red: horizontal (x) envelope; Green: vertical (y) envelope. The plotted envelopes are 2 rms.

Choosing a scheme with a long LEBT which includes 3 focusing solenoids and a bending magnet and, with a significant part of the beam transport being space charge dominated is not quite conventional. The bending dipole magnet allows switching the beam between ion sources, which ensures a high availability of the front-end given the ion source relatively short lifetime. The choice of implementing un-neutralized transport over a significant portion of the LEBT arises mainly from the commissioning scheme of the downstream beam line, which will be accomplished with a pulsed beam (generated via the LEBT chopper). Hence, because the nominal beam in the PXIE LEBT runs dc, the beam envelopes during commissioning and normal operation would differ significantly - this is illustrated on Figure 3.4, which shows the beam envelopes for the beam current beam line design with and without space charge. It is not the case for pulsed beam machines. Thus, designing the LEBT with an un-neutralized transport section for normal operation, i.e. continuous beam, should render the transition from the commissioning optics solution to the nominal optics solution more straightforward.

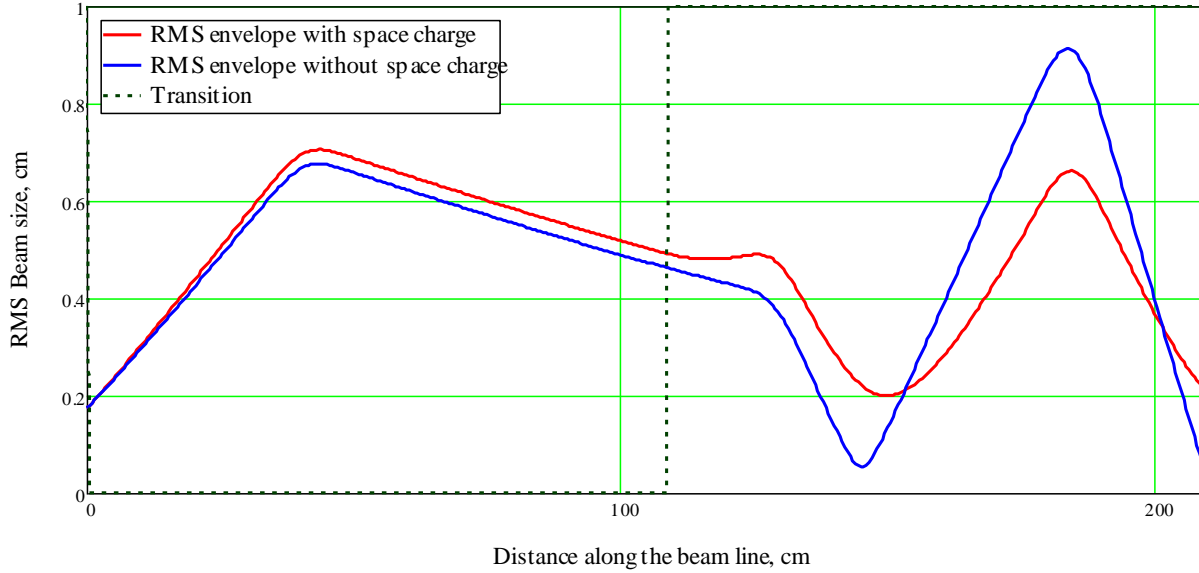


**Figure 3.4:** Beam envelopes (rms) in the LEBT with and without space charge for 5 mA, 30 keV beam (with PIC-like code written in MathCAD). The  $\beta$ -functions for the un-neutralized case nearly match those specified at the entrance of the RFQ.

Moreover, traditional designs usually have a very short distance between the chopper and the entrance of the RFQ to avoid re-neutralization and consequently transition effects. Removing the neutralization of the beam by design ahead of the RFQ might alleviate the transitional effect of going from an almost fully neutralized beam to a completely uncompensated beam. Although the beam current in PXIE is smaller than for most machines by a factor of 5 to 10 the smaller beam emittance and LEBT low energy result in approximately the same space charge field strength as in the SNS. However numerical simulations show that the un-neutralized beam transport over the length of the space charge dominated region may not result in unacceptable emittance growth (Figure 3.5 and 3.6). It is also conceivable to implement some slight scraping to diminish the amount of tail particles that form and would propagate downstream (see Figure 3.6).

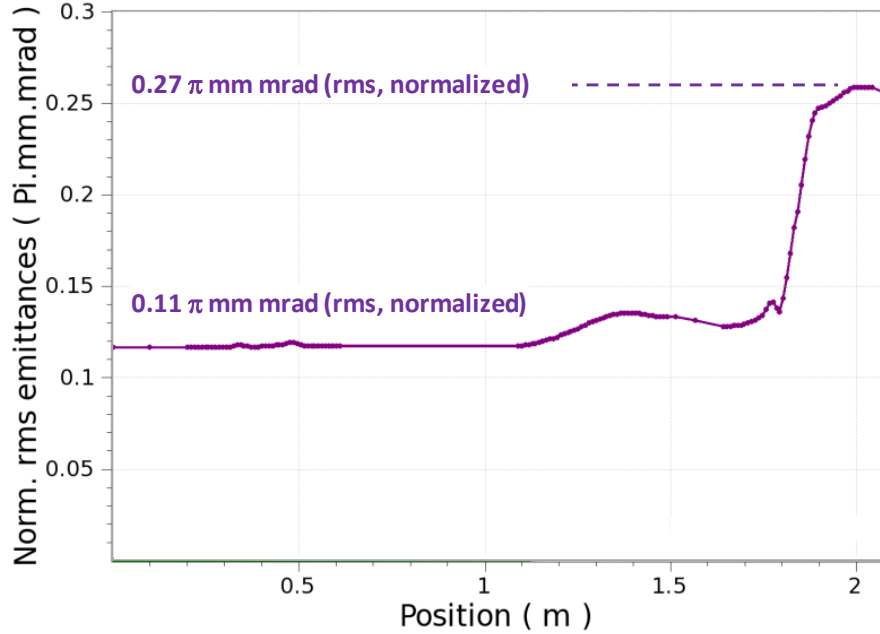


**Figure 3.5:** Emittance evolution along the PXIE LEBT for a 5 mA, 30 keV (with Tracewin). The start of the emittance growth shows where the transition between the neutralized and un-neutralized beam transport occurs.

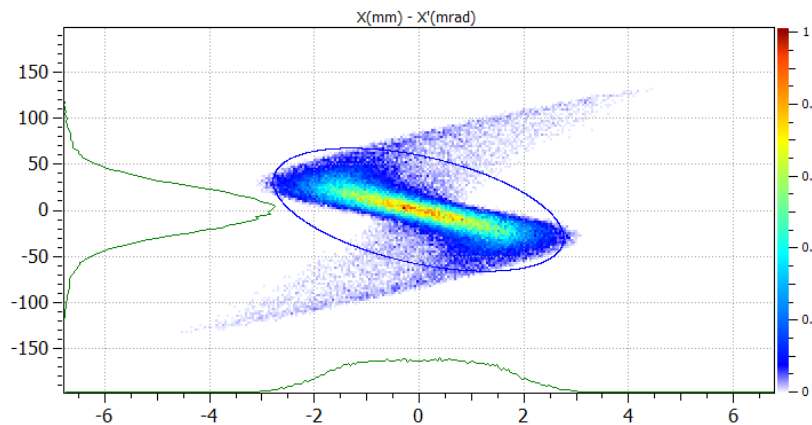


**Figure 3.6:** Phase space distribution ( $x-x'$ ) at the entrance of the RFQ (with Tracewin). The initial distribution was Gaussian.

Therefore a study of the differences between dc and pulsed beam transport has to be carried out before the RFQ commissioning can start. The goals of the study are to characterize the beam stability in the beam-plasma system, the phase space dilution due to space charge and the dynamics of beam neutralization. After completion of these studies the space charge dominated

transport scheme might or might not be chosen for Project X. Note that from an optics point of view, the lattice is not incompatible with a fully neutralized transport (DC operation, Figure 3.7). In this case the scraper located in front of the RFQ can serve as trapping electrode to prevent the effect of the RFQ fields on the beam neutralization. If required an additional trapping electrode can also be installed.

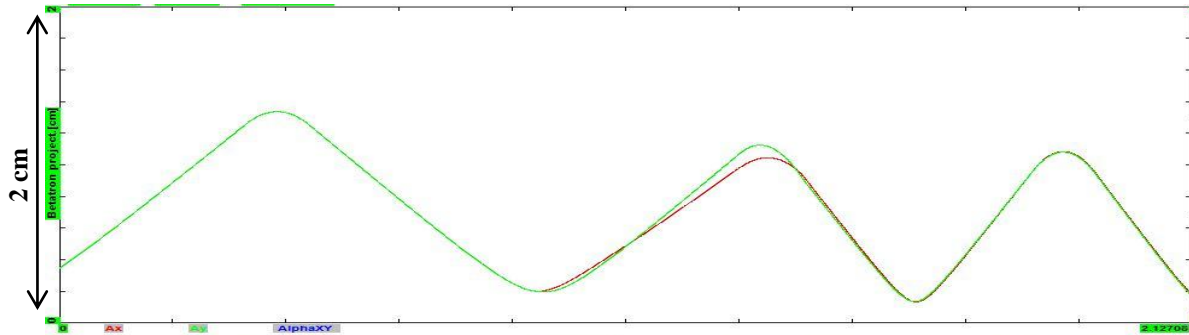


**Figure 3.7:** Optics simulation of the LEBT with neutralized transport only (with OptiM). All optical elements are identical to those on Figure 3.3. Only the magnetic field values were adjusted.

Additionally, a downside of the present SNS LEBT configuration is that it is not possible to have any sort of diagnostics for the beam entering the RFQ. The longer LEBT proposed for PXIE allows the implementation of additional diagnostics, in particular after the chopper. Purposely limiting neutralization and devising space charge dominated optics downstream of the kicker allows installing diagnostics before the RFQ entrance, hence leading to a better control of the beam entering it. Also, it helps to identify potential issues appearing during operations faster, and consequently, provides better machine availability. Thus, having proper diagnostics in the LEBT becomes a must.

## References

- [1] <http://www.dehnel.com/index.html>
- [2] L. Prost et al., “Project X and PXIE Ion Source Functional Requirement Specifications as of time of PXIE review”, Project X Document 968
- [3] Q. Ji, J. Staples, “Project X H<sup>-</sup> Ion Source Acceptance Test and Future Plan”, Project X Document 897
- [4] L. Prost et al., “Project X LEBT: Functional Requirement Specifications”, Project X Document 912
- [5] V. E. Scarpine, “PXIE LEBT Beam Transverse Emittance Station FRS”, Project X Document 1077
- [6] A. Shemyakin, “PXIE Design Handbook” (*this document*) Section 6
- [7] OptiM input files can be found at <http://www-bdnew.fnal.gov/PXIE/Optics/index.htm>

## 4. Radio-Frequency Quadrupole

Steve Virostek and Derun Li

### Introduction

The PXIE RFQ design is a 162.5 MHz, 4.45 m long, four-vane CW structure of four longitudinal modules that will accelerate a 5 mA  $H^-$  beam from 30 keV to 2.1 MeV using a 60 kV vane-to-vane voltage. Most of the RF input power is dissipated on the cavity walls to establish the needed RF field with only about 12% beam loading. Each of the approximately 1.1 m long RFQ modules will consist of four solid OFHC copper vanes that are modulated prior to being brazed together. A brazed copper structure has been chosen due to the high power CW operation. A series of 32 water-cooled pi-mode rods provides quadrupole mode stabilization, and a set of 80 evenly spaced fixed slug tuners is used for final frequency adjustment and local field perturbation correction.

The PXIE RFQ design incorporates selected portions of the technology validated by the Spallation Neutron Source (SNS) Front End RFQ [2] designed and constructed at LBNL. By combining specific proven fabrication and assembly methods with the use of other appropriate high reliability, low cost features, LBNL has developed a design that poses low risk and is easily manufactured using readily available machinery. Images from a 3-D CAD model of the completed RFQ design are used here to present detailed descriptions of various design characteristics. An overall view of the full four-module RFQ is shown in Fig. 4.1.

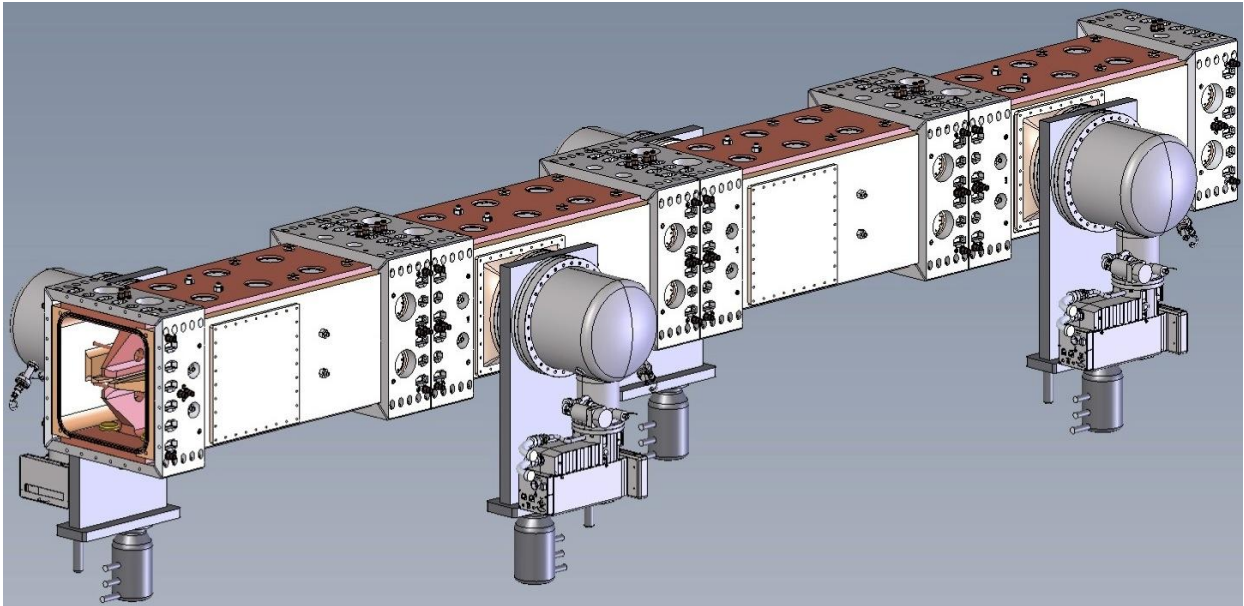


**Figure 4.1:** CAD model of the full four-module RFQ.

## Beam Dynamics Design

The beam dynamics design of PXIE RFQ is optimized using the measured beam distribution from the H<sup>-</sup> ion source. The design has over 96% transmission for beam current from 1 to 15-mA. At 5-mA nominal current, 99.8% beam capture is achieved with output transverse and longitudinal emittances of  $0.15\text{-}\pi\text{-mm-mrad}$  and  $0.64\text{-keV-nsec}$ , respectively. The beam dynamics design was conducted using PARMTEQM; Figure 4.2 shows the simulation results at 5-mA. Error analyses have been completed; the analyses indicate that the RFQ design tolerates very well with mechanical, TWISS parameters and field errors. A comparatively low value of the beam input energy reduced the length of adiabatic beam buncher and, consequently, the total RFQ length and required beam power.

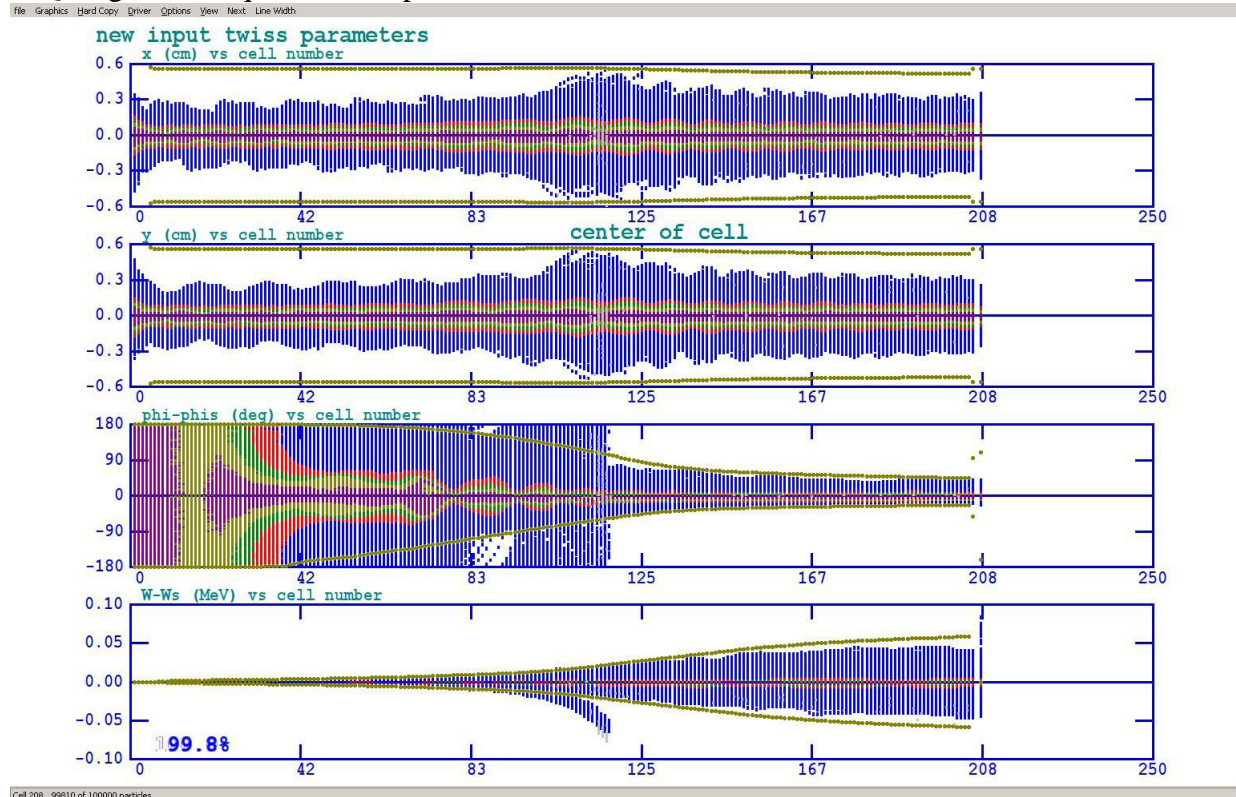


**Figure 4.2:** PARMTEQ simulations of the RFQ at 5-mA

## RF Design Studies

The RF design studies have been conducted through a close collaboration with Fermilab, detailed EM simulation studies can be found in [1]. These studies include mode stabilization (schemes), the field flatness due to  $\pi$ -mode stabilization rods, radial matcher, entrance and exit terminations (cut-backs). Table 4.1 summarizes the RF design results.

**Table 4.1:** Main parameters of the PXIE RFQ EM design

<b>Parameters</b>	<b>RFQ</b>
Frequency, MHz	162.493
Frequency of dipole mode, MHz	181.99
Q factor	14660
Q factor drop due to everything, %	-14.7
Power loss per cut-back, W (In/Out)	336/389
Max power density at cut-back, W/cm <sup>2</sup>	~ 7.9
Total power loss, kW	73.8

### RFQ Mechanical Design Details

Each of the four vanes in a module are to be machined from a single piece of copper and will include simple cooling channels produced using an established gun boring technique. The RFQ vane tips are to be modulated by means of a fly cutter technique previously developed at LBNL using a programmable mill. Fiducial surfaces that also act as mating surfaces will be machined directly onto the vanes to provide high precision during both machining and assembly. Two vane geometries will be used (horizontal and vertical) with the opposing vanes being identical. Other features such as tuner ports, RF coupling ports, vane cut backs, cooling passage taps, vacuum pumping ports, pi-mode rod penetrations, sensing loop ports and tapped holes for the stainless steel joint plates are to be machined prior to finish machining of the cavity surfaces and vane tips. An exploded view of a single four-vane module and a cross section view of the RFQ body showing the cooling passage locations are provided in Fig. 4.3.

The finished vanes are to be brazed together along axially running joints. A zero-thickness brazing process will be used in order to maintain the tight vane tip-to-vane tip tolerance, which is dictated by the high dependence of cavity frequency on vane tip spacing. Wire braze alloy will be loaded into grooves in the joint surfaces such that the alloy spreads throughout the joint during the braze cycle by means of capillary action. This technique permits the RFQ modules to be assembled and the cavity frequency measured prior to the braze cycle to allow for dimensional adjustments, if necessary.

A series of stainless steel joint plates are to be bolted to the outer RFQ surfaces at the ends of each module. These plates contain embedded bolt pockets to allow joining of the modules. No special alignment fixtures or procedures will be required to join the RFQ modules together as the ends are designed to be self-aligning by means of embedded dowel pins. The bolted end connections are sufficiently strong and stiff such that the fully assembled RFQ can be lifted and handled as a single unit. This characteristic also allows the RFQ body to be supported using a simple kinematic (or 6-strut) system that will not impart any direct bending stresses on the assembled RFQ. The joint plate concept is shown in Fig. 4.4.

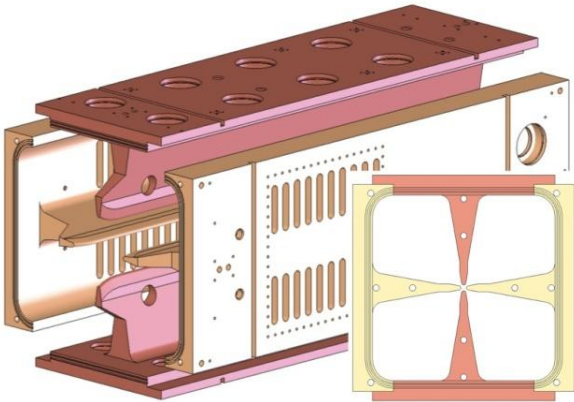


**Figure 4.3:** Exploded 4-vane module; RFQ cross-section.

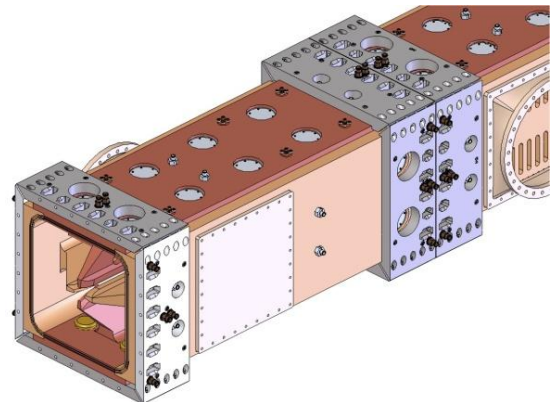


**Figure 4.4:** RFQ modules connected by joint plate method.

A set of 8 cooling passages in the RFQ cavity walls are to be fed and controlled separately from the 4 channels embedded in the vanes. During operation, a combination of RF power dissipated in the cavity walls and heat removal through the cooling passages will cause the cavity to expand and shift in frequency. Continuous differential control of the cavity vane and wall water temperatures provides a fine-tuning of the structure frequency during operation. Since the cavity frequency is very dependent on vane tip spacing, separate temperature control of the vane water provides up to six times the frequency range of an isothermal control circuit.

The passages are to be gun drilled from one end of the vanes with e-beam plug welds at the end penetrations. Each 12 mm diameter passage will carry approximately 16 liters per minute of cooling water. At the beginning of the first module and at the end of the fourth module, there will be vane cutbacks for proper termination of the RF cavity. The vane cooling passages will run close to the root of the cutbacks in order to accommodate the high local heat loads at the ends. A section view of a Module 1 horizontal vane is provided in Fig. 4.5 showing the geometry of the central cooling passages.

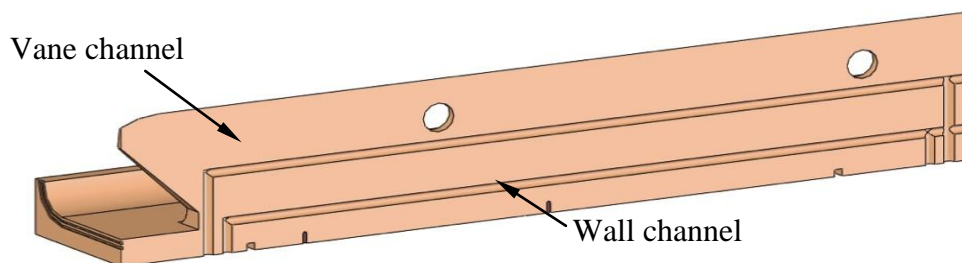


**Figure 4.5:** Section view of Module 1 horizontal vane.

Cavity tuning will be achieved with fixed slug tuners distributed along the length of the modules. The design uses 20 tuners per RFQ module (1 per quadrant at 5 evenly distributed locations). Based on bead pull field measurements of the assembled RFQ, each set of four tuners at a given axial location will be custom machined to predetermined lengths. Primary RF sealing will be accomplished by a step in the tuner flange surface that interfaces with the RFQ wall. Behind the step, an RF coil spring will protect the O-ring, also located on the tuner flange. Load plates using setscrews will be held in place by a snap rings recessed in the copper vane wall and will provide the necessary sealing load. The tuners are to be machined from solid slugs of copper. CAD images of the tuner design are provided in Fig. 4.6.

A series of Pi-mode stabilizer rods (4 pairs per module) will be incorporated to provide RF mode stabilization (to separate the dipole mode and symmetrize the quadrupole mode). The rods will pass through the vanes and provide a direct connection between opposing cavity walls. The rods will be brazed into the cavity walls at the same time that the four vanes are brazed together. The rods will be 10 mm diameter hollow copper tubes with active water-cooling. Details of the rod geometry are shown in Fig. 4.7.

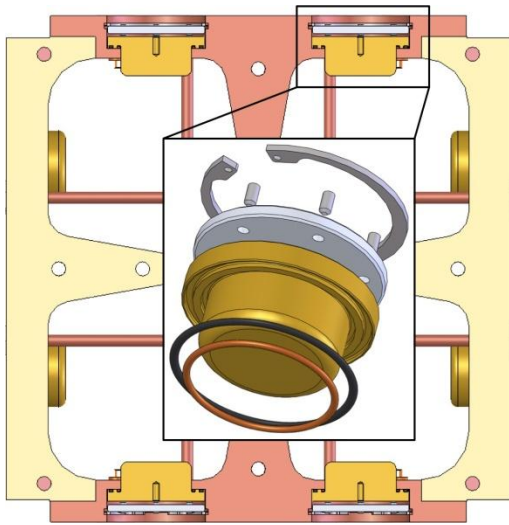


**Figure 4.6:** Fixed slug tuner details.

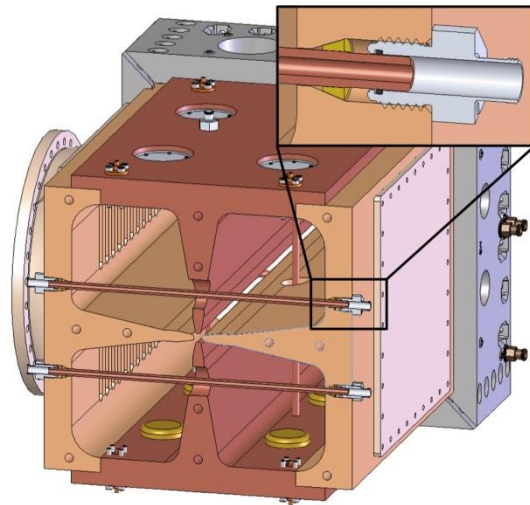


**Figure 4.7:** Pi-mode rod details.

The primary module-to-module RF connection will consist of a 3 mm wide, 250  $\mu\text{m}$  high raised surface machined into the module ends around the periphery of the cavity. This sealing surface is to be backed up by a canted coil spring, which will absorb any RF that leaks past the primary seal. Outside of the canted spring is an O-ring, which provides the vacuum seal. The modules are bolted together at these joints as previously described.

## Thermal Analysis

A series of RF and thermal finite-element models of the RFQ have been developed using ANSYS®[3]. The primary model consists of a one quadrant, 1 mm thick 3-D slice of the RFQ cross section. The thermal loads and constraints applied to the model include cavity wall heat flux from the RF, convective heat transfer on the cooling passage surfaces and symmetry boundary conditions. Examples of the temperature contour plots for the cavity body and vane cutback region are shown in Fig. 4.8.

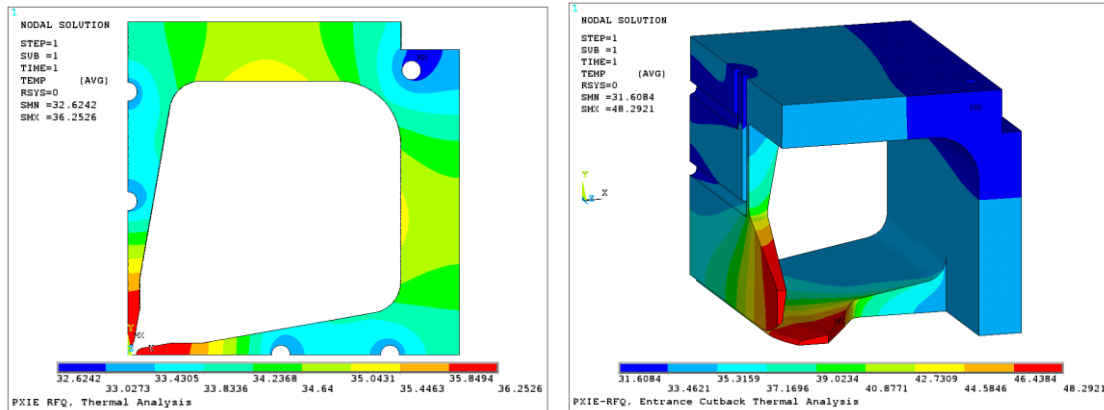


**Figure 4.8:** Temperature distribution in one RFQ quadrant: cavity body (left) and vane cutback (right).

From the RF analysis, the average linear power density was determined to be 137 W/cm with a peak heat flux on the cavity wall of only 0.7 W/cm<sup>2</sup>. With 30°C water in the vane and wall cooling passages, the resulting temperature profile in the cavity body ranges between 32 and 37°C at full RF gradient.

Additional modeling that has been carried out includes stress and displacement analyses, thermal analyses of the tuners, pi-mode rods and vane cutbacks, and prediction of the frequency shift of the RFQ cavity due to thermal loading and changes in the cooling water temperature.

The RFQ cooling scheme will use differential water temperature control in the vane and wall passages. This technique provides active tuning of the RFQ by holding the wall water temperature constant and adjusting the vane water temperature up and down. The frequency of the RFQ can be shifted by -16.7 kHz for every 1°C rise in the vane cooling water temperature. For uniform water temperature control, the shift would only be -2.8 kHz/°C.

## References

- [1] G. Romanov, et al., “Project X RFQ EM Design”, Proceedings of IPAC-2012
- [2] A. Ratti, et al, “The Design of a High Current, High Duty Factor RFQ for the SNS,” EPAC '00, Vienna, Austria, pp. 495-497.
- [3] ANSYS, Inc. (<http://www.ansys.com>).

## 5. Medium Energy Beam Transport

Alexander Shemyakin

### Introduction

To make the Project X a versatile multi-user facility, the bunch structure of the beam coming out of the linac should satisfy needs of each experiment quasi – simultaneously (see Sec. 1). A proper selection of bunches from the CW train will be made in the MEBT, the ~10m section between RFQ and HWR cryomodule. The heart of the MEBT is the wideband chopping system that directs unneeded bunches to an absorber according to a pre-selected pattern and sends the bunches to be accelerated into the SRF linac with minimum distortions. Beam chopping in MEBT is used in other facilities (e.g. SNS [1]), but the concept of bunch-by-bunch selection results in significantly more demanding requirements to the chopping system. Demonstration of this scheme at PXIE will be an important step toward establishing the feasibility of the Project X concept.

In addition, MEBT should provide proper optical matching between the RFQ and the SRF cryomodules, include tools to measure the properties of the beam coming out of the RFQ and transported to the SRF cavities, and have means of protecting the SRF section from excessive beam loss.

### Functional specifications

The MEBT allows for bunch-by-bunch selection, normally chopping out ~80% of the bunches with a wideband chopper. The main requirements [2] are summarized in Table 5.1.

**Table 5.1** Main MEBT functional requirements

Beam line height from the floor	1.3m
Ion type	H <sup>-</sup>
Input beam energy	2.1 (+/-1% ) MeV
Nominal output energy (kinetic)	2.1 (+/- 1%) MeV
Maximum frequency of bunches	162.5 MHz
Nominal input beam current	5 mA
Beam current operating range	1- 10 mA
Nominal output beam current	1 mA
Nominal charge per bunch	30 pC
Relative residual charge of removed bunches	$< 10^{-4}$
Beam loss of pass through bunches	$< 5\%$
Nominal transverse emittance (n, rms)	0.27 mm mrad
Nominal longitudinal emittance (rms)	0.8 eV- $\mu$ s
Longitudinal emittance tolerance	$<10\%$ increase over input
Transverse emittance tolerance	$<10\%$ increase over input
Beam displacement at exit	$< +/- 0.5\text{mm}$
Beam angle at exit	$< 0.5$ mrad
Scraping to trans. emittance (pulsed mode @10W avg beam power)	$<0.05$ mm mrad (n, rms)

All these requirements are identical to that of the present Project X scenario.

### MEBT scheme

Transverse focusing in the MEBT is provided mainly by equidistantly placed quadrupole triplets; the only exception is two doublets matching the beam at the RFQ exit to the triplet focusing of MEBT (see Fig. 5.1 and the optics description in Section 2). This creates a lattice

structure of MEBT. Below in this Section the spaces between neighboring triplets or doublets are referred as MEBT sections. The sections are presented in Fig. 5.1 by rectangles with their color corresponding to the main function of a section, and the arrows show pictorially the focusing elements. The period in the regular part is 1140 mm, which leaves 650 mm (flange-to-flange) space for equipment (350 mm in the section between doublets labeled #0 in Fig. 5.1).

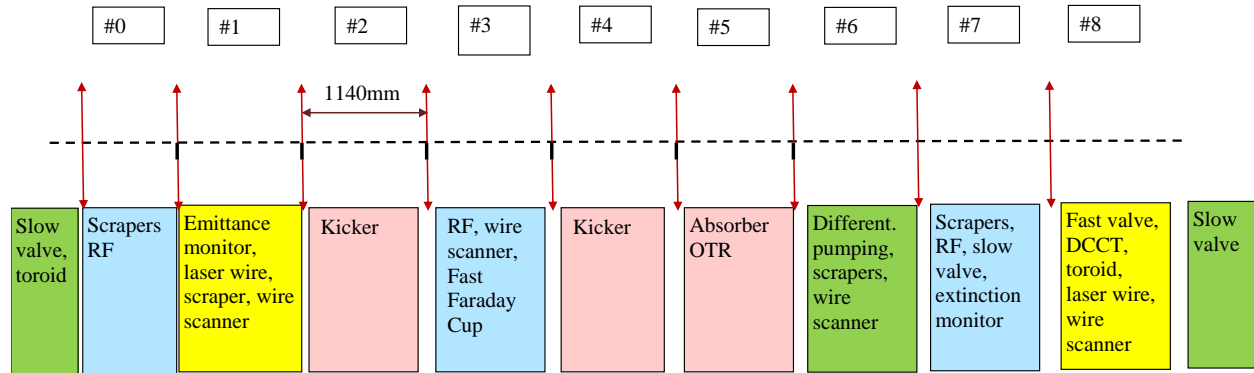


**Figure 5.1:** MEBT structure.

The red rectangles represent sections of the chopping system, which consists of two identical kickers separated by  $180^\circ$  transverse phase advance and an absorber ( $90^\circ$  from the last kicker).

The main function of the blue-colored sections is to provide longitudinal focusing by bunching rf cavities. In addition, they include other equipment, for example, scrapers and diagnostics.

Two sections marked in yellow are designated mainly for diagnostics. The section #1 provides the information about properties of the beam coming out of RFQ, and the section #8 (in combination with instrumentation in the upstream sections) characterizes the beam supplied to the SRF linac.

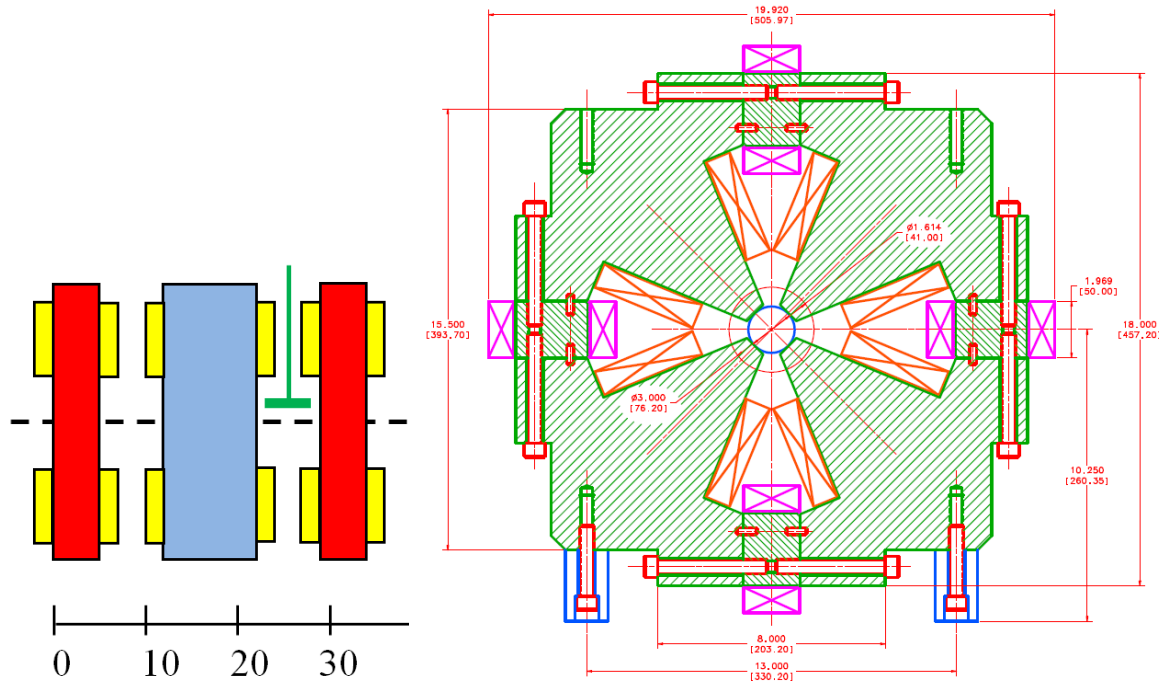
Green coloring means that the section design is determined by vacuum requirements. Two boundary rectangles correspond to interfaces of MEBT with the RFQ (left) and HWR cryomodule (right). The section #6 separates  $\sim 10^{-9}$  Torr vacuum in the last sections of MEBT from the absorber section (#5), where a large gas flow from the absorber surface will result in pressure  $\sim 10^{-6}$  Torr. This is achieved by inserting a vacuum restriction in the form of a 10 mm ID, 200 mm- long vacuum tube.

Fig. 5.1 also indicates location of scrapers. Each of sections #0, 1, 6, and 7 contains a set of 4 movable scrapers that are used for scraping of the transverse beam tails as well as a part of the protection system, indicating undesirable changes in the beam position and envelope.

## MEBT subsystems

### *Transverse focusing*

The triplets and doublets providing transverse focusing in the MEBT are formed by two types of quadrupoles: with 10-cm effective magnetic length (called type F quads) and 6-cm (D-type). Specifications for the quads are in Ref. [3], and the conceptual design is shown in Fig.5.2.



**Figure 5.2:** Pictorial view of the triplet (left) and the conceptual design of the F-type quadrupole (Vl. Kashikhin, A. Makarov).

The triplet consists of one F-type and two D-type quadrupoles, and the doublet has two F-type. F-type quadrupoles include dipole coils to steer the beam. The quadrupoles are designed for a 1.25" OD vacuum tube.

### *Kicker*

The undesired beam bunches will be removed in the MEBT by a chopping system consisting from two identical kickers and an absorber. In the broadband, travelling-wave kicker, the transverse electric field propagates through its structure with velocity equal to the speed of H<sup>+</sup> ions (~ 20 mm/ns) so that to make vertical kick sufficient to displace the bunches designated to be removed to the absorber. The specifications for the kicker can be found in Ref. [4]. Because of critical importance of the kicker performance, presently two versions of the kicker are being investigated [5].

The first version has 50 Ohm characteristic impedance of the kicker structure and deflects the beam by voltage applied between planar electrodes connected in vacuum by coaxial cables with the length providing necessary delays, similar to the design used at LAMPF [6]. The 50cm-long structure (Fig. 5.3) has 25 copper plates of 14.6 mm length (along the beam trajectory), 50mm width and 1 mm thickness. The total power loss in the electrodes induced by the electromagnetic signal is expected to be ~50 W per structure, and the structure is required to withstand additional 40 W of the beam loss. Cooling of the Teflon-insulated cables is provided by clamps, which, in turn, are cooled by water flowing through the channels in the structure base.

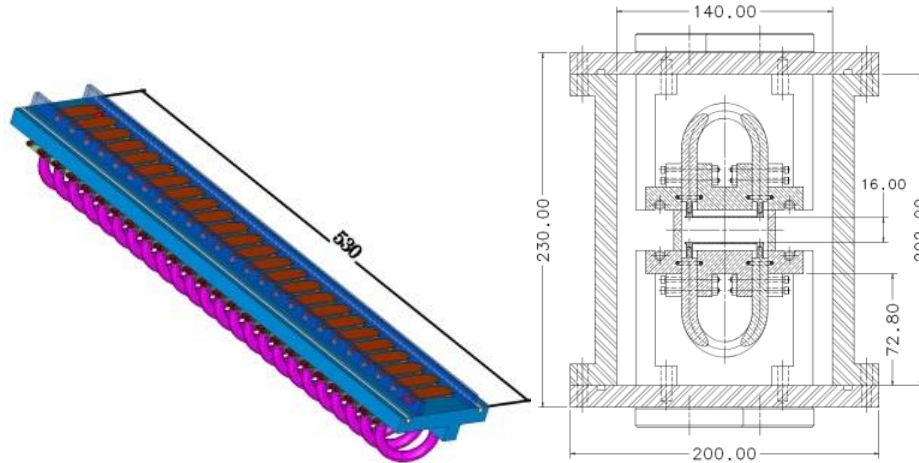


**Figure 5.3:** Mechanical schematic of the 50-Ohm kicker structure and the cross section of the kicker assembly (D. Sun, V. Lebedev, A.Chen, M.Jones).

The 50-Ohm kicker is driven by a commercially available linear amplifier. To compensate for a low frequency phase distortion in the amplifier, its driving signal is formed by an arbitrary waveform generator so that to obtain desired pulse shape at the structure input. The amplifier band is 50 – 1000 MHz. An absence of DC amplification requires pulses to be bipolar. The amplifier band allows forming pulses with the flat top of about 2 ns. The pulses for bunch removal or “passing through” have opposite polarity.

The second version of the kicker consists of two helical structures (Fig. 5.4). A helical deflector was used at LAMPF [7] (with a significantly slower rise time) and in Tektronix oscilloscope 7104. A high impedance of the helices, 200 Ohm decreases the current through the structure but requires development of a driver (though with a lower power than for 50 Ohm version) and the set of infrastructure such as 200 Ohm load, feedthroughs, and transmission lines. The 200 Ohm kickers are driven by broadband, DC coupled switches in push-pull configuration that are under development.

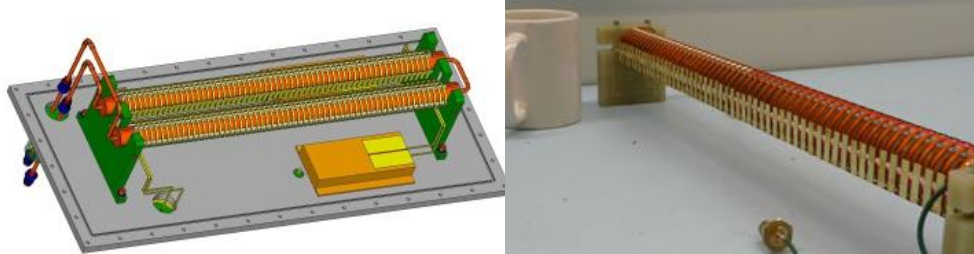


**Figure 5.4:** Mechanical drawing of 200 Ohm dual-helix kicker and photo of a single 200 Ohm helix prototype.

For both versions, the separation between plates is 16 mm, while the vertical aperture at the entrance and exit of each kicker is limited to 13 mm by special electrodes. An excessive current to these “protection” electrodes would mean a mismatched beam and would trigger a beam interruption by the protection system to avoid damaging the kickers.

### *Absorber*

The unwanted bunches are directed to an absorber located in the vicinity of the beam passing through. Nominally, the absorber accepts 80% of the 2.1 MeV, 5 mA beam. However, the absorber is being designed for the maximum power of 21 kW that corresponds to a 10mA beam completely diverted to the absorber (see specifications [8]). The power density in the beam with ~2mm rms radius exceeds by an order of magnitude what is technically possible to absorb without melting the surface. To decrease the surface power density, the absorber is positioned with a small angle, 29 mrad with respect to the beam (Fig. 5.5).

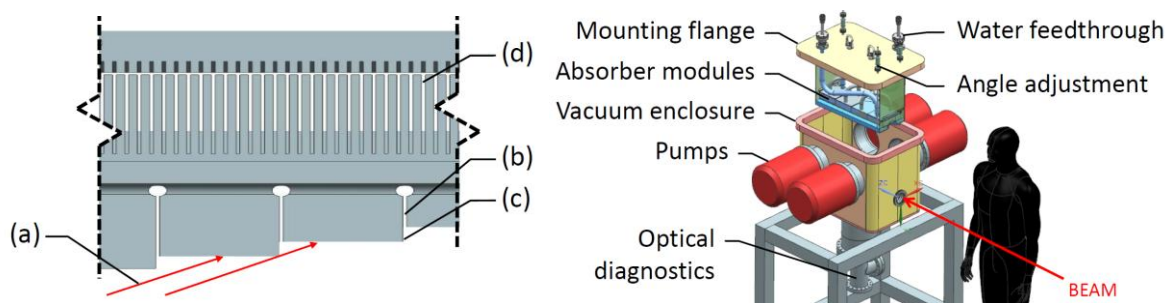


**Figure 5.5:** Conceptual design of the MEBT absorber. Left: side view of absorber showing (a) beam incident on surface, (b) axial stress relief slits, (c) shadowing step increment (magnitude exaggerated), (d) 300µm wide by 1mm pitch water cooling channels. Horizontal scale exaggerated. Right: exploded view.

Challenges presented by the absorber design include maintaining vacuum quality, managing surface effects (sputtering and blistering), containing secondary particles, accommodating radiation effects, spreading energy deposition, and the survival of temperatures and temperature-

induced mechanical stresses. Presently the design choice is a monolithic absorber made from the molybdenum alloy TZM [9].

At the ion energy of 2.1MeV, the mean stopping length is about 20 $\mu$ m. Therefore, heating of the absorber is essentially a surface phenomenon, and thermal properties of the absorber can be adequately tested with an electron beam of the same surface power density. For this purpose, such electron beam test bench is assembled using parts of now dismantled Recycler electron cooler.

### *Bunching cavities*

To keep the beam properly bunched, the MEBT includes 3 identical bunching cavities [10]. Each cavity is a quarter-wave 162.5 MHz resonator (QWR) with the nominal accelerating voltage of 70 kV (at  $\beta=0.067$ ). Geometrically, the minimum beam aperture is 30 mm, total height of the cavity  $\sim$ 540 mm, and the space occupied along the beam line is  $<$  340 mm (flange-to-flange). The conceptual design and some results of simulations are shown in Fig. 5.6.

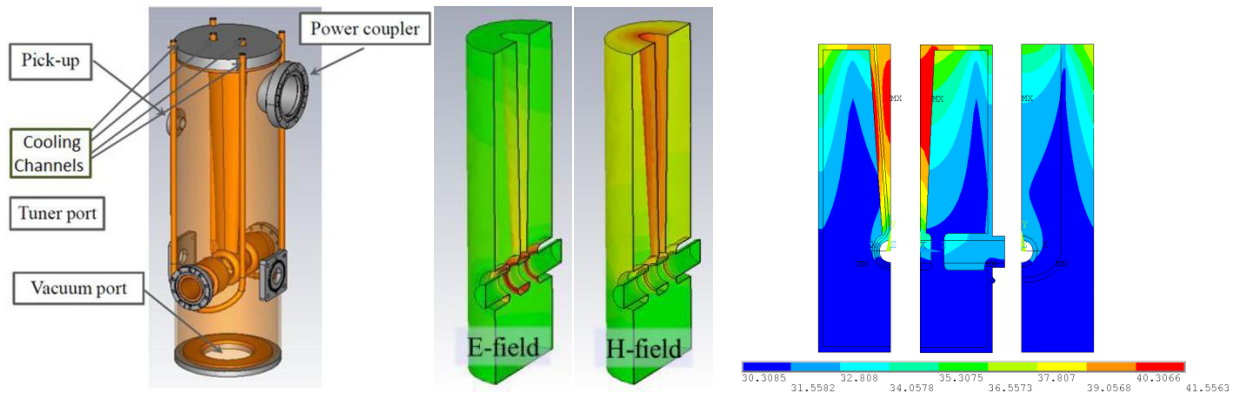


**Figure 5.6:** Conceptual design of the MEBT bunching cavity (left), simulated surface field distributions (center), and the temperature distribution (right) (from Ref. [11]).

### *Scrapers*

As it has been mentioned, each of sections #0, 1, 6, and 7 will contain a set of 4 scrapers. Each of these 16 scrapers is envisioned as an electrically isolated, 100W-rated plate precisely movable across the half-aperture [12]. The scrapers will be used for several purposes:

1. For beam halo measurements and removal
2. To protect the downstream equipment from a beam loss caused by beam envelope and trajectory mismatches. A high-loss signal from a scraper will trigger turning the beam off.
3. As an axillary beam density distribution diagnostics (pulse mode)
4. To form a pencil H beam for measurements downstream (pulse mode)

The scrapers sets in the upstream and downstream pairs are separated by  $\sim 90$  degree of the transverse phase advance to insure an effective removal of particles with large transverse actions.

### *Vacuum system*

The vacuum requirements for MEBT are determined by the electron detachment in  $H^-$  beam and by the necessity to have a low gas flow into the HWR cryomodule [13]. Obviously, the electron detachment results in a loss of  $H^-$  beam intensity; an additional restrictive effect is a flux of created neutral hydrogen atoms that may reach the SRF cavities. These atoms have roughly the same velocity as the primary  $H^-$  ions and, therefore, the divergence of the neutral beam is determined by the  $H^-$  angles in the location of detachment. For the design of the vacuum system, we adopted the requirement of keeping the integral of the pressure over the distance of MEBT to be below  $1 \cdot 10^{-6}$  Torr·m, which corresponds to losing  $\sim 10^{-4}$  in the beam intensity and adding an additional  $\sim 0.1$  W heat load to SRF by the neutrals.

The gas flow from the room-temperature MEBT to the 2K HWR cryomodule causes a gas deposition on the cryogenic surfaces. While there are no exhaustive experiments or a cohesive theory on the subject, in literature there are indications that such coverage at the surface of the cryo cavities degrades their performance. On the other hand, the closest analog, a HWR in the Argonne National lab successfully operates at the pressure of  $5 \cdot 10^{-8}$  Torr immediately upstream of the cryomodule, though with unknown gas composition. To be on a safe side, we aim to the pressure upstream of PXIE's HWR of  $1 \cdot 10^{-9}$  Torr (hydrogen).

The vacuum scheme based on these requirements is discussed in detail in Section 14.

### *Diagnostics*

Elements of diagnostics to be used in the MEBT are listed in Fig. 5.1, and the detailed description is in Section 11.

### **MEBT commissioning and tests**

With the full set of instrumentation, the MEBT allows complete characterization of the beam coming of RFQ. This makes possible a scenario when RFQ and MEBT are being installed and commissioned at the same time, with a temporary  $\sim 2$ -kW beam dump at the end of MEBT (likely to be borrowed from previous experiments). By that time, the LEBT is supposed to be commissioned and capable of injecting into RFQ either DC or pulse beam with the duty factor that can be varied widely by adjusting both the pulse duration and repetition frequency. Also, in addition to routine acceptance procedures, major MEBT elements are passed preliminary tests:

- The kickers and their drivers are fully characterized in RF measurements, including effective amplitude and shape of pulses as well as the wave velocity. Vacuum tests with the full applied RF power are performed.

- The absorber prototype is tested with an electron beam.
- Buncher cavities are tested with the full RF power.
- Thermal capabilities of the scrapers are tested with an electron beam.

As soon as the RFQ is ready, a  $\sim 5$  mA,  $\sim 1$   $\mu$ s, 60 Hz beam is accelerated and injected into the MEBT. In this mode, the average power,  $\sim 0.6$ W is low enough to avoid any damage. The beam is characterized and tuned using the toroid, scrapers, emittance monitor, and the wire scanner in the first sections. Also, the pulsed beam scraped to a small emittance by the first set of scrapers can be passed through MEBT to commission the BPM system with minimum direct irradiation of the BPM plates.

After passing this pencil beam through the entire MEBT and characterization of the RFQ beam, the next step is tuning on the full peak current beam all the way to the dump. It allows optical measurements of the beam line, possible correction of quadrupole calibrations and wiring errors etc. The BPM calibrations can be cross-checked with the wire scanners. Time-of-flight measurements verify the beam energy.

Knowing optics, we can start commissioning of the kickers (still in the pulse mode). BPMs and the wire scanners give information about the beam deflection; deflection optimization allows to phase the kickers. The effective emittance of the bunches selected for passage can be judged through the combination of beam scans by wire scanners (for the beam core) and by the scrapers downstream of the absorber (for the transverse tails). Also, the kicker protection system using the protection electrodes is tested and tuned. An extinction monitor (see Section 11) is used to measure the amount of ions left in the longitudinal buckets scheduled to be cleared.

The absorber is commissioned by steering the beam with the dipole coils built into the quads (with the kickers off) to the absorber surface and slowly increasing the intensity of the beam injected into RFQ. The absorber vacuum chamber is equipped with an optical system that allows observing the visible light from the absorber. This system is expected to be an important tool in measuring the beam spot size. First, the Optical Transition Radiation (OTR) light might be measurable with long averaging times (seconds) even in the pulse mode, though the signal-to-noise ratio is difficult to estimate. Then, at intensities approaching the nominal regime, the thermal radiation should be easily detectable because the working temperature of the absorber surface is expected to be as high as 1000C. The spot size is optimized varying the beam line optics and the angle between the beam and the absorber surface. The absorber is tested for the maximum power of 2.1 kW and thermocycling at relevant parameters.

Commissioning of the scrapers will include, in addition of testing their scraping capabilities, a calibration of the current measured from a scraper plate versus the beam loss to it. The calibration allows incorporating the scrapers into the protection system. If an error in focusing or steering that may be dangerous for creating beam losses in the SRF linac occurs upstream of the

scrapers, the resulting beam loss to a scraper plate generates a signal large enough to trigger turning the beam off by the protection system.

The preferable way of MEBT commissioning is with the fully assembled MEBT line. However, if the HWR cryomodule progresses faster than the MEBT tests, one can dismount one or two last sections to move the temporary dump into the new position and free the space enough for assembling the HWR. By splitting the time between two activities, we should be able to continue most of the tests (for example, working with the absorber), while progressing with HWR installation.

When all MEBT elements are commissioned in full, performance of the entire line is tested. The goal is to either demonstrate that the PXIE MEBT is adequate for the Project X by reaching simultaneously all parameters of Table 6.1 or clearly identify its deficiencies and specific ways of modifications the beam line for the use with the Project X.

Note that even if the latter is the case, in the most of scenarios the front end has enough flexibility to provide the beam needed to test the performance of the cryomodules. For instance, if the absorber can't sustain the full average power or the kicker system is not capable of the high repetition rates, part of chopping can be made in LEBT. While it would be a clear step down from the requirement of an arbitrary bunch selection, the bunch structure would be close enough to perform all other tests. Another example is a failure by the kicker system to reach the nominal deflection. The emittance of the beam entering the kickers can be decreased by scraping the beam tails with scrapers. As a result, the beam size in the absorbed location is lower, and, in turn, the bunch cleaning can be effective even at a smaller separation between the bunches scheduled for passing and for being dumped.

## Summary

The proposed design of the PXIE MEBT addresses all requirements of the Project X, including bunch-by-bunch selection and optical matching. Also, it provides enough diagnostics to characterize the beam properties at the RFQ exit and at the entrance of the SRF linac. At the same time, the MEBT has enough flexibility to address a variety of uncertainties in commissioning scenarios.

## References

- [1] A. Aleksandrov and C. Deibele, "Experimental study of the SNS MEBT chopper performance", Proc. of IPAC'10, Kyoto, Japan, May 23-28, 2010, MOPD063
- [2] "PXIE MEBT Functional Requirements Specification", Project X Document 938.
- [3] "PXIE MEBT quadrupoles specifications", Project X Document 933
- [4] "PXIE MEBT kicker specifications", Project X Document 977
- [5] V. Lebedev et al., "Progress with PXIE MEBT chopper", Proc. of IPAC'12, New Orleans, USA, May 20 - 25, 2012, WEPPD078

- [6] J.S.Lunsford and R.A.Hardekopf, IEEE Trans.on Nucl.Sci., NS-30, 4, 1983, p.2830
- [7] J.S.Lunsford et al., IEEE Trans.on Nucl.Sci., NS-26, 3, 1979, p.3433
- [8] “Functional specifications for PXIE MEBT absorber”, Project X Document 964
- [9] C. Baffes et al., “Design Considerations for an MEBT Chopper Absorber of 2.1MeV H<sup>-</sup> at the Project X Injector Experiment at Fermilab”, Proc. of IPAC’12, New Orleans, USA, May 20 - 25, 2012, WEPPD035
- [10] “FRS for Bunching cavity for PXIE MEBT”, Project X Document 1071
- [11] G. Romanov et al., “CW room temperature re-buncher for the Project X front end”, Proc. of IPAC’12, New Orleans, USA, May 20 - 25, 2012, THPPP063
- [12] “Functional specifications for PXIE MEBT scrapers”, Project X Document 1067
- [13] V. Lebedev, “Beam - related vacuum requirements for PXIE”, Report at PX meeting, December 13, 2011, Project X Document 971
- [14] A. Chen, “PXIE vacuum”, Report at the Project X collaboration meeting, April 10-12, 2012, Berkeley, CA, Project X Document 1022

## 6. Half-Wave Resonator Cryomodule Design

Peter Ostroumov

### Introduction

The Project-X injector includes a single cryomodule with 8 superconducting 162.5 MHz  $\beta_{\text{OPT}} = 0.112$  half-wave resonators interleaved with 8 superconducting solenoids for acceleration of high-intensity proton or  $\text{H}^-$  beams in the energy range from 2 MeV to 11 MeV. This cryomodule [1] is being designed and built by ANL with the intent of delivering a device which has all external connections to the cryogenic, RF, and instrumentation systems located at removable junctions separated from the clean cavity vacuum system. A special care was devoted to ease assembly, cavity cleanliness, interfacing to subsystems (e.g., cryogenics, couplers, tuners, etc) satisfy the ANL/FNAL/DOE guidelines for vacuum vessels. We employ proven warm-to-cold low-particulate beam line transitions to minimize unused space along the linac, a top loading box design that minimizes the size of the cleanroom assembly, and compact beam-line devices to minimize the length of the focusing period.

### Half-Wave Resonators

The 162.5 MHz half-wave resonator (HWR) design [2] is based on recent advances in SRF technology for TEM-class structures being developed at ANL. The beam dynamics optimization has resulted in an optimal cavity beta of  $\beta_{\text{OPT}}=0.11$ . Highly optimized EM parameters were achieved by adjusting the shapes of both inner and outer conductors [3]. The highest performing HWR geometries use a center conductor with a race-track shaped cross section in the high-electric field region. Detailed studies of the electric field distribution in the accelerating gaps revealed an appreciable defocusing quadrupole component of the electric field in the HWR with a race-track shape central conductor. The latter is not acceptable in high-intensity ion linacs with a solenoid-based symmetric focusing and leads to emittance growth. Therefore, we developed a “donut” shaped drift tube in the center conductor as is shown in Figure 6.1. Table 6.1 summarizes the relevant cavity parameters. Figure 6.1 shows MWS simulation results of the electric and magnetic surface field distributions in the “donut” HWR and engineering 3D model of the HWR. The cavity engineering model includes stainless steel helium vessel, RF coupler, slow tuner and kinematic alignment mount. The quadrupole component of the RF field depends on particle speed and therefore cannot be compensated in the entire energy range of cavity operation. Figure 6.2 presents dependence of quadrupole component on particle  $\beta$  for the optimized cavity geometry. This effect will be compensated by correction coils located inside nearby focusing solenoid capable to create dipole and skew-quadrupole fields.

A pneumatically actuated mechanical slow tuner which compresses the cavity along the beam axis is located outside of the helium vessel and will be attached to the SS flanges as is shown in Figure 6.1. The slow tuner is an improved version of the previous design used successfully for the past 3 years in the ATLAS Energy Upgrade Cryomodule [4]. A fast tuner is not required for the PXIE application once a 4 kW RF power source is available. This power is sufficient to support the 1 mA beam loading with an 80 Hz loaded bandwidth.

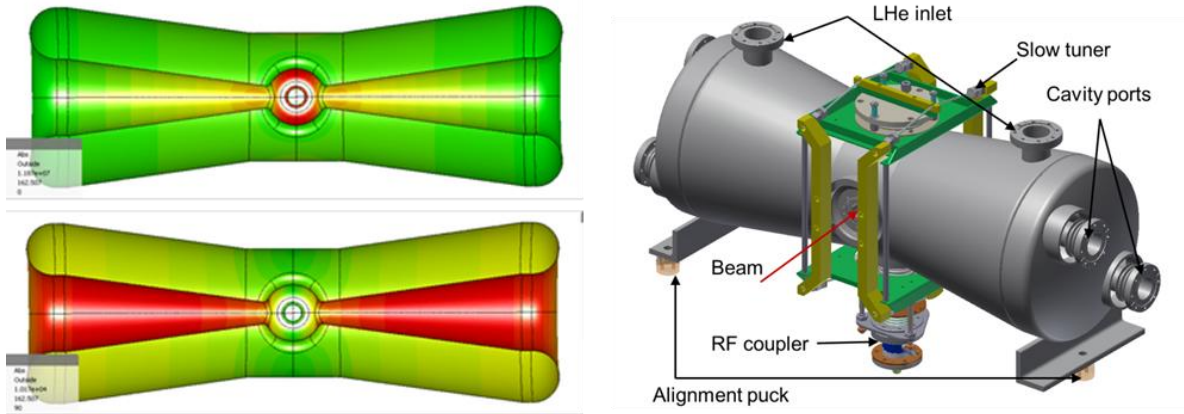


**Figure 6.1:** A half-wave resonator model in MWS (left). The electric (top) and magnetic field (bottom) distributions on the surface were obtained with tetrahedral mesh. Red is high intensity and green is zero. 3D engineering model of the HWR is shown on the right.

<b>Table 6.1:</b> Cavity main parameters	
<b>Parameter</b>	<b>Value</b>
Frequency, MHz	162.5
Optimal beta, $\beta_{OPT}$	0.112
$L_{EEF} = \lambda \beta_{OPT}$ , cm	20.7
Aperture, mm	33
$G = Q_0 R_s$ , $\Omega$	48
$R/Q_0$ , $\Omega$	272
$E_{PEAK}/E_{ACC}$	4.67
$B_{PEAK}/E_{ACC}$ , mT/(MV/m)	5.0
Nominal Voltage,/(MV)	1.8

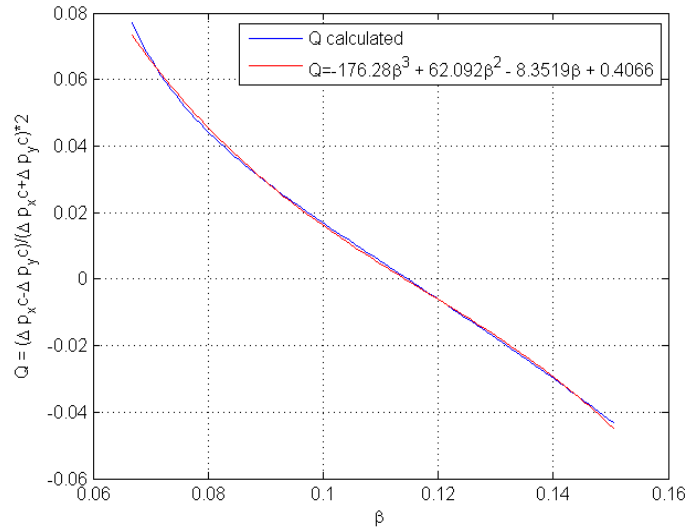


**Figure 6.2:** Quadrupole effect in the HWR cavity versus the particle velocity  $\beta$  in operating domain; red and blue line show simulation and approximation.

### RF Input Coupler

A power coupler has been designed and being built at ANL for use with the 162.5 MHz HWRs [5]. The 50 Ohm coaxial capacitive coupler will operate CW with up to 15 kW of forward power under any condition for the reflected power. The coupler should not adversely impact the cleanliness of the high-gradient SC cavities. The design is similar to already demonstrated ANL 4 kW, 72 MHz coupler [6] which serves as the starting point for the new coupler. The modular design has four separate components. These are a cold bellows, a cold rf window, a 70-to-300 K transition and a 300 K rf window as shown in Figure 6.3. The disc is brazed between the inner and outer conductors. The adjustability of the center conductor by 30 mm into and out of the cavity is performed by compressing the cold bellows, formed from thin-walled stainless steel with 20  $\mu\text{m}$  of copper on the inner (rf) surface. The cold window is anchored to 70 K by circulating cold He or N<sub>2</sub> gas, as shown in Figure 6.3, and also separates the cavity and cryomodule vacuum spaces. The window conductively cools the center conductor, so that it operates near 70 K for all operating modes. The cold bellows and rf window are readily cleanable for assembly onto the clean SC cavity. The warm window, located near the bottom wall of the cryomodule, separates the cryomodule vacuum from atmosphere. Detailed multi-physics simulation of the coupler and mechanical design were presented in ref. [7].

<b>Table 6.2: Coupler Design Parameters</b>	
<b>Parameter</b>	<b>Value</b>
Design RF power, kW	15
Outer diameter, mm	50
Impedance, $\Omega$	50
S11 @ 162.5 MHz, dB	-30
Static load to 2K, W	0.06
Static load to 5K, W	1.6
Static load to 70K, W	2.6

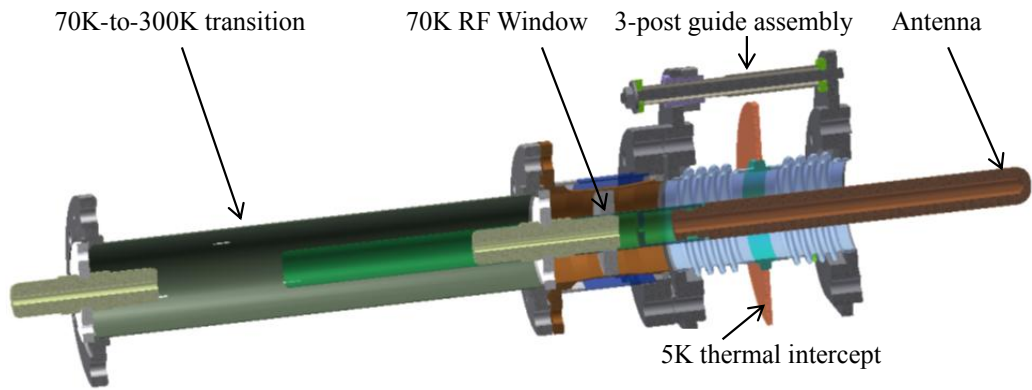


**Figure 6.3:** Input coupler

### SC Solenoid and BPM

The focusing period in this cryomodule has been minimized by following a novel approach to the solenoid, beam-position-monitor (BPM), and interconnecting spools. Instead of using the traditional Con-Flat® type flanges, EVAC CeFix [8] flanges are used. These flanges eliminate all the threaded fasteners in a low-particulate region which must be kept clean to minimize field emission in the cavities, a significant improvement over the Con-Flat® flanges. The superconducting magnets are being developed in collaboration with Cryomagnetics, Inc. and Meyer Tool and Manufacturing, Inc. The magnet design integrates the  $x$ - $y$  steering coils with the focusing solenoid to save length. A compact BPM is connected to the solenoid through EVAC CeFix flanges. The solenoid and BPM assembly together with support stands and alignment pucks is shown in Figure 6.4.

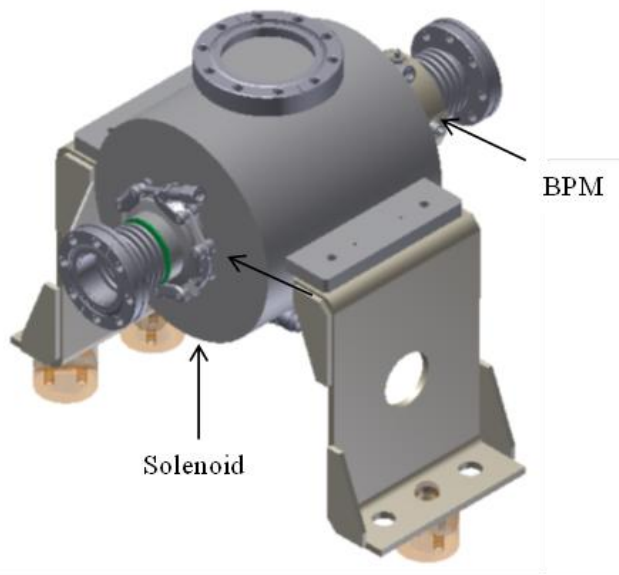


**Figure 6.4:** Solenoid and BPM assembly

### **Cryomodule Assembly**

The PXIE HWR cryomodule design is an evolution of the top-loaded box cryomodule design used successfully for the ATLAS Energy Upgrade Cryomodule [4]. Several improvements have been made as well as modifications for 2 K operation. Currently, we are working on an optimized vacuum vessel design to minimize the cost of fabrication, reduce the space required in the accelerator hall, and satisfy the pressure vessel safety guideline set forth by FNAL.

The PXIE HWR cryomodule layout was determined with careful beam-dynamics simulations and estimates of recent cavity performance [9]. This work determined that a focusing period contains a magnet-BPM-cryomodule sequence and that 8 of these units were required. The cryomodule design is developed around these requirements. The cryomodule beam-line assembly along with the strong-back, cavity subsystems, and strong-back hangers is shown in Figure 6.5. The main difference between this cryomodule and our previous designs is the operating temperature, 2 K. To account for this we are incorporating thermal shielding at 70 K, intermediate thermal intercepts at 5 and 70 K, and a cryogenic distribution system compatible with FNAL requirements. The helium distribution system does not supply gas but rather supercritical 5 K helium gas. Internal to the cryomodule the 5 K supply is split to supply the 5 K thermal intercepts and a heat exchanger followed by a J-T throttle valve to supply the 2 K liquid for the cavity and magnetic cooling. The heat exchanger and J-T valve combination are based upon a similar configuration used for the past 3 years in the ANL test cryostat. The heat exchanger is based upon the models developed for the LHC cryogenic distribution system and described in [10]. The cryomodule is designed for clean assembly of the cavities, couplers, magnets, interconnecting beam-pools, beam-line gate valves, and vacuum manifold. All of these parts have been designed to be cleanable via ultrasonic cleaning and high-pressure ultra-high purity water rinsing. The cryomodule design for the clean assembly builds upon our previous work and minimizes the number of components and connections which must be handled/made in the cleanroom.

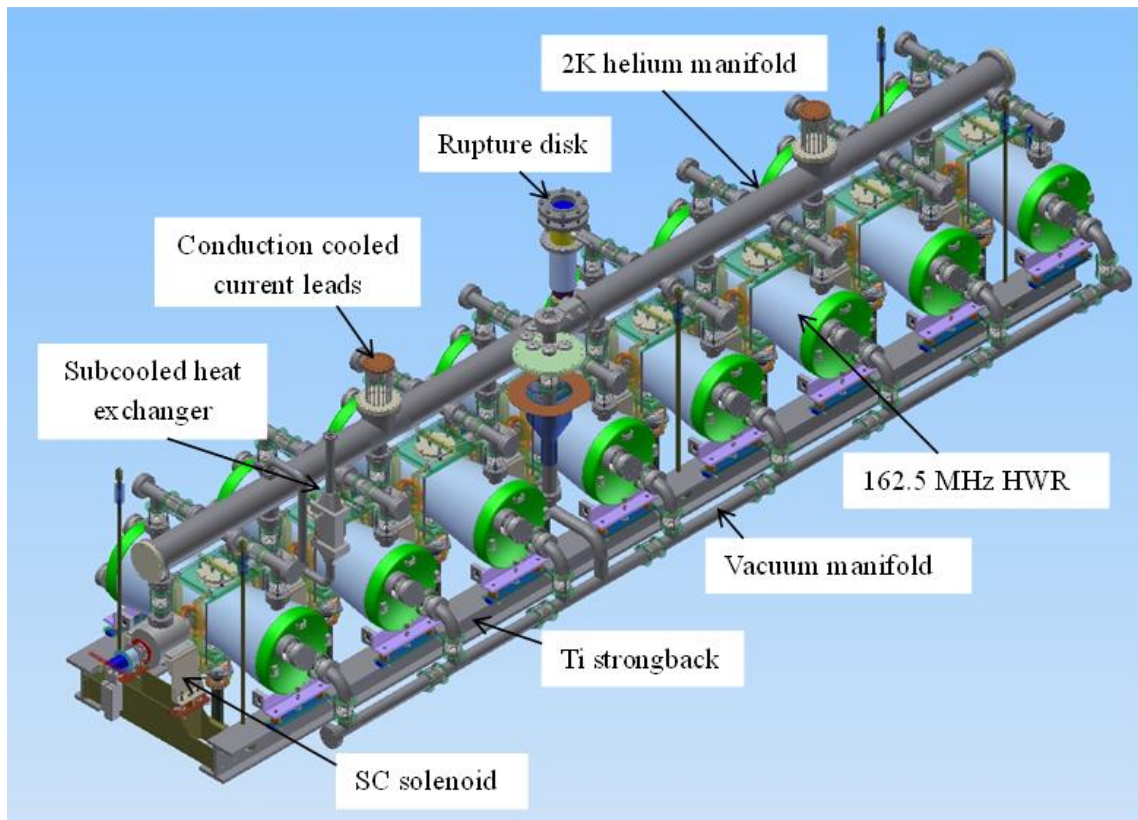


**Figure 6.5:** Cavity string assembly

The cavity/magnet support and alignment system provides a rigid platform for each cavity and magnet and allows for the independent alignment of each element. This system is structurally supported by a titanium I-beam rail system which runs the length of the cryomodule and supports all of the beam-line elements. The cryomodule spanning strong-back alignment technique has been in use at ATLAS for the past 25 years and was recently measured to hold the alignment of elements to better than  $250\ \mu\text{m}$  and  $0.1^\circ$  typically. Each individual element will be supported by a Maxwell-type kinematic mounting arrangement [11] and the alignment targets for the elements. Here notice that we are in the process of assembling a new cryomodule for the ATLAS Intensity Upgrade which will serve as a proving ground for the technology to be used in the HWR cryomodule. The Maxwell kinematic support structure was chosen because the beam axis of the cavity does not displace along the x-axis during cooldown. This arrangement is shown in Figure 6.6. Each cavity and magnet will have 4 targets, mounted on fiducial surfaces referenced to the electrical axis of the devices, which will be used for alignment with the beam axis and optical monitoring for misalignment measurements during all stages of the cryomodule life-cycle: assembly, pump-down, cool-down, operation, warm-up etc. 3D engineering model of the HWR cryomodule assembly is shown in Figure 6.6.

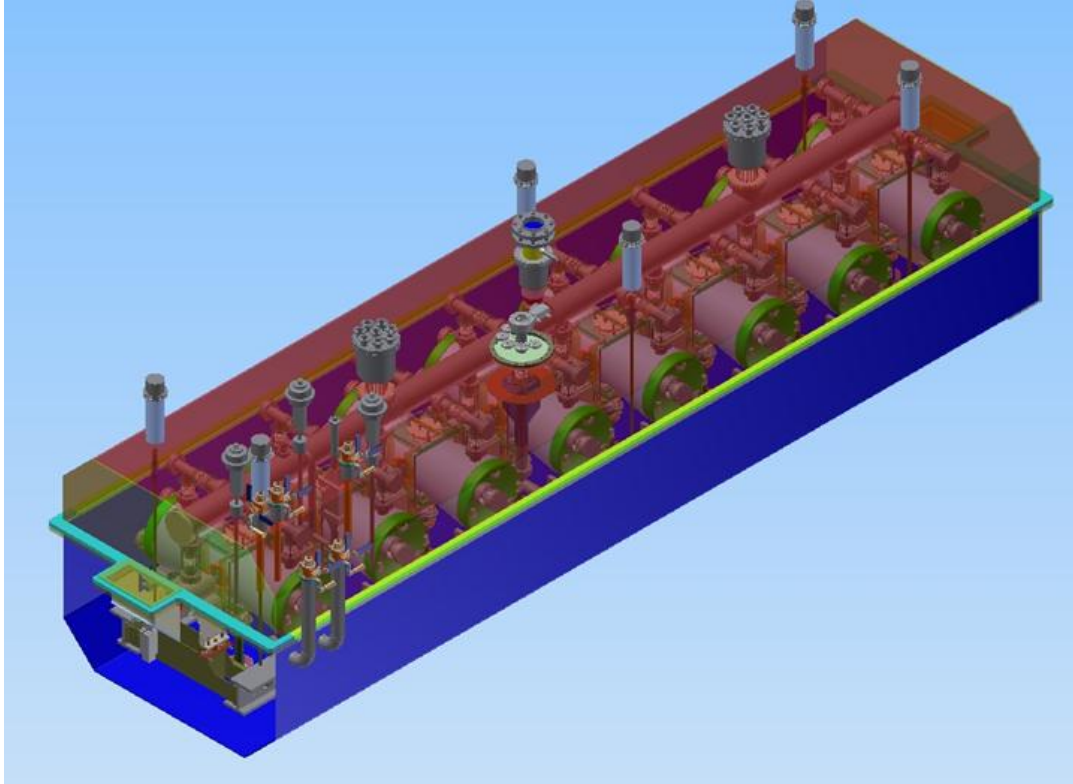


**Figure 6.6:** Cryomodule assembly

### Heat Load Estimate

Table 6.3 summarizes the estimated static and dynamic heat loads to each temperature level in the cryomodule assembly from all sources. The following sources were included in the calculation of 2K heat load: cavities, rf couplers, helium manifold, radiation from 70K to 2K, instrumentation, high current leads, strongback hangers, cavity and solenoid cooldown lines, vacuum manifold, slow tuners, gate valves. Changing operating voltages by +20% and -20% will result to 28W and 21 W total 2K heat load correspondingly.

<b>Table 6.3: HWR Cryomodule Heat Load Estimate</b>	
<b>Temperature</b>	<b>Load, W</b>
2 K, static	14
2 K, dynamic	10
4.5 K	60
70 K	250

### References

- [1] Z.A. Conway et al., “A New Half-Wave Resonator Cryomodule Design for Project-X”, Proceedings of the IPAC’12, p. 3865.
- [2] P.N. Ostroumov et al., “Development of a Half-Wave Resonator for Project X”, Proceedings of the IPAC’12, p.2295.

- [3] B. Mustapha, et al., "A Ring-shaped Center Conductor Geometry for a Half-wave Resonator", Proceedings of the IPAC'12, p. 2289.
- [4] P.N. Ostroumov et al., "Commissioning of the ATLAS Upgrade Cryomodule", Proceedings of HIAT'09, Venezia, 2009, p. 151.
- [5] M.P. Kelly et al., "Design and Construction of a High-Power RF Coupler for PXIE", Proceedings of the IPAC'12, p. 2284
- [6] M.P. Kelly et al., "A New Fast Tuning System for the ATLAS Intensity Upgrade Cryomodule", Proc. of LINAC'10, p. 884.
- [7] S.V. Kutsaev, M.P. Kelly, and P.N. Ostroumov, "Electromagnetic Design of 15 kW CW RF Input Coupler", Proceedings of the IPAC'12, p.2286.
- [8] <http://www.evacvacuum.com/index.php?id=152>
- [9] M.P. Kelly et al., "SRF Advances for ATLAS and other  $\beta < 1$  Applications", SRF'11, p. 680.
- [10] N. Gilbert et al, "Performance Assessment of 239 Series Helium Sub-Cooling Heat Exchangers for the LHC," Adv. Cryo. Eng. 51a (2006), p. 523.
- [11] L.C. Hale and A.H. Slocum, "Optimal design techniques for kinematic couplings," Precision Engineering 25 (2001), p. 114-127.

## 7. SSR1 Cryomodule Design

Tom Nicol

### Introduction

The SSR1 cryomodule will operate with continuous wave (CW) RF power and support peak currents of 5 mA chopped with arbitrary patterns to yield an average beam current of 1 mA. The RF coupler design employed should support a future upgrade path with average currents as high as 5 mA. The RF power per cavity at 1 mA average current and 2.2 MV accelerating voltage ( $\beta=0.22$ ) should not exceed 4 kW with an overhead reserved for microphonics control. The RMS normalized bunch emittance at the CM exit should not exceed 0.25 mm mrad for each of 3 planes.

The current beam optics design for Project X requires that the SSR1 cryomodule contains eight cavities and four solenoids in the following order: C-S-C-C-S-C-C-S-C-C-S-C. Horizontal and vertical dipole corrector are located inside each solenoid. A four-electrode beam position monitor is located at each solenoid.

The intent is that this cryomodule has all external connections to the cryogenic, RF, and instrumentation systems made at removable junctions at the cryomodule itself. The only connection to the beamline is the beam pipe itself which will be terminated by “particle free” valves at both ends. Minimizing mean time between failure and repair and in-situ repair of some internal systems are important design considerations in the cryomodule design. Figure 7.1 shows the linac layout including the location of the SSR1 cryomodule.

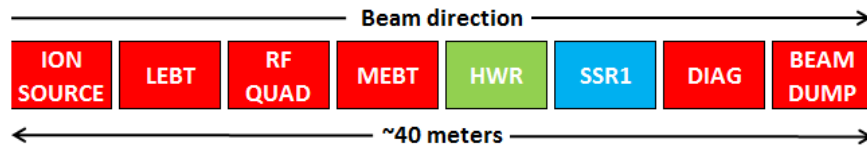


Figure 7.1: PXIE layout

### Cryomodule Design

Eventually, Project X will require several different cryomodule designs for cavities operating at 162.5, 325, 650, and 1300 MHz. The SSR1 for PXIE is the first of these being developed at Fermilab. Some details of individual cryomodule components are described in the following sections.

#### *Cryogenic Systems and Vacuum Interfaces*

There are two ways that cryogenic and vacuum systems are distributed to individual modules in superconducting magnets or cavity strings. The first, sometimes called coarse segmentation, refers to systems in which the cryogenic circuits and insulating vacuum inside individual cryostats are more or less continuous for long lengths, at least over the length of several cryomodules. Most accelerator magnet systems are configured this way as are the cryomodules envisioned for the ILC and the XFEL at DESY. The second, referred to as fine segmentation, refers to systems in which the insulating vacuum and the cryogenic circuits are confined to an individual cryomodule, the only connection between modules being the at beam tube. The cryomodules for the SNS and CEBAF are one example of fine segmentation. Fine segmentation is the configuration choice for Project X and PXIE cryomodules. Each individual vacuum vessel

will be closed at both ends and the cryogenic circuits will be fed through bayonet connections at each cryomodule. Each cryomodule will have its own connection to the insulating vacuum pumping system. Also, each cryomodule will have its own 2 K heat exchanger and pressure relief line exiting near the middle of the module. This configuration provides flexibility in terms of cryomodule replacement, and cooldown and warm-up times at the expense of requiring more individual cryogenic connections, cold-to-warm transitions at each end of each cryomodule, and extra space at each interconnect to close the beam tube. The choice of fine segmentation results in larger static cryogenic losses. However they are still significantly smaller than the dynamic losses for the Project X CW part to which the SSR1 cavities belong.

### ***Vacuum Vessel***

The vacuum vessel serves to house all the cryomodule components in their as-installed positions, to provide a secure anchor to the tunnel floor, to insulate all cryogenic components in order to minimize heat load to 80 K, 4.5 K, and 2 K, as well as maintain the insulating vacuum. It is 1.219 m (48 inches) in diameter and manufactured from 300-series stainless steel.

### ***Magnetic Shield***

Just inside the vacuum vessel, virtually in contact with the inner wall, is a magnetic shield to shield the cavities from the earth's magnetic field. Preliminary tests show that a 1.5 mm-thick mu-metal shield at room temperature reduces the residual field inside the cryostat to less than 10  $\mu$ T. It is possible that additional separate magnetic shields will be installed around individual magnetic elements to further reduce the potential for trapped fields in the superconducting cavity structures.

### ***Thermal Shield and Multi-Layer Insulation***

Each cryomodule will have a single thermal shield cooled with helium gas, nominally at 45-80 K. It is currently envisioned to be made from 6000-series aluminum with cooling channels on both sides. Two 15-layer blankets of multi-layer insulation, between the vacuum vessel and thermal shield will reduce the radiation heat load from the room temperature vacuum vessel to approximately 1.5 W/m<sup>2</sup>. A 5 K circuit will be available to intercept heat on the rf couplers and current leads, but there is no plan to install a full 5 K thermal shield.

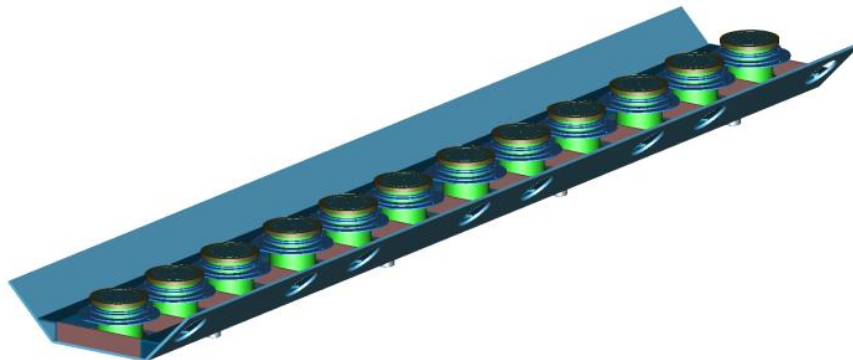


**Figure 7.2:** Strongback with supports

### *Support System*

All of the cavities and solenoids will be mounted on individual support posts which are in turn mounted to a full-length strongback located between the vacuum vessel and thermal shield. This enables the entire cavity string to be assembled and aligned as a unit then inserted into the vacuum vessel during final assembly. The strongback is envisioned to be aluminum, but stainless steel is an option. Maintaining the strongback at room temperature helps minimize axial movement of the cold elements during cooldown, reducing displacement of couplers, current leads, and many of the internal piping components.

The support posts are similar to supports utilized in SSC collider dipole magnets and ILC and XFEL 1.3 GHz cavity cryomodules. The main structural element is a glass and epoxy composite tube. The tube ends and any intermediate thermal intercepts are all assembled using conventional shrink-fit assembly techniques in which the composite tube is sandwiched between an outer metal ring and inner metal disk [1]. The strongback and support posts are shown in Figure 7.2. All of the cavities and magnetic elements are mounted to the support posts using adjustable positioning mechanisms.

### *Cavity and Tuner*

The cryomodule contains eight single spoke,  $\beta=0.22$ , 325 MHz cavities operating in CW mode at 2 K in stainless steel helium vessels. The cavity electro- magnetic (EM) parameters are shown in Table 7.1. The cavity operational and test requirements are summarized in 0.

**Table 7.1:** EM Cavity parameters

<b>Parameter</b>	<b>Value</b>
Frequency	325 MHz
Shape	Single Spoke Resonator
$\beta_g, \beta_o$	0.215, 0.22
$L_{\text{eff}} = \beta_o \lambda$	203 mm
Iris aperture	30 mm
Inside diameter	492 mm
Bandwidth	90 Hz
$E_{\text{pk}}/E_{\text{acc}}$	3.84
$B_{\text{pk}}/E_{\text{acc}}$	5.81 mT/(MV/m)
G	84 $\Omega$
R/Q	242 $\Omega$

**Table 7.2:** Cavity operational/test requirements

Parameter	Value
Max leak rate (room temp)	$< 10^{-10}$ atm-cc/sec
Operating gain per cavity	2.0 MeV
Maximum gain per cavity	2.4 MeV
$Q_0^*$	$>5 \times 10^9$
Max. power dissipation per cavity at 2 K	5 W
Sensitivity to He pressure fluctuations	$< 25$ Hz/Torr
Field flatness	Within $\pm 10\%$
Multipacting	none within $\pm 10\%$ of operating gradient
Operating temperature	1.8-2.1 K
Operating pressure	16-41 mbar differential
MAWP	2 bar (RT), 4 bar (2K)
RF power input per cavity	6 kW (CW, operating)

\*Note that the measurements of the first three SSR1 cavities in the vertical test stand showed  $Q_0$  of  $7-9 \times 10^9$  at the operating acceleration field.

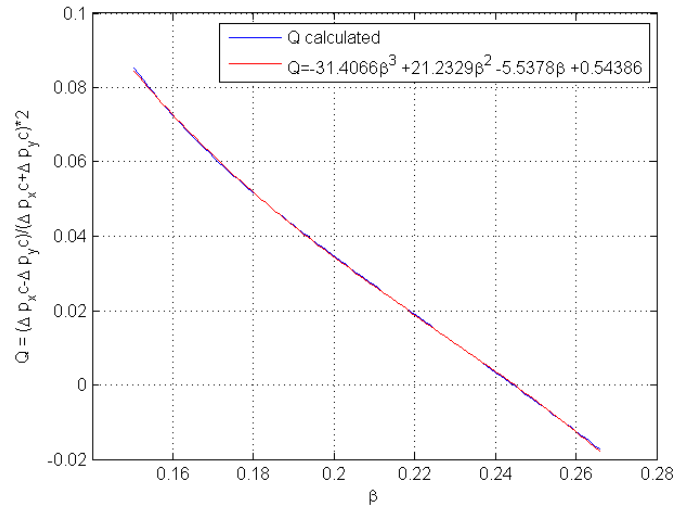


**Figure 7.3:** Quadrupole effect in SSR1 cavity versus the particle velocity  $\beta$  in operating domain; blue and red line present simulation and approximation.

A spoke cavity has no axial symmetry. Therefore its quadrupole component cannot be compensated in the entire range of cavity operation. Figure 7.3 presents dependence of quadrupole effect on the beam  $\beta$ . Due to engineering limitations mainly related to the rf couplers the cavities are rolled by 45 deg.; consequently, their quadrupole field is also rolled and is equivalent to the skew-quadrupole field. The cavity skew-quadrupole fields will be compensated by correction coils located inside nearby focusing solenoids capable to create dipole and skew-quadrupole fields.

In order to attain the requirements for frequency range and resolution (Table 7.3), the tuning systems for cavities of narrow bandwidths such as SSR1 typically integrate a coarse and a fine mechanism engaged in series. The first normally utilizes a stepper motor with large stroke capability and limited resolution, the latter usually contains piezo-electric actuators with limited stroke but virtually infinite resolution.

The coarse tuner is predominantly used to achieve consistently the resonant frequency during the cool-down operations. The range necessary to compensate for the cool-down uncertainties is estimated to be 50 kHz. In the event that a cavity must be detuned as a result of a malfunction, the coarse tuning system must be able to shift the frequency away from resonance by at least 100 bandwidths which equal to  $\approx 10$  kHz, so that the beam is not disturbed. The requirement on the range was set arbitrarily considering a safety margin of 2.7.

The requirement on the resolution of the coarse tuning system was set arbitrarily to a value that would allow operation in the event of a failure of the fine-tuning system. Based on other applications, it is believed that such resolution can be achieved with a coarse tuning system.

It is conservatively assumed that the coarse system cannot be operated during beam acceleration, it is thought that the vibration of a stepper motor may induce vibrations in the cavity severe enough to disrupt the operation.

Fine tuners shall be designed to compensate, at a minimum, the frequency shifts of the cavity induced by fluctuations of the helium bath pressure. The use of fine tuners will reduce considerably the hysteresis of the system by limiting the elements in motion during the tracking of the frequency.

A particular design effort shall be dedicated to facilitate the access to all actuating devices of the tuning system from access ports on the vacuum vessel. All actuating devices must be replaceable from the ports, either individually or as a whole cartridge.

**Table 7.3:** Tuning system requirements

<b>Parameter</b>	<b>Value</b>
Coarse frequency range	135 kHz
Coarse frequency resolution	20 Hz

The Helium vessel shall be fabricated from a non-magnetic stainless steel (e.g. 316L) designed to house a 2 K helium bath sufficient to remove up to 5 watts average dissipated power, with appropriately sized supply and return piping. It must meet the requirements of the Fermilab ES&H Manual for cryogenic pressure vessels and be rated at an MAWP (Maximum Allowable Working Pressure) of no less than 2 bar at room temperature and 4 bar at 2 K. Every effort should be made to minimize the weight and physical size of the helium vessel in all dimensions.

The cavity vessel with tuner system is shown in Figure 7.4 and described more completely in [2].



**Figure 7.4:** Spoke cavity, helium vessel, and tuner

**Table 7.4:** Design parameters of couplers

<b>Parameter</b>	<b>Value</b>
CW Power	30 kW
Multipactor threshold	25 kW (TW)
Passband	50 MHz
Input	3-1/8'' coaxial
Output	3''× 0.5'' coaxial
Output impedance	105 Ohms

***Input Coupler***

The input coupler is a 105-ohm coaxial design that supplies approximately 2 kW CW to each cavity in PXIE and ultimately up to 18 kW CW in Project X. The coupler contains a single warm ceramic window that provides separation of the warm and cold coupler sections. During

cryomodule fabrication, the cold section can be installed on the cavity in the cleanroom prior to assembly of the string. The warm section can then be installed from outside the vacuum vessel during final assembly. The inner conductor is solid copper with phosphor bronze bellows to accommodate motion due to misalignment and thermal contraction. The cold end of the outer conductor is 316L-stainless steel. The warm end is copper with phosphor bronze bellows. Heat load estimates don't suggest a significant penalty for not copper plating the outer conductor. A forced-air cooling tube is inserted into the inner conductor after assembly that supplies air to cool the coupler tip. The input coupler design is described more thoroughly in [3]. The coupler parameters are shown in Table 7.4. Figure 7.5 shows the current coupler design.

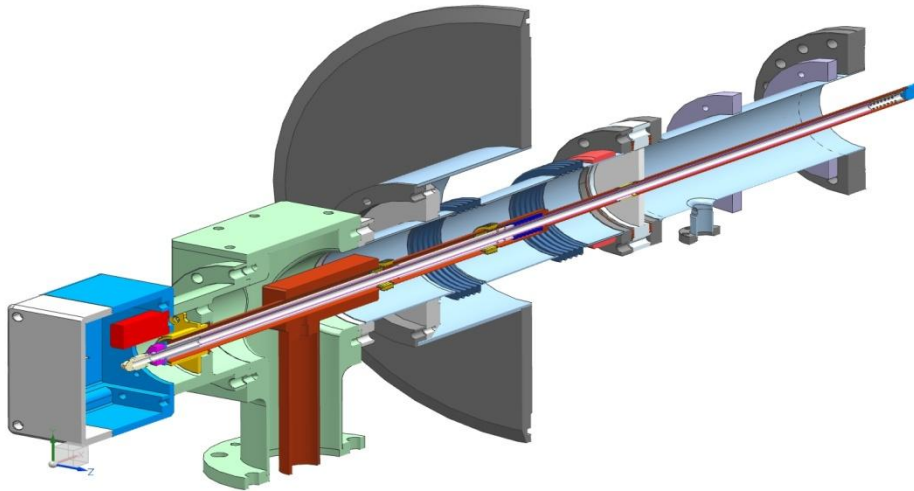


**Figure 7.5:** Input coupler

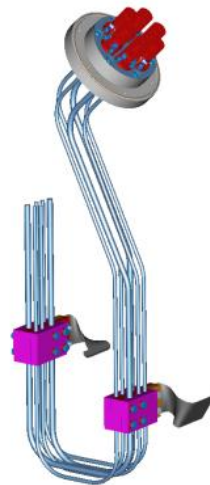


**Figure 7.6:** Conduction cooled lead assembly

### ***Current Leads***

Each focusing element package contains three magnet coils: the main solenoid, operating nominally at 100 A and two steering correctors each operating nominally at 50 A. A conduction

cooled current lead design modeled after similar leads installed in the LHC at CERN is being developed for use in the SSR1 cryomodule [4]. Figure 7.6 illustrates the conceptual design for the lead assembly. Thermal intercepts at 45-80 K and at 5 K help reduce the heat load to 2 K, nonetheless, these current leads represent a significant source of heat at the low temperature end. There will be one lead assembly for each magnetic element.

### ***Solenoid and Beam Position Monitor***

The four magnet packages in the cryomodule each contain a focusing solenoid and two dipole correctors all operating in a helium bath at 2 K.

The general design requirements for the lenses in the SSR1 cryomodule are summarized in the list below:

1. Requirements essential for the beam dynamics in the linac:
  - Integrated focusing strength of the lens must be not less than  $4 \text{ T}^2\text{m}$ ;
  - Each lens must contain two dipole correctors; bending strength of each corrector must be not less than  $0.0025 \text{ T}\cdot\text{m}$ ;
  - Clear aperture in the lens must be not less than 30 mm;
  - Uncertainty of the location of the effective magnetic axis in the focusing solenoid of the lens relative to reference points on the outer surface of the device must be better than 0.1 mm RMS.
2. Requirements essential for proper functioning of the cryomodule:
  - Maximum current in the solenoid of the lens must be less than 100 A;
  - Maximum current in the dipole correctors must be less than 50 A;
  - LHe vessel must be used for cooling the windings down to 2 K;
  - The lenses must be quench-protected; the energy deposited in the lenses after quenching must be as low as reasonably achievable;
  - The LHe vessel must meet the requirements of the Fermilab's ES&H manual chapters for pressure vessel;
  - The design of the LHe vessel must ensure reliable and reproducible mechanical connection to the alignment fixture of the cryomodule;
  - Maximum magnetic field generated by lenses in the cryomodule in the area near the surface of the SSR1 superconducting cavities must not exceed the level that would result in more than two-fold reduction of the intrinsic quality factor after quench event at any point on the surface of the cavity.

The Project X lattice, especially the low-beta section, provides little room along the beamline for beam diagnostics either inside individual cryomodules or between adjacent modules. In order to conserve axial space along the beamline a button-type beam position monitor (BPM) has been chosen for installation in the SSR cryomodules. A total of four will be installed in the cryomodule and tested in PXIE, one at each magnetic element. These devices are compact and lend themselves well to incorporation right into the solenoid magnet package as shown below in Figure 7.7. The bellows in either end of the beam tube allow independent adjustment of each magnet.

### ***Final Assembly***

The final assembly of the SSR1 cryomodule for PXIE is shown in Figures 7.8 and 7.9. Figure 7.8 shows the cavity string consisting of the cavities, solenoids, beam position monitors, and internal piping mounted on support posts which are in turn mounted to the strongback. Figure 7.9 shows the entire cryomodule assembly.

### ***Heat Load Estimate***

Table 7.5 summarizes the estimated static and dynamic heat loads to each temperature level in the cryomodule assembly from the primary sources. As mentioned earlier, the nominal 80 K thermal shield and intercepts may operate anywhere between 45 and 80 K.

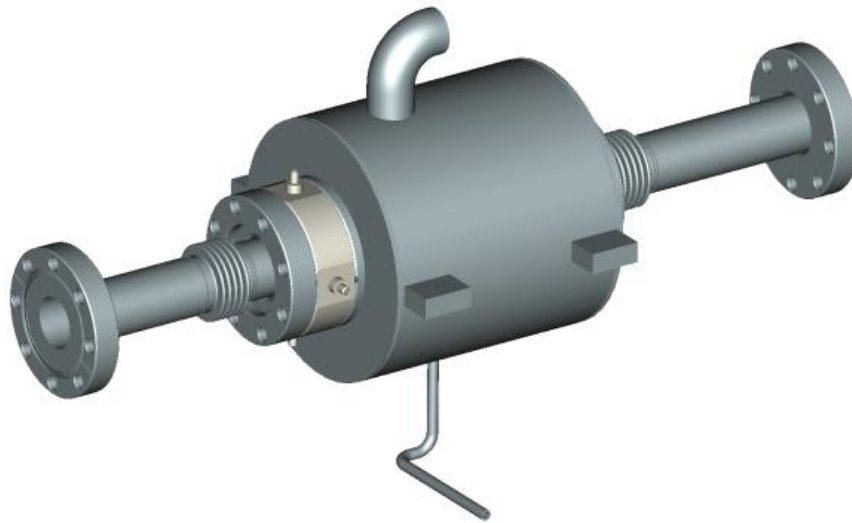


**Figure 7.7:** Solenoid and BPM assembly

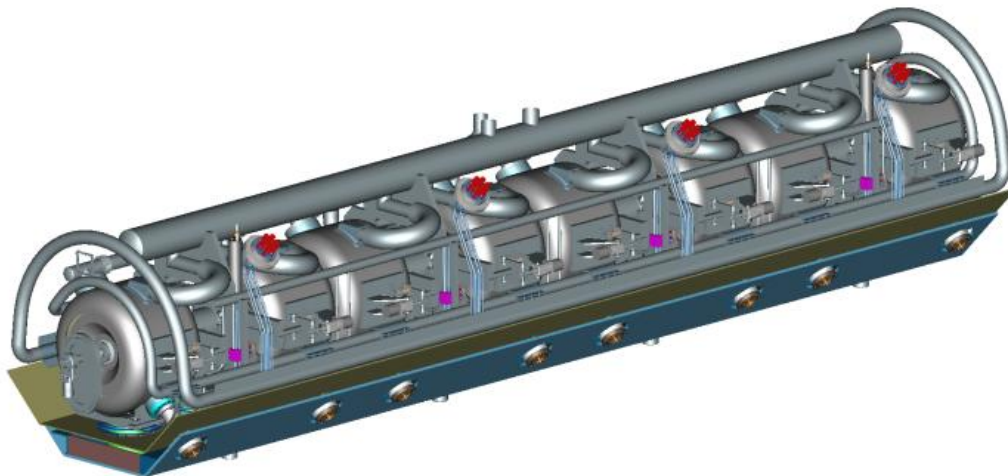


**Figure 7.8:** Cavity string assembly

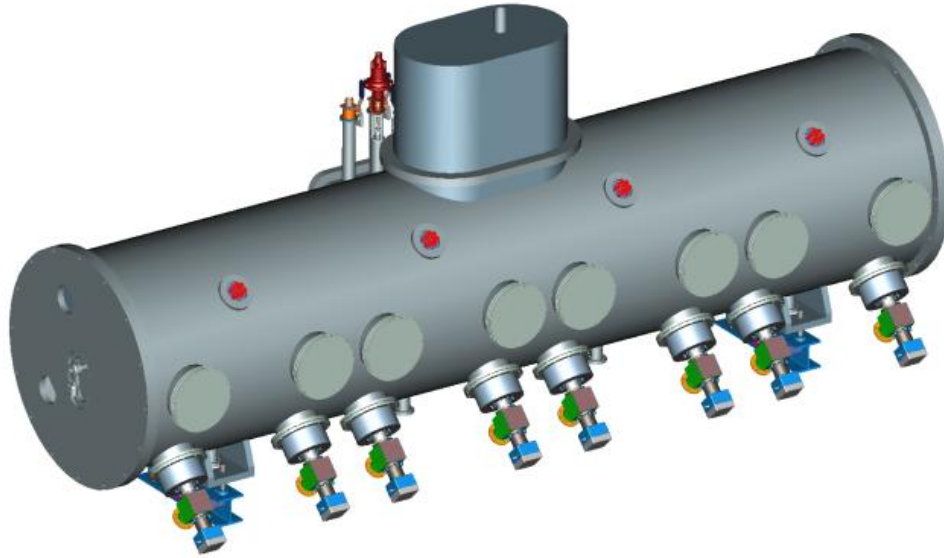


**Figure 7.9:** Cryomodule assembly

<b>Table 7.5: SSR1 Cryomodule Heat Load Estimates</b>							
SSR1 8 cavities, 4 solenoids	Each unit			Mult	Total		
	80 K	5 K	2 K		70 K	5 K	2 K
Input coupler static	5.36	2.82	0.50	8	42.88	22.56	4.00
Input coupler dynamic	0.00	0.00	0.25	8	0.00	0.00	2.00
Cavity dynamic load	0.00	0.00	1.78	8	0.00	0.00	14.24
Support post	2.76	0.36	0.05	12	33.12	4.32	0.60
Conduction lead assembly	36.80	13.20	1.24	4	147.20	52.80	4.96
MLI (total 70 K + 2 K)	30.54	0.00	1.42	1	30.54	0.00	1.42
Cold to warm transition	0.72	0.08	0.01	2	1.44	0.16	0.02
<b>Total</b>					<b>255.2</b>	<b>79.8</b>	<b>27.2</b>

**References**

- [1] T.H. Nicol, R.C. Niemann, and J.D. Gonczy, “Design and Analysis of the SSC Dipole Magnet Suspension System”, Supercollider 1, p. 637 (1989).
- [2] L. Ristori, et al, “Design of Single Spoke Resonators for PXIE”, presented at IPAC 2012, paper ID: 2689-WEPPC057.
- [3] S. Kazakov, et al, “Main Couplers Design for Project X”, presented at IPAC 2012, paper ID: 2523-WEPPC050.
- [4] A. Ballarino, “Conduction-Cooled 60 A Resistive Current Leads for LHC Dipole Correctors”, LHC Project Report 691 (2004).

## 8. Diagnostics Line and Beam Dump

Nikolay Solyak and David Johnson

### Introduction

After acceleration in the SSR1 cryomodule up to 25-30 MeV the H- beam will be transported through diagnostic line and dumped in the beam absorber. Transverse and longitudinal beam envelopes in the beamline are shown in Figure 8.1, where diagnostics beamline starts at 21.5 m downstream (distance from the end of RFQ).

### Beam Diagnostics

Diagnostics beamline will be equipped with BPMs, beam current monitor, laser wire profile monitor, halo monitor and beam loss monitor which will allow the measurements of basic beam parameters after acceleration, namely:

- Beam current (used for machine protection)
- Beam energy
- Beam 3D profiles and transverse and longitudinal emittances
- Halo measurements
- Beam loss measurements
- Beam extinction measurements

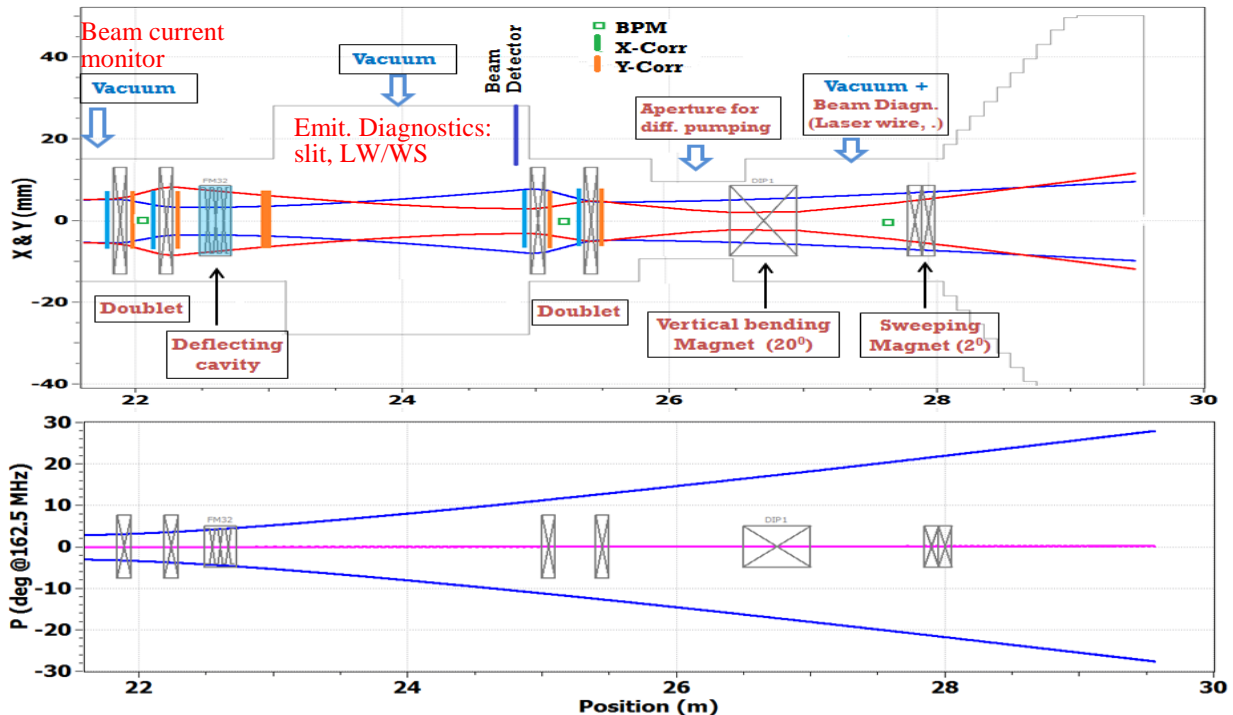


**Figure 8.1:** Transverse (top) and longitudinal 3-sigma beam envelope in diagnostics line. Locations of magnets, beam diagnostics and vacuum pumps are shown.

The beam energy is determined by measuring the beam position downstream of a 20 degrees spectrometer bending magnet; time-of-flight measurements with a phase locked BPMs can also be used. While the beam current monitor installed in the beamline is the main device to measure beam current, with proper calibration, BPMs can also be used. Beam loss monitors will monitor radiation from beam losses. Transverse emittances can be extracted from sets of beam profile measurements done by laser wire for different settings of upstream quadrupoles. Direct measurement of the transverse emittances by using slit and profile monitor, installed before bending magnet is a complementary option. To minimize longitudinal space needed for beam monitoring, vacuum pump and gauges, the beam halo monitor can be installed in a multi-port box along with other devices. Additional diagnostics include an RF deflector and beam detector used for extinction measurements.

### *Extinction measurements and deflecting cavity*

Project X will provide beams for different HEP experiments. Some of them (for example mu2e) have a strict requirement ( $<10^{-9}$ ) for beam extinction for removed bunches. Consequently, the populations inside these “empty” buckets (previously occupied by the bunches chopped out in MEBT) should be very small. An extinction level better than  $10^{-4}$  is specified for the MEBT. This number is mainly determined by available in MEBT diagnostics. Further cleaning happens during acceleration in the SC cryomodules which additionally filter out halo particles. A schematic of the extinction measurement experiment is shown in Figure 8.2. Particles from “empty” and filled buckets are rf separated vertically. The charge in empty buckets is measured by a sensitive particle detector. Bunches from filled buckets are returned back toward the axis and propagate through the rest of beamline to a beam dump. Such RF separation promises to measure the extinction level well below  $10^{-9}$ .

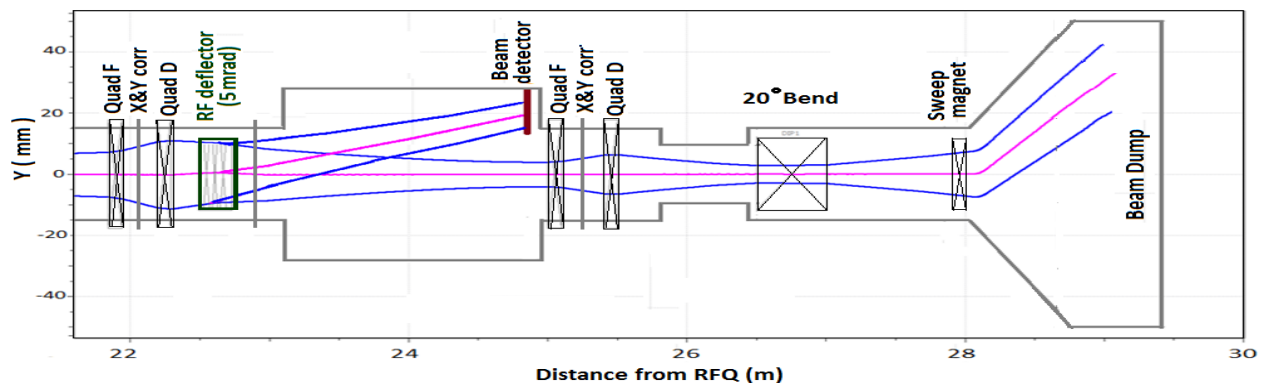


**Figure 8.2:** Schematic of extinction measurement experiment, 3-sigma envelopes for passing and deflecting bunches are shown in blue.

Bunch separation is provided by an rf separator and vertical DC corrector. Rf separator kicks bunches from empty and filled buckets in opposite directions with a deflecting angle of  $\sim 5$  mrad. A DC corrector located immediately downstream doubles the deflecting angle for “empty” bunches and cancels out the one experienced by “full” bunches. The rf deflector frequency is chosen to be 243.75 MHz corresponding respectively to 1.5 times of the bunch spacing

frequency (162.5 MHz) and providing a  $180^\circ$  phase difference between kicked out and propagating bunches. A proposed baseline design for a 243.75 MHz copper deflecting cavity is shown in Figure 8.3 and corresponding basic parameters for this design and alternatives are presented in Table 8.1. A high frequency (243.75 MHz) cavity with 30 mm gap was chosen as a baseline because of smaller dimensions, sufficiently large aperture and acceptable power consumption. For the extinction measurement experiment, the chopper will provide a special beam structure where all odd bunches are removed.

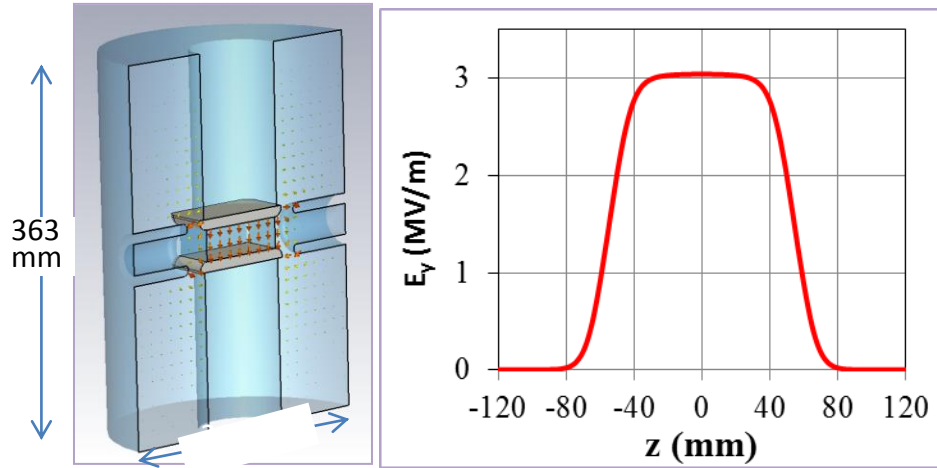


**Figure 8.3:** Configurations (left) and deflecting electric field along beam axis (right) of baseline 243.75 MHz RF separator.

**Table 1:** Parameters of the deflecting cavity

Parameter	243_Baseline gap 30 mm	243 MHz gap 20 mm	162_low loss gap 30 mm	162_low loss gap 20 mm
Frequency, MHz	243.75	243.75	162.5	162.5
Inner height, mm	363	413	368	331.5
Inner diameter, mm	260	260	420	360
Flange-to-flange (approx.), mm	350	350	510	450
Gap, mm	30	20	30	20
E_surf_max, MV/m	5.2	4.8	4.56	4.39
E_y_max, MV/m	3.04	4.3	2.58	2.75
Power losses, kW	2.9	1.44	1.94	1.65
Q	12575	14864	16934	13440
Kick voltage, MV	1.07	1.07	1.07	1.07
Proton $\beta$ (23.5 MeV)	0.22	0.22	0.22	0.22
Deflecting angle, mrad	5.0	5.0	5.0	5.0

### Vacuum

Vacuum requirements in the diagnostics line and the beam dump are dictated by requirement of good vacuum near the SSR1 cryomodule. We identify three areas with different requirements.

The dump area receives a lot of gas generated from the incident  $H^-$  ions which initially penetrate inside the beam dump receiving surface but then diffuse out. This  $H^-$  flux also results in sputtering of absorber material and degassing its surface. A turbo pump needs to be connected to the dump internal volume so that to create differential pumping through the nearby beam pipe. This pump has to remove large flux emitted by the beam dump and to keep pressure at the level of  $10^{-5}$  -  $10^{-6}$  torr outside the dump. The second area of differential pumping is located between two doublets (see Figure 8.2) and is separated from the dump by a  $\sim 0.5$  m long and a 20 mm pipe introducing additional differential pumping. Vacuum requirements in this area are  $10^{-7}$  -  $10^{-8}$  mbar. The third and last region is next to the SSR1 cryomodule where a high vacuum ( $<10^{-9}$  mbar) is needed to prevent gas and micro-particle migration to the cryogenic area. The exact locations of vacuum equipment and pumping requirements are yet to be determined. Development of functional requirements and conceptual design of the entire vacuum system are in progress.

### Beam Dump

The primary beam absorber (dump) for the PXIE 30 MeV CW  $H^-$  accelerator is located at the end of the diagnostics line downstream of a  $20^\circ$  vertical bending magnet. The current layout is shown in Figure 8.4. The nominal elevation of the accelerator axis is 1.3 meters above the floor of the enclosure. The bending angle and distances were chosen to have the absorber and its shielding above the floor. The absorber does not receive particles from the “empty buckets vertically deflected by the upstream rf separator. They will be stopped in a detector upstream of the vertical dipole.

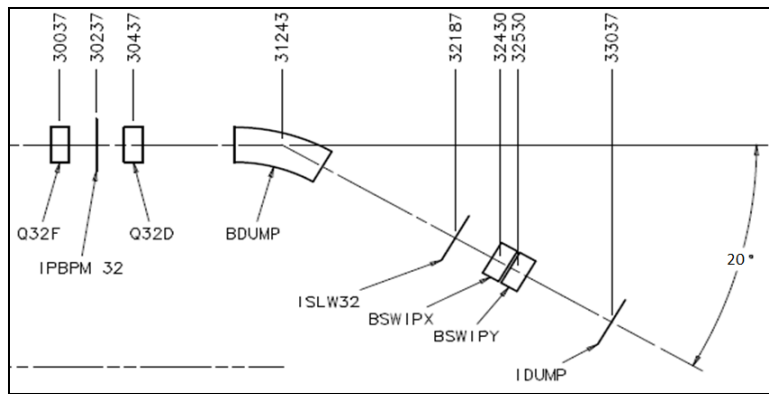


**Figure 8.4:** Mechanical Engineering layout of the end of the diagnostics line and the beam dump.

The primary beam dump is to be designed for continuous operation with 50 kW 30 MeV beam. The dump has to have radiation shielding so that the outgoing radiation would not exceed 0.1% of the radiation corresponding to 100% loss in an unshielded area. This local dump shielding reduces radiation to the level sufficient to avoid accelerator equipment degradation and to have residual radiation sufficiently small for servicing the accelerator (see Section 10). Taking

into account that for low energy beam with fixed power the radiation grows fast with energy the radiation shielding estimate was carried out for the maximum energy expected to be achieved in the PXIE. Corresponding beam parameters are presented in Table 8.2.

**Table 8.2:** Beam parameters used for radiation shielding estimate

Parameter	Value	Units
Energy	30	MeV
Beam current	1.7	mA
Beam power	50	kW
H flux	$3.7 \times 10^{19}$	Ions/hr
Operation time	2300	hrs/year
Total particles to absorber	$8.5 \times 10^{22}$	Ions/year

*Absorber geometry and materials*

The proposed absorber system consists of a long cylinder capped at the downstream end. Six poles sweeping magnets, powered by 3-phase 60 Hz source will produce rotating deflecting magnetic field just upstream of the absorber. A cross section of the proposed magnet and list of basic parameters are shown in Figure 8.5. The amplitude of deflecting angle can be varied in range of 1 - 2° to impinge at a oblique angle on the inside surface of the cylinder. Figure 8.6 shows the proposed layout of the sweeping magnet and absorber geometry and the density of the power losses in absorber. In the current proposal, the absorber is sized for a 2° deflecting angle.

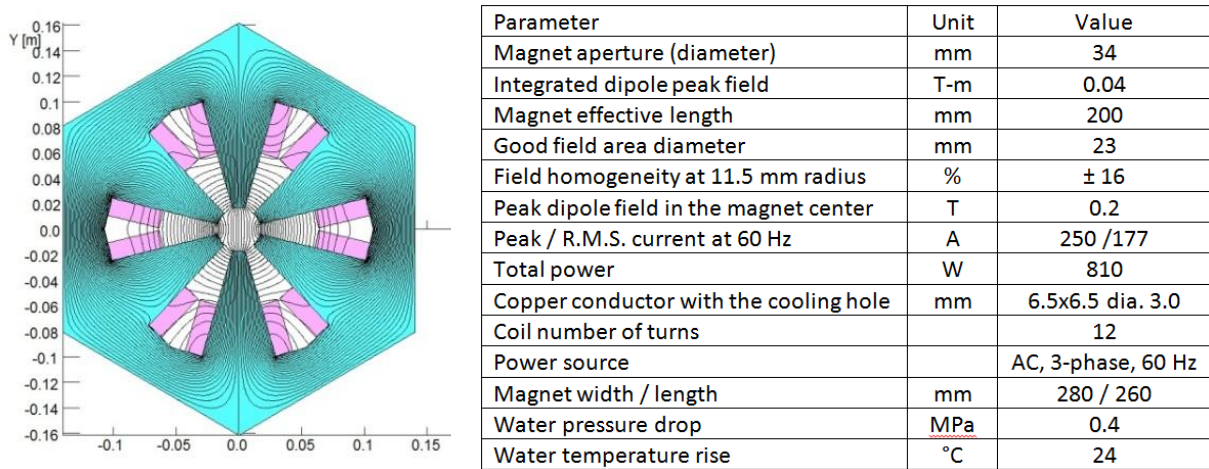


**Figure 8.5:** Magnet cross section of proposed sweeping magnet and parameters.

If the absorber can be made longer then the amplitude to the sweeping magnets may be modulated to effectively paint the beam over a larger area. This would reduce not only the temperature but spread the energy deposition over a larger area.

Due to grazing incidence approximately 25% of the particles are forward scattered from the surface with much wider energy and angular distributions ( $\sigma_E = 7.4$  MeV,  $\sigma_\theta = 6^\circ$ ). The process was simulated by the code SRIM [1] used to investigate the effects of the back scattering and sputtering in the beam dump. The forward scattered particles carry out approximately 6% of the power of the incident beam and impinge on the rear inner surface of the absorber resulting in a density of power dissipation almost order of magnitude smaller than in the cylindrical part of absorber. The simulation for  $2^\circ$  incident angle also shows that the maximum penetration depth in the absorber material is substantially different for the forward scattered ( $MD_{fs} = 13.9 \pm 11.2$   $\mu\text{m}$ ) and stopped in material particles ( $MD_{stop} = 86.3 \pm 55.6$   $\mu\text{m}$ ).

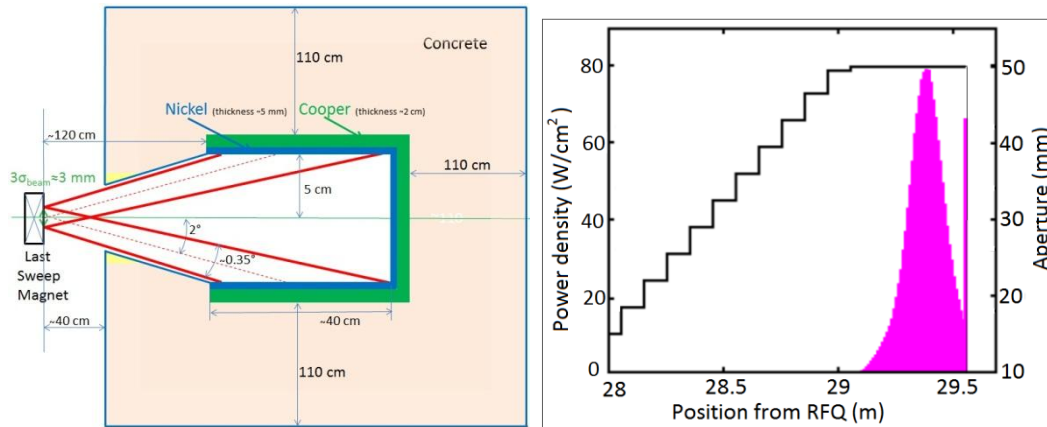


**Figure 8.6:** A sketch of the beam dump (not to scale), including the first layer of its local radiation shielding (left). Red lines show sweeping of the beam. Right: beam power distribution in the absorber (magenta).

The absorber material must have at least a 5 years lifetime under assumed irradiation conditions. Material of its receiving surface has to be chosen to minimize neutron flux. The blistering and sputtering properties of this material are also important. Several materials were considered as candidates for the inner surface of the absorber: graphite, aluminum, copper, and nickel. The current choice for the primary absorber material is nickel [2]. Nickel has good thermal properties, low residual activation, can be brazed to copper and has a stopping range (at 30 MeV a  $90^\circ$  incident angle) of 1950  $\mu\text{m}$ . At the proposed incident angle of  $2^\circ$  the stopping depth from the surface is  $\sim 70$   $\mu\text{m}$ , consistent with SRIM simulations. Further analysis of the absorber material is needed, including expanding the list of material to be considered.

#### *Effects of sputtering, blistering and flaking*

Protons penetrating inside a material are trapped and form gas molecules clustered near defects. The gaseous ions create bubbles with high pressure causing blistering and flakes. Bad thermal contact with surface causes material evaporation with higher exposition. This is the mechanism for surface erosion. Typically, first blistering is observed at deposition in the range of  $\sim 10^{21}$ -  $10^{24}$  ions/ $\text{m}^2$ ; above  $10^{23}$  ions/ $\text{m}^2$  flakes and blisters start to be eroded by sputtering.

Nickel is considered to be one of the best materials for reactor walls; blistering in nickel starts later than in many other materials (Cu, AL, Nb, Mo etc.) [3]. Taking into account this rate, the surface of the dump of  $\sim 0.1 \text{ m}^2$  and the total expected particle flux per year we estimate that the lifetime of the absorber with 5 mm nickel thickness is  $\sim 10$  years. We assume the penetration length in nickel to be  $\sim 70$  microns for  $2^\circ$  incident angle and that this layer will be removed when fluence exceeds  $10^{23}$  ions/m<sup>2</sup>.

#### *Absorber cooling*

The current proposal utilizes copper cooling channels just outside the nickel cylinder with parallel channels looped around its surface. The cooling water enters at the rear of the absorber passes through the channels and comes out at the front of the absorber. A number of cooling channel and their sizes will be adjusted so that the temperature rise of the absorber water cooled wall would be in the range of  $30\text{-}40^\circ \text{ C}$ . Temperature inside absorber at the nickel surface is expected to below  $120^\circ \text{ C}$ . Based upon the power density and the cooling water flow, cooling does not seem to be an issue.

#### *Radiation shielding*

The requirements for local shielding are determined by Fermilab radiation safety standards. The proposed configuration of the shielding (walls and ceiling thickness, labyrinths, and various penetration) is based on an assumption of a 5-W uncontrolled single-point beam loss in the PXIE beamline. This means that local shielding of the dump should provide at least a  $10^{-3}$  attenuation of prompt radiation. Conceptual design for the dump and local radiation shielding is shown in Figure 8.6. The dump itself with the 50-kW beam power has local shielding, designed as a concrete cube with  $\sim 230\text{-cm}$  sides. Outside of the enclosure, the radiation level should not exceed  $0.5 \text{ mrad/hrs}$ . Radiation shielding design is based on simulations performed with the MARS code and described in Section 10.

An absorber baffle is installed at the front surface of the absorber to protect the sweeping magnets from radiation coming out of absorber.

#### *Instrumentation and Interlocks*

At minimum we would like to monitor the absorber temperature and vacuum pressure to assure integrity of the dump.

Interlocks designed to protect the absorber hardware must be integrated into the machine protection system. For example, in case of sweeping magnet failure the beam should be prohibited from being accelerated. In addition, we envision interlocks on the water system, vacuum system, absorber temperature, or excessive or unusual loss pattern. Design of this system has not started yet.

## References

1. J.F. Ziegler, J.P. Biersack, M.D. Ziegler. “SRIM – The Stopping and Range of Ions in Matter”. <http://www.srim.org/SRIM/SRIMLEGL.htm>.
2. N.Mokhov, “HINS Beam Absorber MARS15 Simulations”. [http://beamdocs.fnal.gov/AD/DocDB/0035/003597/002/HINS\\_mokhov\\_042810.pdf](http://beamdocs.fnal.gov/AD/DocDB/0035/003597/002/HINS_mokhov_042810.pdf).
3. “Sputtering by Particle Bombardment II”. Editor R. Behrisch, Springer-Verlag, 1983.
4. Yu. Eidelman, et. al. “the Conceptual design of the Shielding Layout and Beam Absorber at the PXIE”, IPAC12 paper
5. Yu. Eidelman, Power point presentation, private communication, ProjectX docDB
6. Vladimir Kashikhin, PXIE magnets for Dump, ProjectX docDB.

# 9. Facility Layout

Richard Stanek

## Site Description

PXIE will be installed and operated in a new concrete block enclosure to be built in the Cryomodule Test Facility (CMTF) building located near the New Muon Lab (NML) building. The PXIE enclosure will be adjacent to the Cryomodule Test Stand (CMTS). Both enclosures will be serviced by the new superfluid cryogenic plant. Support equipment, electronics and RF power stations will be positioned near the enclosures in the open area and on the second floor mezzanine. Plan and elevation views of the enclosure are shown in Figures 9.1 and 9.2, respectively.

The enclosure will contain all of the PXIE elements including the ion source, LEBT, RFQ, MEBT, HWR and SSR1 cryomodules, the diagnostic section and the beam dump. The high energy end labyrinth of PXIE will be shared with CMTS. A second labyrinth located at the low energy end of the PXIE enclosure will serve as the main entrance to the PXIE enclosure. The cryogenic lines for the HWR and SSR1 cryomodules will penetrate the enclosure vertically through the upstream ceiling section away from the higher energy areas. RF transmission lines and supporting signal and instrumentation cables will enter the PXIE enclosure through specially designed header shielding blocks intended to provide adequate radiation attenuation and located at the low energy end of the enclosure. It is desired to have a short path for the signal and instrumentation cables. Such cables for the diagnostic section will enter the enclosure through a penetration located near the downstream end. This penetration will be designed for use in a higher energy beam loss area.

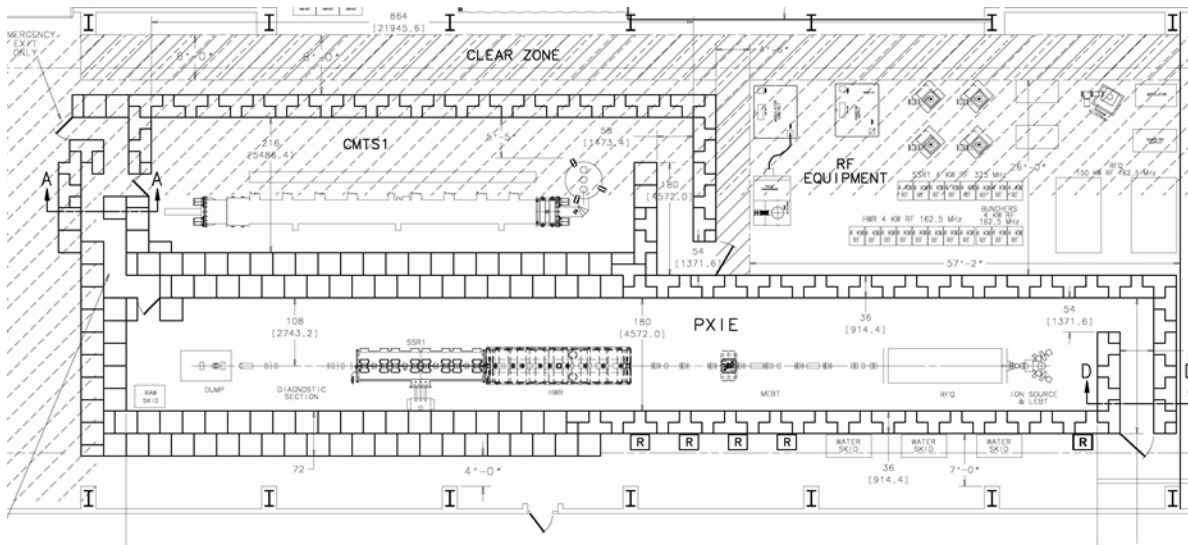
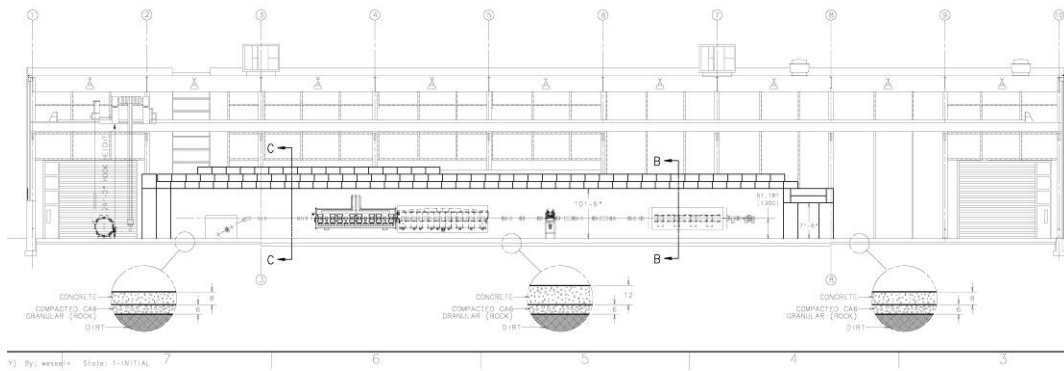


Figure 9.1: Plan view of PXIE CW linac and CMTS concrete enclosures within CMTF

The PXIE concrete enclosure will be built with overlapping, prefabricated concrete shielding blocks. The low energy walls will be 3 feet thick and constructed from T-shaped concrete blocks to allow overlap and eliminate straight seams. The high energy walls will be 6 feet thick and made from rectangular shaped blocks arranged in a dual-layer overlapping pattern. The concrete block ceiling is a minimum of 3 feet thick; however, a significant section of the ceiling beginning midway through the HWR cryomodule and ending just downstream of the beam dump will be 4.5 feet thick. The ceiling block layout will allow for easy removal and stacking thereby enabling larger components to be placed in position using the building's overhead 20 ton crane. The exact arrangement of concrete shielding blocks will be consistent with the PXIE Radiation Shielding Assessment.



**Figure 9.2:** Elevation view of PXIE CW linac in concrete enclosure within CMTF.

The plan for layout of the PXIE/CMTF facility is to construct a 3D CAD model of the building, shielding cave and beamline elements. Through the use of this technology, the exact positions as well as accurate lengths for connecting piping and cabling can be determined. Priority will be given to achieving the optimum layout for components that are costly to construct such as RF coax transmission lines and cryogenic transfer lines. The PXIE/CMTF project team will also develop a set of standards for items such as valves, seals, connectors, and instrumentation so that each element type will be consistent within the facility.

## 10. Shielding and Radiation safety

Valeri Lebedev, Yuri Eidelman, and Anthony Leveling

### Method of Shielding Assessment

The Accelerator Division requirements for the conduct of radiation shielding assessments are given in ADSP-02-0110. The scaling rules used to define the “Shielding Requirements” mentioned in ADSP-02-0110 are only applicable at energies above 1 GeV and break down entirely in the energy range relevant to PXIE. More appropriate energy scaling formulae to determine source terms and attenuation factors for the PXIE shielding assessment are described below (see also [1]).

The upstream half of the PXIE accelerator transports and accelerates  $H^-$  beam to 2.1 MeV. This beam energy was chosen in part to avoid the production of ionizing radiation including neutrons by the  $H^-$  beam [2]. In addition, materials chosen for the low energy sections of the accelerator have been verified to have no significant production cross sections for neutrons by the 2.1 MeV  $H^-$  beam. Consequently, the evaluation of the enclosure shielding, labyrinths, and penetrations is based upon potential beam loss in the downstream half of the PXIE accelerator beginning with the HW cryomodule.

The HW and SSR1 cryomodules are intended to be operated with very high efficiency and extremely low losses. Beam current monitoring of the machine protection system will be developed to limit losses between the upstream end of the HW cryomodule and the downstream end of the Diagnostic Section below 0.1%. Beam losses in the HW and SSR1 cryomodules must be limited to prevent damage to those cryomodules. Losses even approaching 0.1% can lead to degraded cryomodule performance and must be prevented for machine protection.

The preliminary shielding assessment [1] determined that the allotted space for PXIE at the Cryomodule Test Facility is not sufficient to accommodate a totally passive radiation shield design. From the preliminary assessment, it is clear that interlocked radiation detectors are required to be used in conjunction with passive shielding in order to meet both the experimental requirements for beam power and the FRCM requirements for health and safety. Thus, the shielding estimate is based on the requirement that the permanent or long time losses cannot exceed 0.01% (5 W) at full energy and that the interlock systems (based on monitoring of radiation in and outside PXIE enclosure) stops the beam operation if this threshold is exceeded. This implies that the beam dump, which has to accept up to 50 kW of beam power at 30 MeV, has to have local shielding which suppresses its radiation by not less than by a factor of  $10^4$ .

Figure 10.1 presents the simulation of local shielding using the MARS code. Shielding consists of concrete cube with shielding layer thickness of 110 cm. The simulation showed that for the PXIE energy such shielding delivers better protection than a combined steel-polyethylene

shielding of the same thickness. As is evident from the data shown in the figure, this shielding provides attenuation of radiation of about 60,000 times.

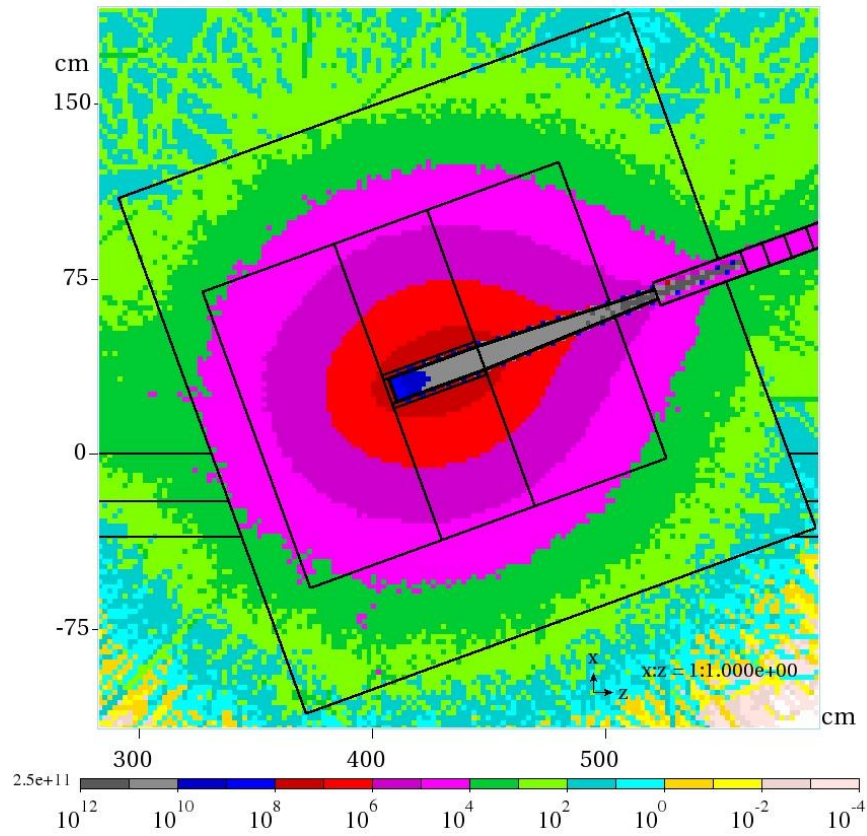


**Figure 10.1:** Results of MARS simulation of the beam dump radiation shielding.

### PXIE Radiation Dose Rate Design Goals

The design goals for radiation dose rates outside the PXIE shielding enclosure are based upon the intended occupancy and are selected from limits permitted by the Fermilab Radiological Controls Manual [3]. The locations and intended radiation dose rates limits for normal and accident conditions are included below in Table 10.1.

### Assessment Parameters and Methodology

The low beam energy radiation source term, the low energy neutron attenuation through concrete, and the off-axis correction factors were used in the HINS shielding assessment [4]. Taking into account PXIE close parameters we use the same equations which are reproduced below.

An established parameterization of Ref. [5] determines the radiation dose equivalent rate as a function of energy, distance, and angle from a low energy proton beam (<1 GeV) incident upon a target:

$$S(E, r, \theta_s) = 2 \times 10^{-5} (1 + E^{0.6}) \left( \frac{1 - e^{-3.6E^{1.6}}}{\left(0.3048r \left(\theta_s + \frac{40}{\sqrt{E}}\right)\right)^2} \right), \quad (1)$$

where  $S$  is the dose equivalent source term (mrem/proton) as a function of proton energy  $E$  (GeV), the distance  $r$  (feet) from the loss point, and  $\theta_s$  (degrees) with respect to the incident proton beam direction.

**Table 10.1: Normal and accident condition radiation dose rate design goals by location for the PXIE enclosure**

Location	Condition	Radiation Dose Rate limit (mrem/hr)	Permitted FRCM Occupancy	Required FRCM Radiologic Postings
Perimeter at floor level around PXIE enclosure	Normal	<0.05	No precautions needed.	No posting required
Perimeter at floor level around PXIE enclosure	Accident	< 1	No precautions needed.	No posting required
PXIE enclosure ceiling	Normal	<0.25	No occupancy limits imposed.	Controlled Area
PXIE enclosure ceiling	Accident	<1	No precautions needed.	Controlled Area

A geometric correction factor,

$$f(R, D) = \cos \left[ \tan^{-1} \left( \frac{D}{R} \right) \right] = \frac{R}{\sqrt{R^2 + D^2}}, \quad (2)$$

is required to adjust the source term at the entrance of labyrinths and penetrations. It takes into account the source term strength when the radiation source is not placed directly in the entrance to a labyrinth or penetration.

For neutron energies below 100 MeV, the attenuation length in concrete is significantly shorter than that for neutrons considered in higher beam energy based assessments. For example,

for high energy shielding problems, 3 feet of concrete provides a reduction factor of 10 in radiation dose rate. The mean free path of low energy neutrons relative to the high energy asymptote has been parameterized in Ref. [5]:

$$\frac{\lambda_{LE}}{\lambda_{HE}} = 1 - 0.8e^{-5E} \quad (3)$$

where the energy dependence of the mean free path for neutrons passing through concrete given as a ratio with respect to its high energy asymptote value,  $\lambda_H$ , and  $E$  is the neutron energy in GeV. Consequently, the reduction in radiation dose rate as a function of energy and concrete thickness is:

$$A(E, T_{conc}) = 10^{\frac{-T_{conc}}{3}(1-0.8e^{-5E})} \quad (4)$$

where  $A$  is the reduction factor achieved by a concrete shield of thickness  $T_{conc}$  (feet) due to a beam loss of protons of energy  $E$  (GeV)

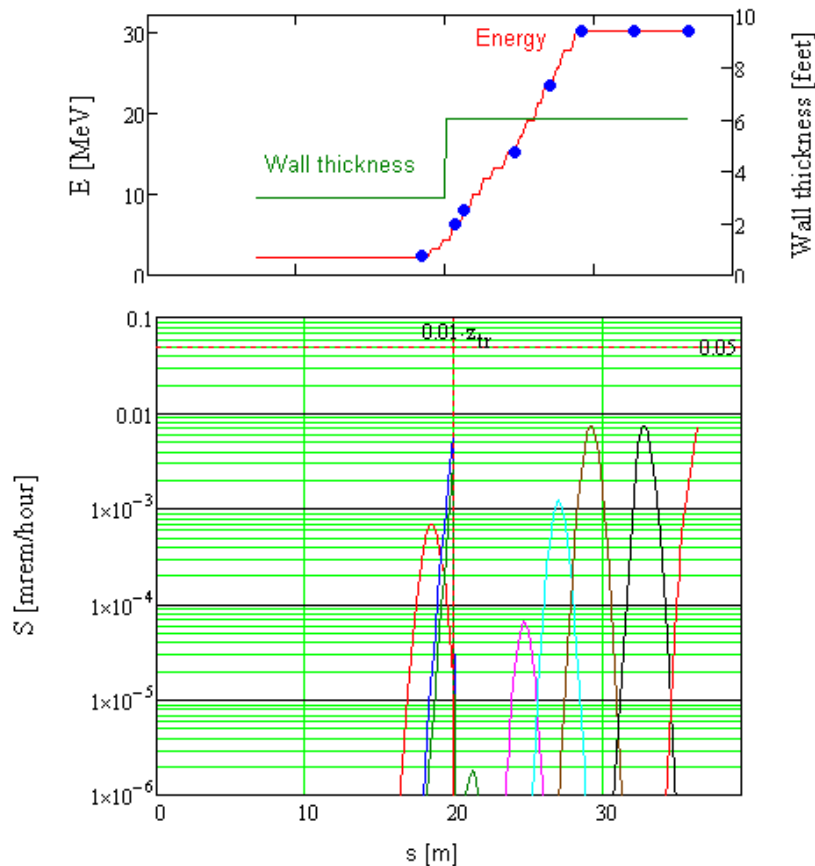


**Figure 10.2:** Dependence of beam energy and the wall thickness (top) and radiation level behind the eastern wall on the longitudinal coordinate in the enclosure.

## Radiation Shielding estimate

Figure 10.2 presents dependences of radiation dose rates behind the enclosure eastern wall for 0.1% beam loss located at longitudinal position marked by corresponding blue dot at the top graph. The dependencies were calculated using Eqs. (1)-(4). One can see that the dose rate does not exceed the limit of 0.05 mrem/hour for the loss at any longitudinal position. In the dose rate calculations presented in Figure 10.2, the peak neutron energy  $E$ , is taken to be equal to the beam energy.

This simplification is conservative in that the real neutron energies are necessarily lower and hence lead to better attenuation provided by the concrete shielding than indicated by calculations. In addition, the dose equivalent per neutron conversion factor is taken as a constant value of 40 fSv/n over the range of the neutron spectrum. Consequently, the resulting shielding calculations for the PXIE shielding assessment are implicitly conservative.

The MARS simulation of radiation Shielding More detailed dose rate distributions were computed using MARS code. The results are presented in Figures 10.3 - 10.5. Corresponding layout of the enclosure presented in Figure 10.6. As one can see the MARS simulations validate the presented above picture.

PXIE is an experimental facility and we expect frequent accesses to the enclosure. Therefore keeping low residual dose in the enclosure is an important requirement. As one can see in Figure 10.5, the suggested thickness of the dump shielding is sufficient to keep the dose rates below 100 mrem/hour. The technical design of the beam dump has not started yet. However the above calculations verify that the space allocated for the beam dump is sufficient and the overall shielding of the enclosure is adequate to the PXIE operational scenario and the expected beam loss.

## References

- [1] A. Leveling, "PXIE Preliminary Shielding Assessment," <http://projectx-docdb.fnal.gov:8080/cgi-bin/ShowDocument?docid=1051>.
- [2] Yu. Eidelman. "Analysis of Material for MEBT Absorber," <http://projectx-docdb.fnal.gov/cgi-bin/ShowDocument?docid=986>.
- [3] Fermilab Radiological Control Manual <http://esh.fnal.gov/xms/FRCM>.
- [4] HINS Linac shielding assessment, Project X document 655-v22
- [5] "A Guide to Radiation and Radioactivity Levels Near High Energy Particle Accelerators": A. H. Sullivan, Nuclear Technology Publishing, (1992).

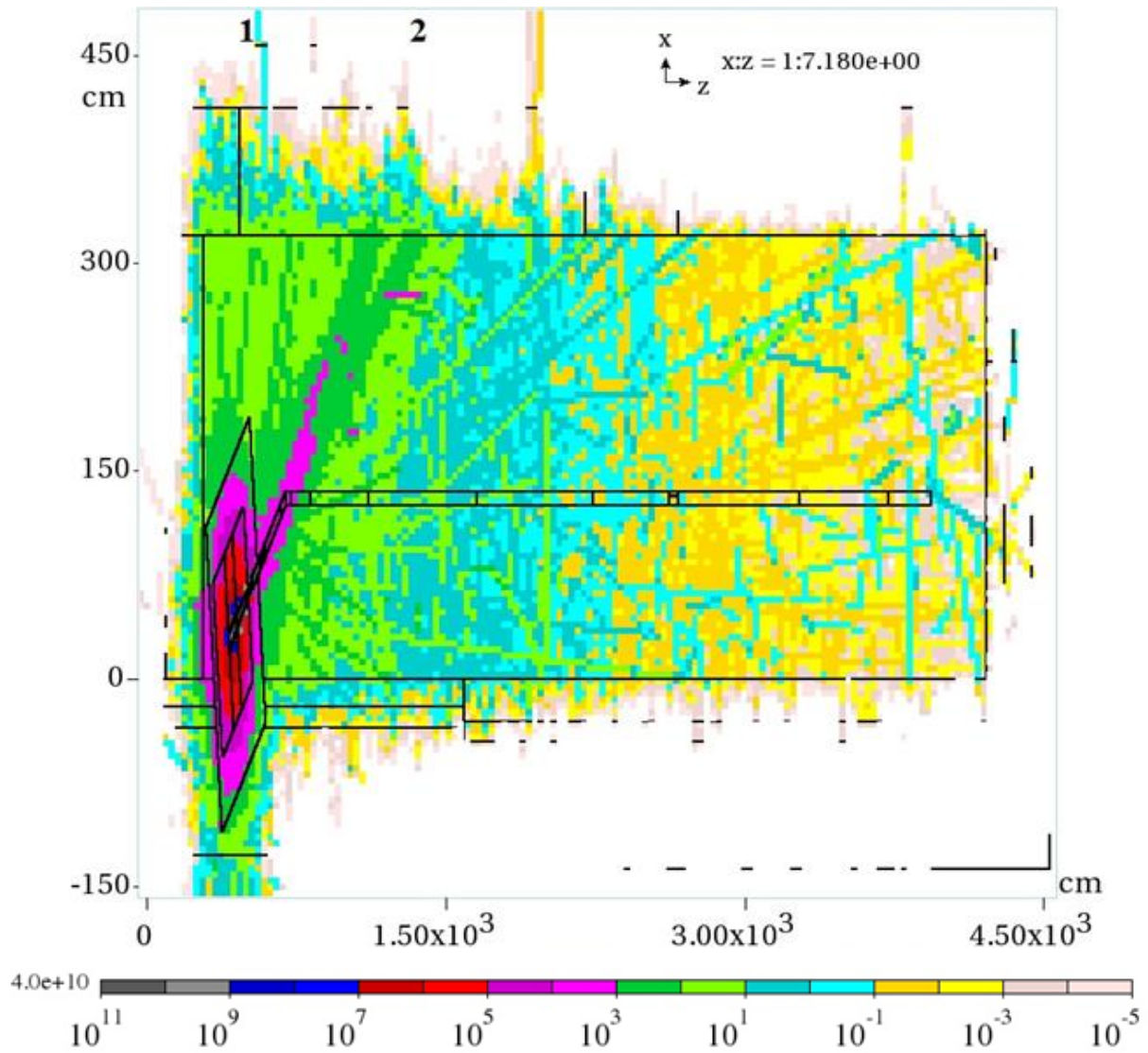


**Figure 10.3:** Total Effective Dose (vertical slice through beam dump) for 50 kW proton beam absorbed in the beam dump (1 mSv/h = 100 mrem/h).

Point	1	2
TED, mSv/hr	$5.0 \cdot 10^{-3}$	$3.5 \cdot 10^{-6}$

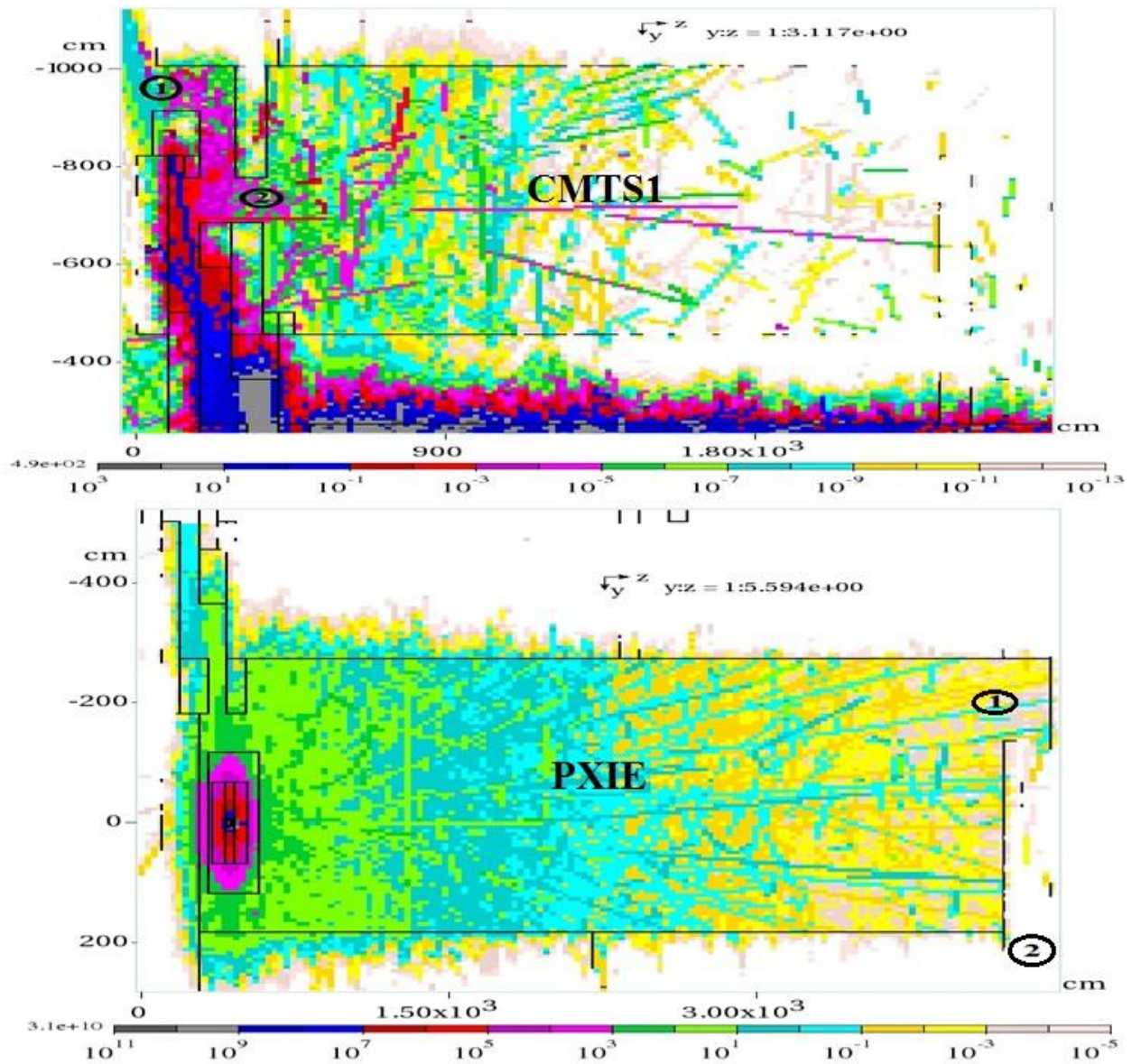


**Figure 10.4:** Total Effective Dose (horizontal slice through beam dump) for 50 kW proton beam absorbed in the beam dump for the CMTS (top) and PXIE (bottom) enclosures

(1 mSv/h = 100 mrem/h).

Point	1	2	1	2
	PXIE Hall	PXIE Hall	CMTS Hall	CMTS Hall
TED, mSv/hr	$(2.1 \div 5.3) \cdot 10^{-5}$	$(.57 \div 1.43) \cdot 10^{-6}$	$4.82 \cdot 10^{-7}$	$4.21 \cdot 10^{-5}$

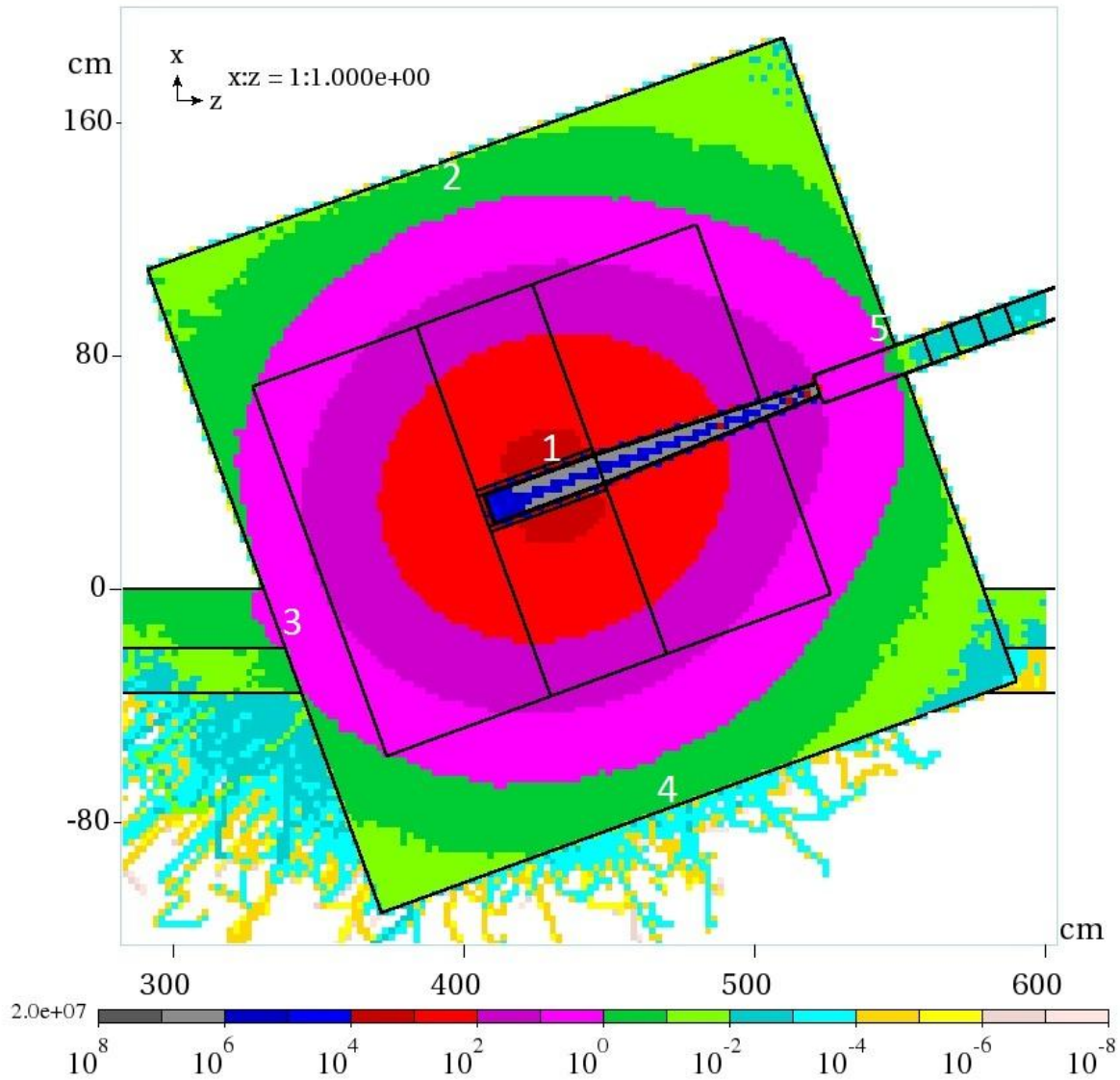


**Figure 10.5:** Distributions of the Contact Residual Dose (30 days irradiation, 1 day cooling);  
(1 mSv/h = mrem/h).

Point	1	2	3	4	5
CRD, mSv/hr	1270±1.5	.1876±.011	2.025±.0487	(2.54±0.13)10 <sup>-2</sup>	.5445±.025

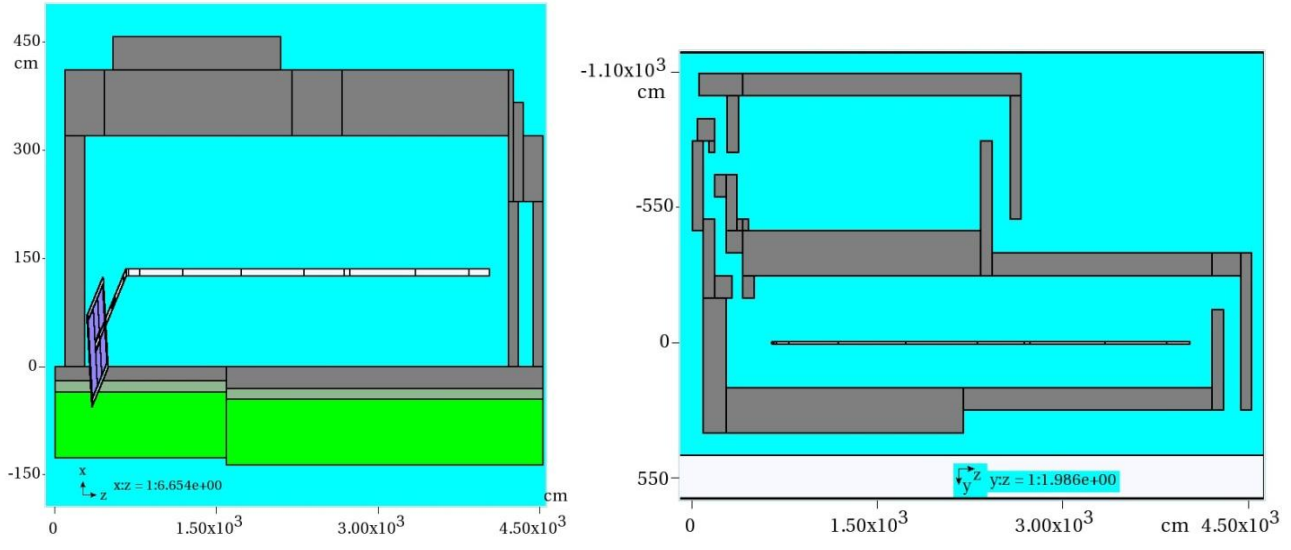


**Figure 10.6:** Layout of the enclosure used in MARS simulations.

# 11. Beam Instrumentation

Vic Scarpine

## Introduction

The successful characterization and operation of PXIE places stringent requirements on the performance of its beam diagnostics. Crucial beam measurements include bunch currents, beam orbit, beam phase, bunch length, transverse profile and emittance and beam halo and tails, as well as the extinction performance of the MEBT. Table 11.1 give a list of measurements and proposed beam diagnostic instruments for PXIE.

**Table 11.1:** PXIE beam measurements and proposed instruments.

Measurement	Instruments
Beam current	DCCT, toroid, resistive wall current monitor
Beam orbit	Button-style BPMs with digital read-out electronics
Beam energy and phase	BPMs, time-of-flight and spectrometer in dump beamline
Transverse profile	Wire scanner, laser-wire
Beam transverse emittance	Allison scanner, slit and wire scanners, laser-wire
Longitudinal profile	Feschenko-style wire monitor, mode-locked laser-wire, fast Faraday cup
Beam extinction measured in MEBT	Broad-bandwidth resistive wall current monitor
Beam extinction measured in the diagnostics line	Single particle detector
Transverse halo	Vibrating wire, collimators, laser-wires, wire scanners
Longitudinal tails	Feschenko-style wire monitor, mode-locked laser-wire

## LEBT Beam Diagnostics

The primary function of beam diagnostics in the LEBT is to characterize and tune the beam during operations. The quality of the beam out of the source will be monitored by periodically measuring the vertical and horizontal transverse emittance using a pair of Allison scanners. Because these scanners are upstream of the LEBT beam chopper, they will need to be water-cooled in order to operate up to 300 W of beam power.

For transverse emittance measurements, the function of the Allison emittance scanners are to map both the vertical and horizontal transverse phase space of the beam ( $x - x'$  and  $y - y'$ ). These scanners will primarily be used to measure beam quality out of the ion source during normal PXIE beam operations. In addition, during LEBT commissioning (before the arrival of the RFQ) these scanners will be used to measure beam at the end of the LEBT. Table 11.2 gives a list of functional requirements for the LEBT transverse emittance measurements [1].

The LEBT current measurement will require a bandwidth from DC to  $\sim 1$  MHz over a current range of  $\sim 0.1$  to 10 mA. Because of the broad bandwidth, beam current will be measured in the LEBT using a DC Current Transformer (DCCT) and a beam toroid. Ideally, the DCCT and toroid are positioned after the LEBT chopper in order to measure both nominal DC beam (DCCT) as well as chopped beam (toroid) entering the RFQ.

**Table 11.2:** LEBT transverse emittance measurement requirements.

Parameter	Value	Units
Measurement planes	2 (horz. and vert.)	
Position measurement range (from beam center)	$\pm 30$	mm
Position measurement resolution	100	$\mu\text{m}$
Angular measurement range	$\pm 80$	mrad
Angular measurement resolution	0.5	mrad
Phase density dynamic range	$10^3$	
Max. beam power dissipation	300	W
Min. beam radius (2 rms)	0.5	mm
Max. power density	375	$\text{W}/\text{mm}^2$
Time slice resolution	1	$\mu\text{sec}$
Measurement time (for 60 position steps)	$\leq 60$	s
Fully retracted position (from beamline center)	40	mm

To measure the beam halo in the LEBT, electrically isolated beam absorbing sleeves will be placed at various locations. Beam impacting these sleeves will be collected similar to a Faraday cup and measured by the instrumentation data acquisition system. It is planned to have these sleeves inside each of the three LEBT solenoids.

At the end of the LEBT, an insert-able Faraday Cup-like device will be located just before the RFQ entrance. This Faraday Cup will stop beam from entering the RFQ as well as measure the beam current at this point. In addition, an insert-able electrically isolated aperture will be part of this Faraday Cup device. This aperture will work similar to the electrically isolated LEBT sleeves and provide a measure of the beam halo at the entrance of the RFQ.

### MEBT Beam Diagnostics

The primary functions of the PXIE MEBT are (1) to match optical functions between the RFQ and the superconducting HWR cryomodule and (2) to generate arbitrary bunch patterns at 162.5 MHz using an integrated wide-band chopper and beam absorbers, capable of disposing of 5 mA average beam current [2]. In addition, the MEBT will include beam diagnostics to measure the beam properties coming out of the RFQ and into the HWR cryomodule.

Two MEBT operating conditions put strict requirements on the choice of beam diagnostics. First, because of the nominal high beam power in the MEBT, beam-intercepting diagnostics can operate only with LEBT chopped beam. However, there is still danger of damage to the

intercepting diagnostics causing possible contamination to the downstream superconducting cavities. To remedy this, we will also utilize non-intercepting laser wire diagnostics for beam profiling. Second, to verify the operation of the arbitrary bunch wide-band chopper, bunch-by-bunch extinction must be measured to a level of  $10^{-4}$ .

In the MEBT, beam position and phase will be measured using button-style BPMs. Eleven BPMs will be used in the MEBT in order to initially phase-in the multiple RF cavities and to adequately monitor the performance of the beam through the MEBT. Table 11.3 gives the beam measurement requirements for the BPM system.

**Table 11.3:** BPM measurement requirements.

Parameter	Value	Units
Transverse resolution	0.1 (for single 1 ms macro-pulse) 0.01 (CW)	mm
Transverse accuracy (absolute)	1	mm
Phase resolution	0.1	deg (at 162.5 MHz)

Horizontal and vertical transverse beam profile measurements in the PXIE MEBT will be made with a combination of wire scanner and laser wire module. This combined module will save space and allow for cross-comparisons between the two profiling devices. Transverse beam profiles will be measured in two locations in the MEBT, (1) near the output of the RFQ before the chopper section and (2) after the chopper section before the entrance to the HWR cryomodule.

Because wire scanners are a proven technology, they will be used to make initial profile measurements. However, to minimize beam interaction, they will rely on short pulsed beam, generated by the LEBT chopper. Laser wires will be commissioned and relied on as the primary beam profile instrument for CW operations with the wire scanners as a fallback instrument. Further discussion of the laser-wire follows below.

Transverse beam emittance will be periodically measured in the MEBT using a standard slit-wire scanner method. The emittance will be measured at the location of the first wire scanner, just after the output of the RFQ. This slit-wire scanner combination will map both the vertical and horizontal transverse phase space of the beam ( $x - x'$  and  $y - y'$ ) and primarily measure the beam quality out of the RFQ. Since this system intercepts the entire beam, it will only be used with short pulsed beam generated by the LEBT chopper.

Longitudinal beam profiles in the PXIE MEBT will be made primarily with a mode-locked laser-wire system additionally locked to the MEBT rf system. The longitudinal profile is measured by scanning (in time) a short-pulse ( $\sim$  few ps) laser pulse through many bunches.

Further discussion of the laser-wire follows below. In addition, during commissioning of the MEBT, longitudinal profiles will be measured with a beam intercepting Feschenko-style wire monitor [3]. This device will be used to cross-check the mode-locked laser-wire system.

Transverse beam halo will be measured in the MEBT utilizing a number of instruments including wire-scanners, laser-wires, vibrating-wires and electrically isolated beam scrappers. It is expected that all of these techniques will be necessary to cover the entire dynamic range required to measure halo.

As part of the MEBT chopper design, unwanted chopped bunches are directed to an absorber located in the vicinity of the beam passing. To monitor the operation of the chopper system, it is desirable to measure the position and shape of the deposited beam on the absorber. Monitoring of the MEBT chopped beam onto the beam absorber will be measured using either Optical Transition Radiation (OTR) or infrared imaging.

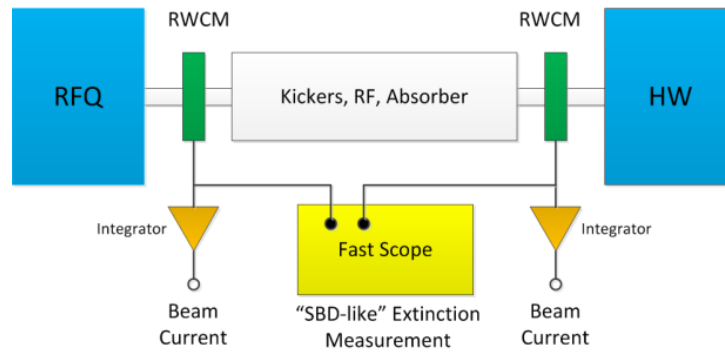


**Figure 11.1:** PXIE MEBT beam current and extinction measurements.

**Table 11.4:** MEBT beam current and chopper extinction measurement requirements.

Parameter	Value	Units
Beam current range	0.05 to 10	mA
Beam current resolution	0.05	mA
Beam current bandwidth	~0.01 to ~2	MHz
Relative resolution of chopped bunch extinction	$< 10^{-4}$	
Bunch extinction measurement bandwidth	~ 1	Hz

#### *MEBT Beam Current and Chopper Extinction Diagnostics*

In order to monitor the operation of the MEBT wide-band chopper, beam diagnostics will need to measure the bunch-by-bunch extinction level [2]. PXIE plans on utilizing a wide-band Resistive Wall Current Monitor (RWCM) initially tested at EMMA [4]. The RWCM has a relatively flat frequency from 10 kHz up to ~ 4 GHz. This enables the RWCM to see individual bunches in the MEBT. Two RWCM signals will use fast integrators to measure the beam current before and after the chopper. The average bunch extinction level will be measured using a high-

bandwidth oscilloscope similar to the Fermilab Sampled Bunch Displays [5]. Table 11.4 gives a list of key requirements for the beam current and chopper operation and Figure 11.1 shows a block diagram of the system in the PXIE MEBT.

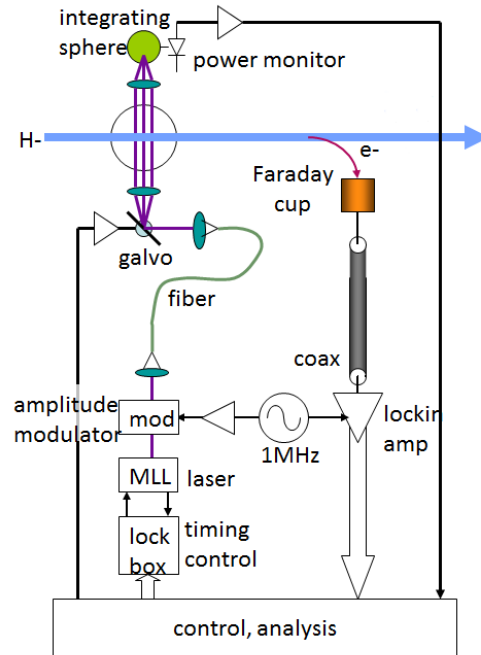


**Figure 11.2:** Fiber optic laser distribution system with synchronous detection for transverse and longitudinal beam profile measurements.

### *Laser Diagnostics for Beam Profiling*

We are pursuing the use of lasers to obtain non-invasive measurements of both longitudinal and transverse profiles of  $H^-$  beam via photo-detachment,  $H^- + \gamma \rightarrow H^0 + e^-$ . Other accelerators, such as SNS, have commissioned transverse beam profiling using a high-power Q-switched Nd:YAG laser [6]. In addition, they have also demonstrated longitudinal beam profiling using 2.5 ps laser pulses from a mode-locked Ti:Sapphire laser [7]. These systems use high peak laser power to saturate the photo-detachment process.

In general, these systems suffer from vibration and temperature drift issues due to the need to transport intense laser pulses from outside the beamline enclosure to the individual profile monitors [6]. To mitigate these issues, we plan to use fiber optics to transport the lower power laser pulses. One technique would distribute low-power, amplitude modulated laser pulse trains via optical fibers. Since lower laser power will not drive the photo-detachment process into saturation, amplitude modulation of the laser pulses with synchronous detection will be used to measure the weaker detached electron signal. Figure 11.2 shows a block diagram of a proposed laser-wire setup using a 1 MHz amplitude modulation [8].

## Cryomodule Beam Diagnostics

The primary functions of beam diagnostics in the cryogenic region of PXIE MEBT are to (1) measure the beam position and phase inside the HWR and SSR1 cryomodules and (2) to measure the beam profiles between the two modules. The beam position and phase will be measured using cryogenic BPMs inside each cryomodule. There are six BPMs inside the HWR cryomodule and four BPMs inside the SSR1 cryomodule. These BPMs will have the same functional requirements as the warm BPMs in the MEBT and test beamline, which are shown in Table 11.3.

Because of the limited space between HWR and SSR1 and the sensitivity of the superconducting cavities to beam loss and contamination, conventional wire scanners cannot be used to measure transverse beam profiles. PXIE will utilize a mode-locked laser-wire, similar to the MEBT laser-wire, between HWR and SSR1 to measure beam profiles. Because there is no space for an electron collector, the beam profiles will be determined by using the SSR1 BPMs to detect synchronous signal in  $H^-$  beam intensity. The use of a short-pulse mode-locked laser allows for both transverse and longitudinal beam profiles to be acquired.

## Test Beamline and Dump Beam Diagnostics

Beam diagnostics for the test beamline and dump beamline are discussed in Chapter 8 of this handbook.

## References

- [1] V. E. Scarpine, “PXIE LEBT Beam Transverse Emittance Station FRS,” Project X Document 1077.
- [2] V. Lebedev et al., “Progress with PXIE MEBT Chopper,” IPAC’12, New Orleans, LA, April 2012, WEPPD078, <http://www.JACoW.org>
- [3] A. Feschenko, “Methods and Instrumentation for Bunch Shape Measurements,” PAC01, Chicago, June 2001, RAOB002, <http://www.JACoW.org>.
- [4] A. Kalinin et al., “The EMMA Accelerator, A Diagnostic Systems Overview,” IPAC’11. San Sebastian, Spain, September 2011, WEPC158, p. 2355. <http://www.JACoW.org>
- [5] R. Thurman-Keup et al., “Longitudinal Bunch Monitoring at the Fermilab Tevatron and Main Injector Synchrotrons,” JINST, 6 (2011) T10004.
- [6] Y. Liu et al., “Laser Wire Beam Profile Monitor in the Spallation Neutron Source (SNS) Superconducting Linac,” Nuclear Instruments and Methods in Physics Research A 612 (2010) 241.

- [7] S.Assadi, “SNS Transverse and Longitudinal Laser Profile Monitors Design, Implementation and Results,” EPAC’06, Edinburgh, Scotland, June 2006 THCPH156, <http://www.JACoW.org>
- [8] R. Wilcox et al., “A Low Power Laser Wire with Fiber Optic Disribution,” DIPAC’11, Hamburg, Germany, May 2011, TUPD53, p. 425, <http://www.JACoW.org>

## 12. Cryogenic Systems

Arkadiy Klebaner

### Introduction

Superconducting radio frequency (SRF) cavities distributed over the length of the PXIE linear accelerator (the Linac) are cooled by superfluid liquid helium. The cavities are grouped in 2 cryomodules – a Half Wave Resonators cryomodule (HWR) and a Single Spoke Resonator 1 cryomodule (SSR1) [1]. The PXIE cryogenic system provides cooling services to these cryomodules.

The cryogenic system includes a cryogenic plant, a cryogenic distribution system, and the ancillary systems (purification system, cryogenic storage, etc.) necessary to support the cryomodules operation in a range of steady state and transient operating modes including RF on/RF off, cool down, warm-up, and fault scenarios. A conceptual layout for the cryogenic system is shown in Figure 12.1.

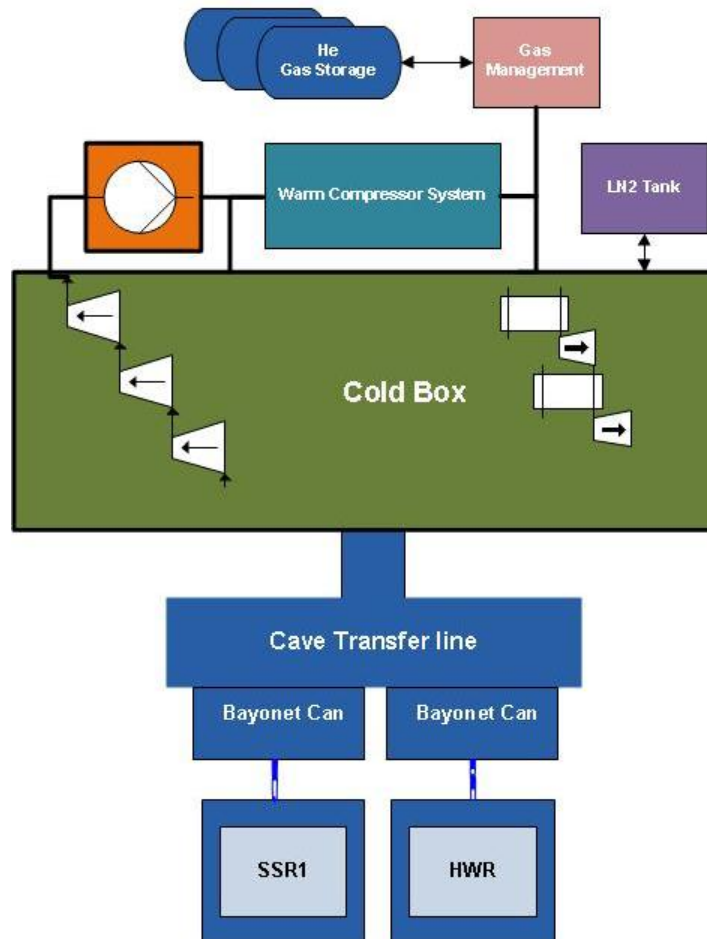


**Figure 12.1:** Conceptual layout of the PXIE cryogenic system

## **Functions and Constraints**

The cryogenic system should support a range of cryogenic loads at various temperature levels and cope with the load fluctuations due to dynamic heat load induced by operation SRF cavities. The system should provide sufficient refrigeration to cover all possible operating scenarios while maintaining stable pressure to avoid phase instabilities in the SRF cavities due to microphonics.

Additionally, the cryogenic system should have features that minimize loss of cryogen and reduce system perturbations during fault conditions. The fault conditions can be induced by the Linac or utilities outage. Also, the cryogenic system should provide for full segmentation of the Linac and allow installation or removal of a cryomodule under cold conditions. It should be possible to commission the cryogenic system independently of cryomodules.

In addition to these basic functional duties, the PXIE cryogenic system should allow for rapid cool-down and warm-up of cryomodules, e.g., for repair or exchange of a malfunctioning module. It should also be able to assist in protecting the SRF cavities from over pressurization beyond their maximum allowable working pressure during fault conditions. The primary protection, of course, is provided by cryomodules. Finally, to ensure reliable operation, the cryogenic system should provide some redundancy among its components and sub-systems.

Combining effective use of the existing Fermilab infrastructure with commercially available components is in the core of the design approach for the PXIE cryogenic system. This approach is chosen to satisfy the project's financial and schedule constraints. Other constraints include existing civil infrastructure, cave design, cryomodule required services, etc. Detailed functional requirements and constraints are listed in [2].

## **Configuration**

The PXIE cryogenics shares several similarities with the Project X cryogenic system. In fact, the PXIE cryogenic system is a scaled down version of a system envisioned for the Project X Continuous Wave (CW) section. As in Project X, PXIE SRF cavities operate in a CW mode, which results in high dynamic heat loads to the cryogenic system. For SRF components, dynamic heat load (due to RF power dissipation) on average is an order of magnitude greater than the static heat load (due to conduction and thermal radiation). Therefore, one of the important requirements for the PXIE cryogenic system is the capability to operate efficiently over a wide range of heat loads. To satisfy this requirement, a hybrid cryogenic cycle that uses both cold and warm compression is chosen. The hybrid cycle has reasonably efficient turndown capability, therefore minimizing the need for resistive heating to compensate for heat load change.

Efficient cryogenic capacity turndown is accomplished by adjusting a cryogenic system helium mass flow rate to match the heat load generated by SRF components. For superfluid

helium system, this requires reducing mass flow rates through a sub atmospheric pumping system. The pumping system for the hybrid cycle comprises of several stages of cold compressors and warm subatmospheric helium compressors (a.k.a. vacuum pumps) connected in series. Vacuum pumps are positive displacement machines, while cold compressors are hydrodynamic machines. Decrease of the warm vacuum pumps suction pressure enables it to linearly reduce the cold compressors mass flow while maintaining the compressors temperatures and speeds at reasonable levels. This in turn enables the cold compressors to stay within their respective working hydrodynamic fields away from surge or stall areas. Additionally, the total pressure ratio, which has to be performed by the cold compressors, is reduced and the speed of some machines can be lowered, therefore reducing the total cryogenic power and saving operating cost.

The major elements of the PXIE cryogenic system include a cold box with heat exchangers, turbo expanders and cold compressors, a warm compressor system, a warm vacuum compressor system, a cryogenic storage and gas management systems, a cave transfer line with bayonet cans, interconnected piping and electrical systems, and associated instrumentation and controls. The cold box and warm vacuum compressor system are being procured from industry, while the rest of the equipment is being reengineered and repurposed from available Tevatron components.

The cryogenic services from the plant are distributed to cryomodules via a compound cryogenic transfer line that runs along the Linac. The transfer line contains five circuits and two bayonet cans. The bayonet cans provide for connection to the PXIE cryomodules and contain a variety of cryogenic valves and instruments. Connection between the bayonet cans and cryomodules is accomplished via vacuum insulated removable cryogenic tubes, so called u-tubes.

## **Goals**

We plan to achieve the following major goals as a result of work on design, construction and operation of the PXIE cryogenic system:

Technical goals:

- a. Project X linac cryogenic segmentation proof of principle: Develop approaches and procedures to install and/or remove a cryomodule under cryogenic conditions;
- b. Operate SRF components in CW mode;
- c. Improve understanding of the SRF component heat loads;
- d. Develop cryogenic system control strategies for all modes of operation, including RF On/RF Off modes;
- e. Develop design solutions and control algorithms to minimize helium pressure fluctuation;
- f. Develop expertise in operating cryogenic turbo expanders with gas bearings, oil free warm vacuum pumps, and cold compressors;

- g. Improve expertise in cryogenic process and component design;
- h. Improve hydrodynamic field models for cold compressors;
- i. Develop expertise in defining three stage cold compressors train hydrodynamic field;
- j. Develop superfluid cryogenic system operational expertise, including efficiently turning down cryogenic capacities.

Cost and schedule goals:

- a. Improve the Project X cryogenic system acquisition strategy and cost estimate based on the procurement experience with PXIE cryogenic system;
- b. Improve capacity margin estimate for Project X cryogenic system;
- c. Develop engineering and technical expertise in support of the Project X superfluid cryogenic system design and operation.

### **References**

1. Nagaitsev, S. et al., “PXIE Functional Requirements Specification”, *Project X Doc DB*, Document 980.
2. Klebaner, A. et al., “PXIE Cryogenic System Functional Requirements Specification” *Project X Doc DB*.

## 13. RF Power Systems

Ralph J. Pasquinelli

### Introduction

The PXIE RF systems will include all continuous wave (CW) amplifiers that are intended for reuse in the Project X front end. The complete PXIE RF system uses three frequencies (162.5 MHz, 325 MHz, and an RF separator at 243.75 MHz) at power levels ranging from 4 kW to 150 kW. Initial investigation of RF power for the RFQ pointed toward using a single tetrode final gain stage. A cost estimate for in house development of such a system was created and showed minimal if any cost savings over commercial products. With limited resources allocated to PXIE, it was decided to go out on bid for commercial solutions. In the last five years, solid-state amplifiers have advanced considerably and now have a very competitive price range and higher power levels in a compact footprint compared with other technologies such as IOTs, klystrons or tetrodes. At PXIE frequencies and power levels, solid-state amplifiers have been chosen for the RF power sources.

There are a total of 21 RF systems included in PXIE. Two 75 kW CW amplifiers will drive the 162.5 MHz RFQ. The bid was awarded to Bruker Biospin [1] in Wissembourg, France. Bruker specializes in the production of MRI scanners, which require significant RF power sources in frequency ranges commensurate with the needs of Project X. Due to the high production volume of MRI systems at Bruker, nonrecurring engineering costs are minimized, making a solid-state amplifier the most economic solution for PXIE RFQ. The beam energy at the RFQ output is 2.1 MeV. Three room temperature buncher cavities and one cryomodule containing eight superconducting half wave resonators (HWR) at 162.5 MHz will have one amplifier each operating at power levels of 4 kWatts or less. Exit energy after the HWR section will be 10.3 MeV. The second cryomodule at 325 MHz will be populated with eight single spoke resonators (SSR1) powered by 4 kW amplifiers. Exit energy after this cryomodule is expected to be 23.7 MeV. A diagnostic separator cavity operating at 243.75 MHz requires a 7 kW amplifier. The separator RF is operated at 1.5 times the RFQ frequency (0.75 times the SSR1) and will be a transverse deflecting cavity. This cavity is to be used to measure adjacent bunch extinction efficiency of the bunch-by-bunch chopper in the MEBT. Only the RFQ amplifier has been procured to date as it the longest lead-time.

A typical RF system configuration is shown in Figure 13.1. The low level RF (LLRF) system will provide a drive signal on the order of 0 to +10 dBm for each RF power source. The amplifier(s) will provide sample signals of the pre-driver and final outputs. All amplifiers will be self contained units complete with integral power supplies, protection circuits, and control interface. The RF distribution system will utilize rigid coax commensurate with system power levels, 6-1/8", 3-1/8", or 1-5/8" EIA flanged sections. The final connection to the cryomodules will utilize a section of flexible transmission line to minimize connector location tolerances.

Each RF system will have a circulator and load to isolate the cavity from the power amplifier. This level of protection is essential in SRF systems due to full power reflection from the cavity in the absence of beam. Cavity and drive sample signals will be provided to the LLRF for vector regulation and frequency control of the cavities.

All of the RF amplifiers will be water cooled to minimize the heat load to the building HVAC system. In the case of the Bruker RFQ amplifier, the DC power supply is also water-cooled, which should result in higher reliability.

While each amplifier has built in protection which includes, water flow, water temperature, pressure differential, and reflected power monitoring; a global interlock and hardware protection system will need to be designed for all RF systems. This will include water flow to loads and circulators, spark detection on cavity couplers, and RF leakage detection.

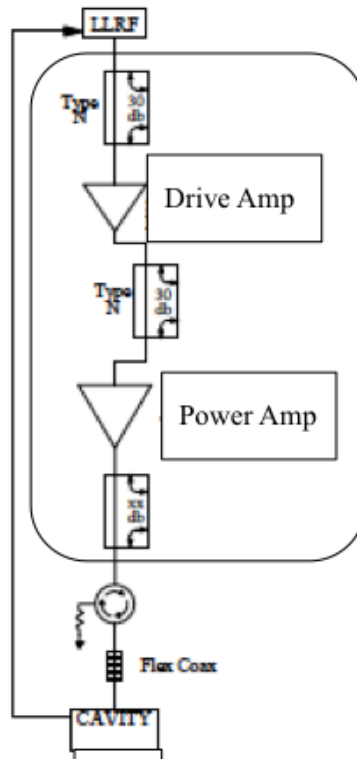


**Figure 13.1:** PXIE typical RF system.

Drive and power amplifiers will be housed in a single enclosure.

The RF systems are designed for robust operation with continuous operation. The PXIE test facility will verify the ability to create an arbitrary pattern of beam bunches for Project X; using the RF separator cavity to measure the extinction ratio of adjacent bunches generated by the fast chopper, and prove that the chopping losses are compatible with operation of SRF cavities in close proximity to the MEBT beam dump.

The sequence of testing will begin with RFQ commissioning. For better control of the gradient vector, it was decided that using two amplifiers, one for each drive port of the RFQ, would allow for better versatility for operations. Any imbalance in coupling impedance could be compensated. If one of the drive amplifiers develops a degraded output, it is possible to compensate output power on the other drive port to allow continued operation. This added level of complexity will require a commissioning period prior to beam acceleration. A vector scan of each subsequent cavity will be necessary with beam to establish the correct gradient for beam acceleration. These procedures have been successfully accomplished with the Fermilab linac and the HINS test accelerator.

### **References**

- [1] <http://www.bruker-biospin.com/>

## 14. Vacuum Systems

Alex Chen

### Introduction

The PXIE Vacuum system will include all beam vacuum environments - from the ion source to the beam dump. The complete PXIE Vacuum system consists of four regions, Ion source-LEBT-RFQ, MEBT, Cryomodules (CM), Diagnosis beamline. There are vacuum gate valves to isolate each other when necessary for commissioning or operation. As PXIE will be a prototype of the Project X front end that will be used to validate the design concept and decrease technical risks. Its vacuum system design will also establish the design guidance for the Project X, especially the quantitative requirement of low particulate vacuum that is sufficient but practical, and is cost efficient to ensure the performance of CM.

### The challenges

The PXIE vacuum system faces significant technical challenges, including a large hydrogen flux from the H<sup>-</sup> ion source (500 mtorr l/s) and large outgassing from the MEBT absorber (~1 mtorr l/s). Therefore, pumps with large effective pumping speed have to be applied within very tight space. Turbo pumps have been chosen for Ion Source, RFQ, Absorber, and Dump. Ion pumps also will be used for distributed pumping among the beamline where applicable.

The greatest challenge is probably to minimize the risk of degrading SRF cryomodules due to the migration of large gas load and microparticles. Therefore, it is important to apply low particulate vacuum practices in the large vicinity (if not all) of PXIE beamline for preventing contamination of the SC cryomodules. The roughing/venting ports will be arranged in the way minimizing the particle migration towards CM, and the flow rate of roughing/venting will be regulated to reduce the risk of particle migration. Differential pumping scheme will be arranged at the vicinity of cryomodules (CM) to minimize the hydrogen gas flux towards CM.

In order to provide design guidance for Project X, the quantitative evaluation of particle generation within classic vacuum devices, such as ion pumps, turbo pumps, valves, Titanium sublimation pumps, RGA etc. will be studied. Also important is the vacuum measurement or monitoring at the cryogenic temperature since it coexists with room temperature vacuum.

As usual, interlocking will be applied on gate-valves as vacuum failure protection and data logging will be implemented for operation and analysis.

The pressure profiles of residual gas in PXIE beamline sections are shown in Figs. 14.1, 14.2 and 14.3, based on the current primary design. The pressure inside beam vacuum of cryomodules will be  $10^{-10}$  torr or less, driven by the temperature of LHe.

### References

- [1] A. Chen, L. Nobrega “PXIE Vacuum Considerations”, Project X-doc-972-v1,

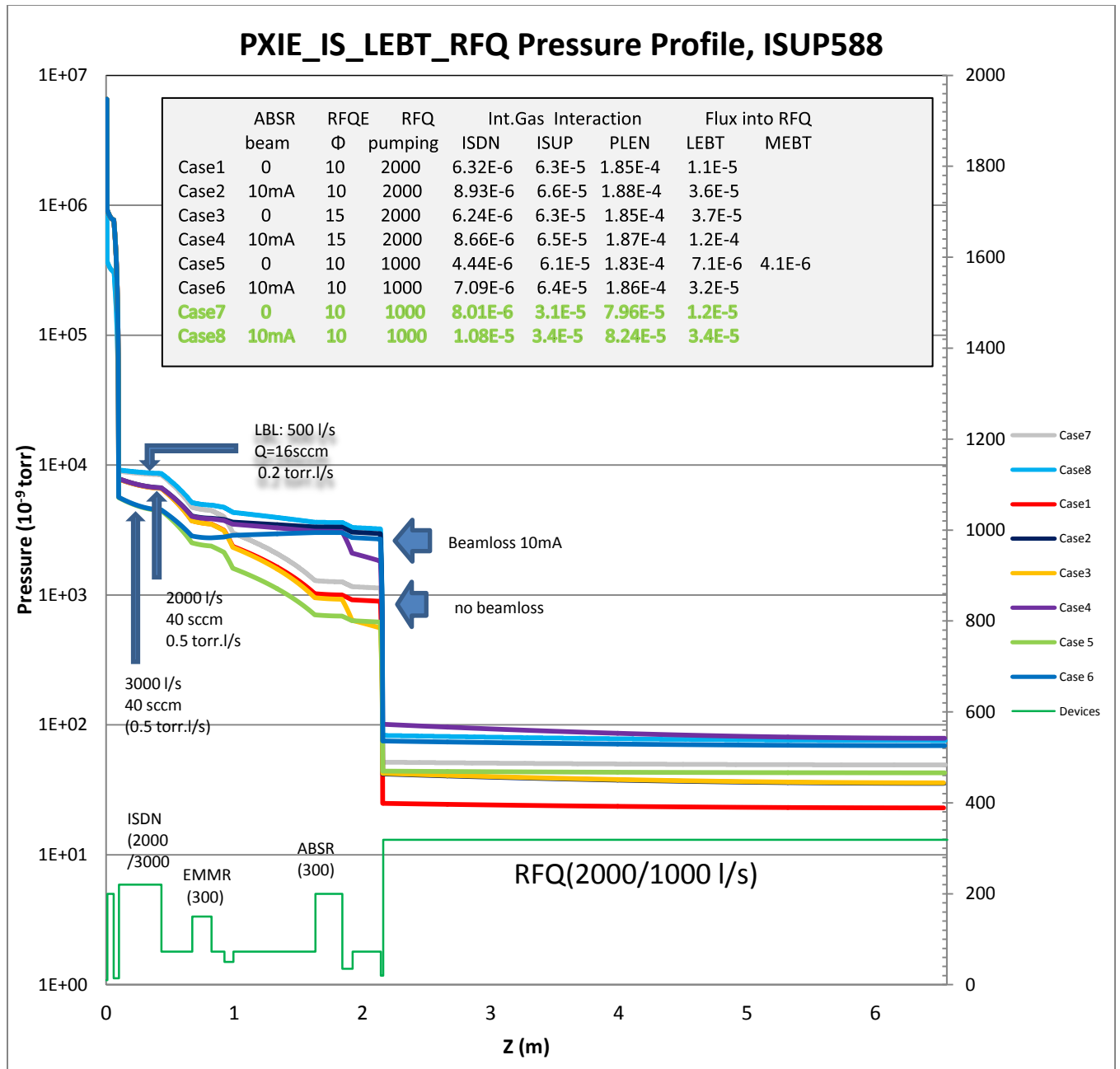


**Figure 14.1:** PXIE residual gas total pressure profile in Ion Source-LEBT-RFQ

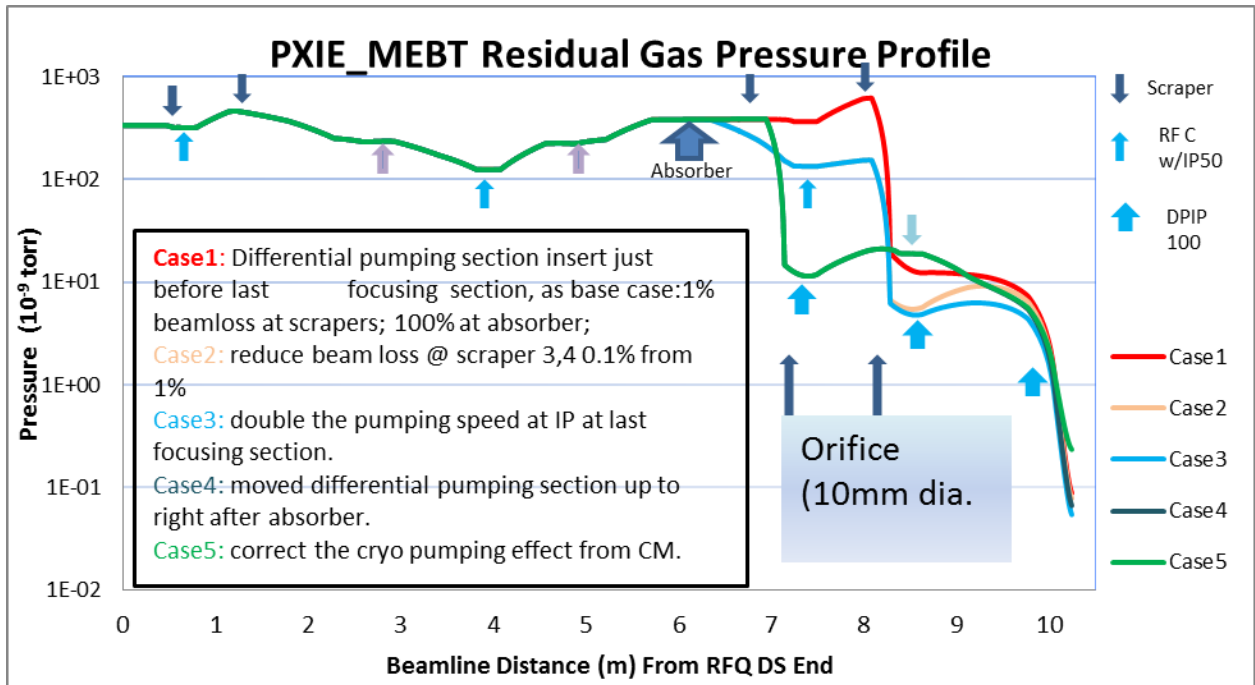


**Figure 14.2:** PXIE residual gas total pressure profile in MEBT

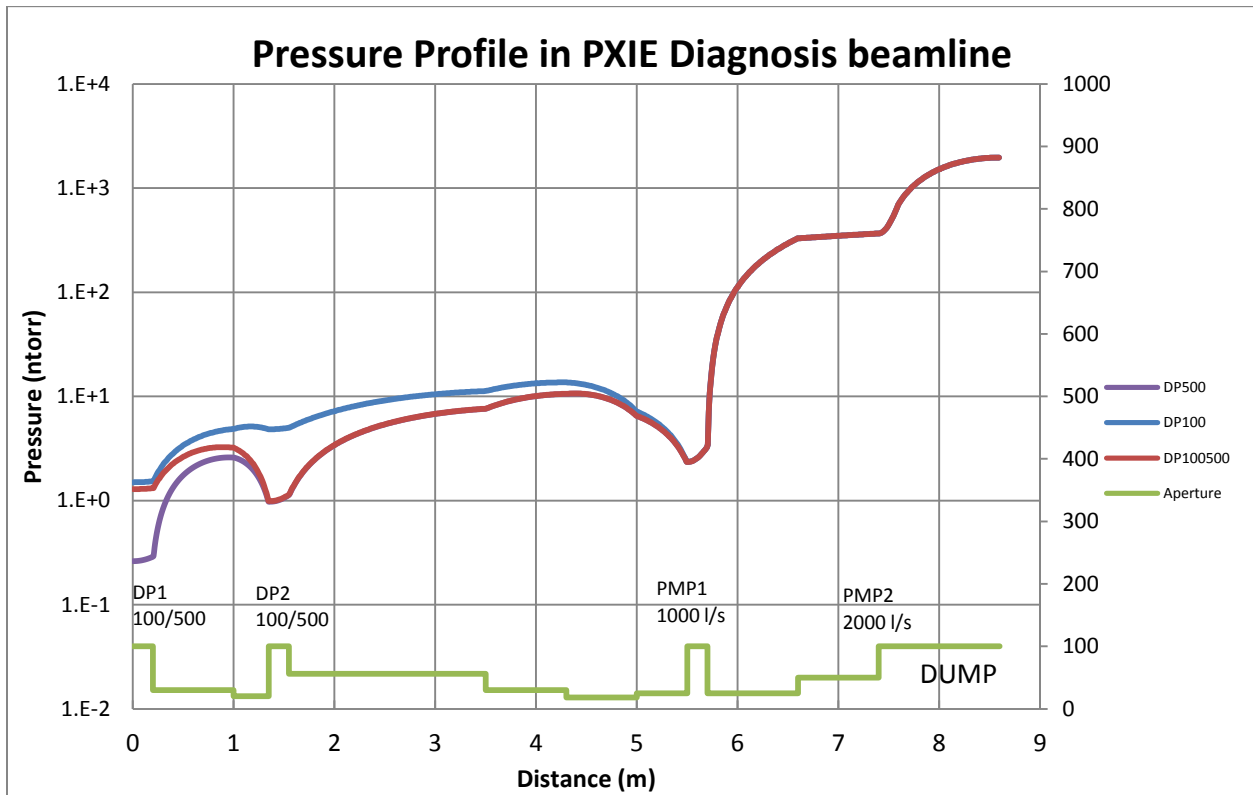


**Figure 14.3:** PXIE residual gas total pressure profile in Diagnosis beamline

## 15. Controls

James Patrick

### Introduction

The control system, schematically shown in Figure 15.1, is responsible for control and monitoring of accelerator equipment, machine configuration, timing and synchronization, diagnostics, data archiving, and alarms. PXIE will use the Fermilab control system ACNET [1]. This is the system that is used in the main accelerator complex and also at the NML/ASTA test facility [2]. ACNET is fundamentally a three tiered system with front-end, central service, and user console layers. Front-end computers directly communicate with hardware over a wide variety of field buses. User console computers provide the human interface to the system. Central service computers provide general services such as a database, alarms, application management, and front-end support. Communication between the various computers is carried out using a connectionless protocol also named ACNET over UDP.

The control system will prefer modern hardware that might be applicable eventually to Project X rather than CAMAC or other legacy equipment in the main complex. General purpose digitization and basic power supply control will be provided by Hotlink Rack Monitor (HRM) front-ends. Each HRM provides 64 analog input channels, 8 analog output channels and 8 bytes of digital I/O Vacuum and LCW controls will be based on PLCs interfaced via standard front-end processors. Instrumentation and RF systems will be based on the standard VME, VXS or VXI platforms.

A new timing system will be developed that is a major enhancement over the TCLK and MDAT links in the main complex. A prototype has been developed based on a 1 Gbps data link that adds a data payload and cycle stamp to each clock event transmission. The latter will allow reliable correlation of data across different front-ends. The prototype design will be updated based on requirements for PXIE, and will serve as a test platform for the timing system for the full Project X accelerator.

PXIE will provide the opportunity to develop and test most of the control system components that would be required for Project X. This includes hardware components and higher level software to control and monitor those components. And it will provide experience with the operational scenarios and the associated global accelerator control applications for Project X.

PXIE can also serve as a place to develop and test new control system technologies before introducing them to the main complex, where reliability requirements are much more stringent. Example technologies under development include a new front-end software framework based on the Erlang programming language that runs on Linux computers, and new more modern console application frameworks. Also more modern VME based modules have been developed for some power supply control and timing functions replacing older CAMAC modules.

A gateway process between ACNET and EPICS based front-ends has been developed. This could be used to interface instrumentation or other devices developed at other labs using EPICS control software. The console environment also supports EPICS displays based on the EDM display manager.

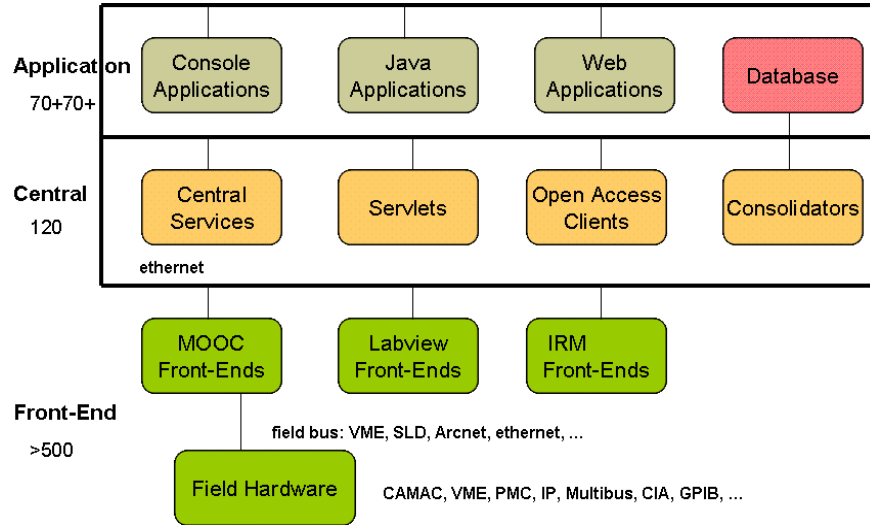


**Figure 15.1:** Fermilab Main Control System Architecture

## References

- [1] K. Cahill, et al., The Fermilab Accelerator Control System, ICFA Beam Dyn.Newslett.47:106-124, 2008.
- [2] J. Patrick and S. Lackey, “Control Systems for Linac Test Facilities at Fermilab”, proc. Linac08, Victoria, BC, 2008.

## 16. Low Level RF System

Brian E. Chase

### Introduction

The *Low Level RF System* for Project X includes all controller hardware and software required to provide many accelerator functions, broken down here as subsystems: the *Field Control System* regulates the RF field vectors in all accelerating structures to maintain the specified beam energy and longitudinal beam emittance throughout the accelerator, the *Resonance Control System* regulates the superconducting cavities tuning frequency by canceling Lorentz forces generated by the RF fields and microphonics. The *Master Oscillator* generates frequency and phase stable multiple frequency references, the *Phase Reference Lines* distribute these Master Oscillator signals throughout the accelerator footprint to phase stabilized tap points, and the *Beam Pattern Generator* which drives the LEBT and MEBT Choppers, generates triggers for kicker magnets and provides beam transfer synchronization with the Recycler Ring.

### LLRF Subsystem Development

The PXIE design allows for the realistic development, deployment and evaluation of most of the critical LLRF systems required for Project X. The PXIE design encompasses the 162.5 MHz RFQ, buncher cavities and eight half wave resonators, the first 325 MHz SSR1 cryomodule and the RF separator at 243.75 MHz. These RF systems present the Field Controllers and Resonance Control Systems with new cavity and cryomodule designs that have not yet accelerated beam. The RF power source for these cavities will be newly designed solid-state amplifiers providing possible new challenges for RF control. Project X RF systems outside the scope of PXIE are partially covered by ASTA, with 1300 MHz pulsed cavities and the test stands which will provide some experience with 650 MHz cavities. The PXIE Master Oscillator will provide all Project X frequencies and will drive shorter versions of the Phase Reference Lines. The full requirements of the Beam Pattern Generator will be addressed with PXIE.

### Key Technologies

There are several key LLRF technologies required for Project X that will be developed and validated in the scope of the PXIE project.

- Development of a *Multi-System Controller* module to handle up to eight PA/cavity systems. This next generation design is an extrapolation of the present MFC module design used at ASTA and is capable of operation in CW or pulsed mode<sup>1</sup>. It will take advantage of state of the art communication industry components. During PXIE commissioning we will learn the unique issues involved with controlling the RFQ, 162.5 MHz half-wave resonators, 325 MHz SSR1 cavities and the 243.75 MHz RF-separator. Requirements such as < 1.0% amplitude and < 1.0 degree phase regulation during beam chopping will be demonstrated. Operability of the RF systems, diagnostics, and the human machine interface are also under the scope of this development.

- Development of a *Multi-Channel Resonance Controller* and a *Piezo Driver* module that is integrated with the Multi-System Controller, stepper motor controllers and piezo actuators. During PXIE commissioning we will optimize the resonance control of several new cavity types. This experience will provide hard data for RF power overhead requirements and will provide feedback to the cavity tuner designs.
- Development of a *Master Oscillator* and a *Multi-Frequency Phase Reference Line* system to generate and distribute all RF references (1300, 650, 325, 243.75, 162.5 MHz) to RF and diagnostic tap points. Challenges here are to maintain phase stability between all frequency standards at many distributed tap points for the accelerator and the experiments within a fraction of a degree.
- Development of a Beam Pattern Generator to drive the LEBT and MEBT chopper. The Beam Pattern Generator takes real-time requirements from the experimental areas and generates the drive signals to the beam choppers. These drive signals are pre-distorted in the generator to remove nonlinearities in the driver amp and dispersion in the choppers. PXIE development and commissioning with beam will determine the full requirement of this system. The chopper performance will affect beam loss and beam quality downstream in the accelerator as well as the general flexibility and reliability of the machine. The MEBT chopper clearly pushes the state of the art on many fronts making it a key and challenging technology for Project X.

### **LLRF Test and Commissioning**

LLRF testing will follow the process of validation in the lab, installation and test in the field and finally commissioned with beam as beam-line components are installed. The quality metrics for Project X and PXIE LLRF align closely with those of the accelerator itself: beam quality, stability, reliability, flexibility, maintainability and operability. These are the qualities of a mature system that has evolved with operational experience. PXIE provides this experience as a precursor to Project X. There is much to learn about the performance of the entire RF and chopper systems, fundamentally if they can meet accelerator performance requirements. Beam diagnostics will provide the final measurements of the performance of these systems.

### **References**

- [1] P. Varghese et al., “A Vector Control And Data Acquisition System For The Multicavity LLRF System For Cryomodule 1 At Fermilab”, LINAC2010 Tsukuba, Sept. 2010, MOPO84.

## 17. PXIE Machine Protection System

Arden Warner and James Steimel

### Introduction

The damage potential of the PXIE is expected to be 150 Watts through the Low Energy Beam transport section (LEBT), 10 kW through the Medium energy Beam transport section (MEBT) and up to 50 KW in the diagnostics section and at the dump. In order to protect the machine and associated diagnostics from beam induced damage and excessive radiation damage a robust Machine Protection System (MPS) is required. The main goals of the MPS will be the following:

- Protect the accelerator from beam induced damage and operator errors
- Manage and monitor the beam intensity
- Safely switch off or reduce the beam intensity in the case of failures
- Determine the operational readiness of the machine
- Manage and display alarms
- Provide a comprehensive overview of the machine status
- Provide high availability
- Provide fail safe operation where possible
- Provide post mortem analysis.

Several signals from devices or systems will be monitored and utilized as actuators to inhibit or reduce the beam intensity loss at various stages of the accelerator. The main actuator for beam is the ion source power supply itself. In the low energy stage of the machine the beam line can be safely tuned with a 100  $\mu$ s beam pulse since only 1 Joule of energy would be deposited in an operational scenario. As a result a 100  $\mu$ s reaction time for the MPS should be sufficient. In addition, signals from the LEBT/MEBT choppers, the Radio Frequency Quadrupole Amplifier (RFQ), cavity power amplifiers as well as beam stops and gate valves status will all contribute as additional control devices. A comprehensive overview of the entire machine will be obtained by carefully monitor all relevant inputs from machine diagnostics and critical systems affecting safe or fail safe operation.

Designing and operating such a system will have broad implications for Project X despite it has much larger damage potential. The protection scheme and techniques developed for PXIE are scalable and can, if required, be implemented on systems with more stringent requirements.

### MPS Configuration

The MPS will be considered to be the collection of all subsystems involved in the monitoring and safe delivery of beam to the dump and not limited to any particular subsystem or diagnostic device. It has connections to several external devices and sub-systems. Figure 17.1 shows a conceptual overview diagram of the MPS. The top layer comprises signal providers such as

beam loss monitors, beam position monitors, magnet power supplies etc. Systems at this level send alarms or status information to the MPS logic subsystems (permit system) which issues a permit based on the comprehensive overview of all inputs and request. Only simple digital signals (e.g. on-off, OK-alarm) are transmitted. All devices or subsystems that are determined to be pertinent to protecting the machine or necessary for machine configuration are included. This permit system layer of the MPS will be FPGA based and is thus fully programmable and handles complex logic task. The logic here will be designed to ensure safe operating conditions by monitoring operational input, chopper performance, the status of critical devices and by imposing limits on the beam power.

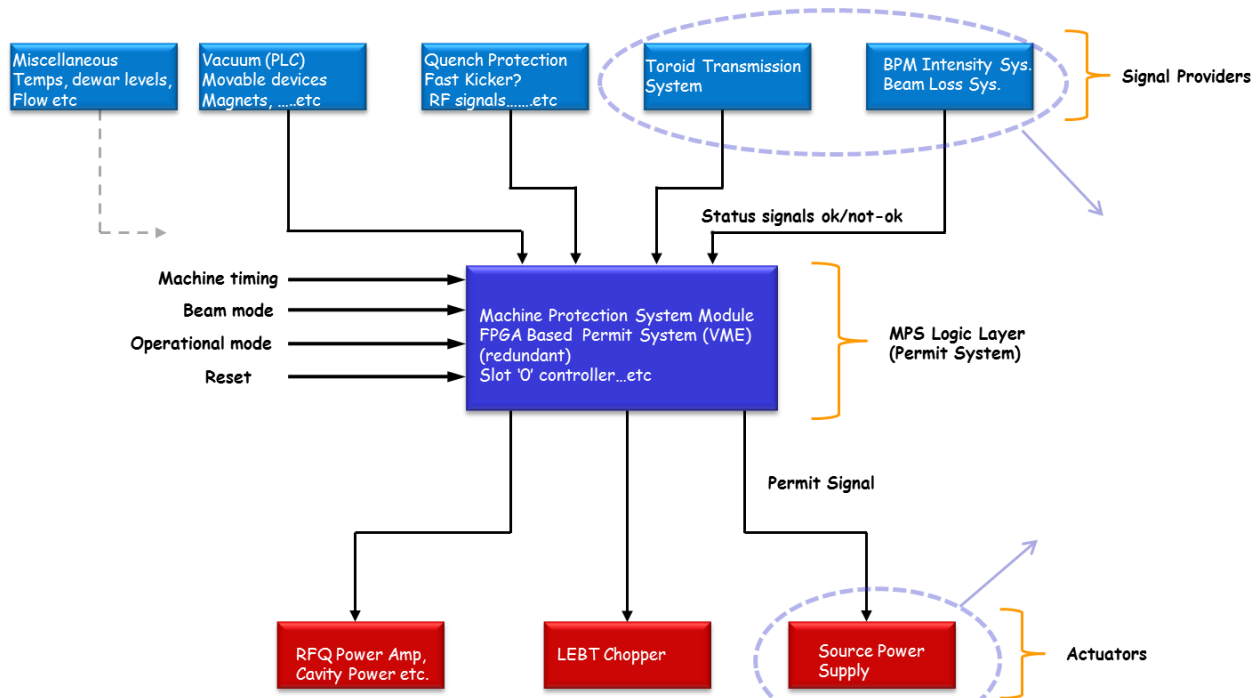


**Figure 17.1: MPS Conceptual Layout**

The final layer of the system shows the main actuators. This will comprise of all points where the MPS logic may act on the operation of the machine to prevent beam from being produced or transported. The entire protection system interfaces with the accelerator control system and machine timing system for configuration management, timing and post mortem analysis as shown in Figure 17.2. The schematic layout would be similar for Project X. The operational modes, operational logic, reaction time and complexity of inputs will differ based on the machine configuration and damage potential at various stages of the accelerator complex.

### Protection System R&D

Protecting the superconducting cavities from low energy protons losses where the particle energies are too low to produce significant detectable radiation will be a major part of the

developmental work needed to effectively inject beam without quenches. To achieve this we will need to research sensitive means for measuring these losses and develop an effective feedback for machine protection. In addition we plan to achieve the following goals as a result of designing, constructing and operating the PXIE MPS:

- Understand and estimate acceptable loss rates in the room temperature sections.
- Develop a strategy to monitor chopped beam from the MEBT.
- Estimate particle shielding effect of superconducting cavities and cryomodules.
- Develop effective algorithms for the FPGA based logic system.
- Demonstrate effective integration with controls/instrumentation and all subsystems.
- Understand dark current effects as it relates to protection issues.

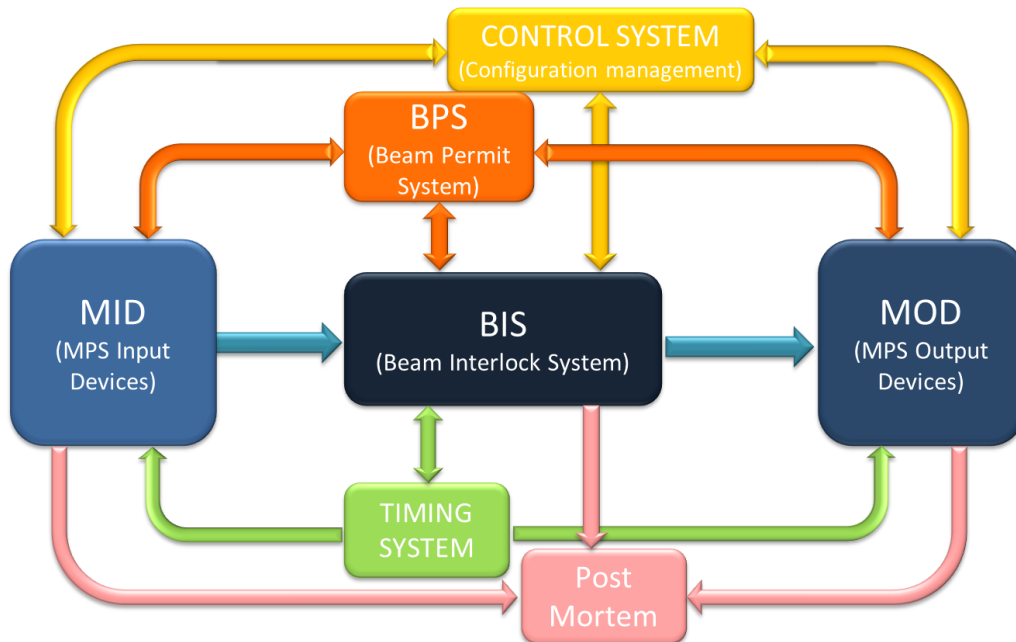


**Figure 17.2:** Conceptual layout integrated with control system

In order to protect the accelerator from damage as the beam transitions from the room temperature sections of the machine to the superconducting sections, some specialized instrumentation will be developed at PXIE. Developing an effective algorithm to monitor the BPM intensities as a feed back to machine protection will be of interest for both PXIE as well as Project X.

### References

[1] S. Nagaitsev et al., “PXIE Functional Requirements Specification”, Project X Document 980.

## Summary

The PXIE program is being designed and constructed at Fermilab as the centerpiece of the Project X R&D program. It will provide an integrated systems test for Project X front end components and validate the concept for the Project X front end, thereby minimizing the primary technical risk element within the Reference Design.

Main technical issues to be addressed by PXIE are:

- LEBT: the beam neutralization, the chopper performance, and the beam stability;
- RFQ: the longitudinal halo formation and the high average power;
- MEBT: the beam dynamics, the chopper kicker and its driver, the absorber, the diagnostics, the extinction, and vacuum near SRF cavities;
- HWR and SSR1: Issues associated with operating SRF cryomodules near a high power absorber, beam losses, beam acceleration, the effect of solenoids magnetic field on SRF cavities, microphonics and LLRF control of low beta CW cavities at 2K;
- Beam line: the beam properties, the beam extinction, the beam losses and halo.

The PXIE design and construction is being carried out by collaboration between Fermilab, ANL, LBNL, SLAC and Indian institutions. It is planned to have PXIE operational by the end of 2016.